

AD-A189 490

ICE PARTICLE CHARGE TRANSFER STUDIES(U) UNIVERSITY OF

1/2

MANCHESTER INST OF SCIENCE AND TECHNOLOGY (ENGLAND)

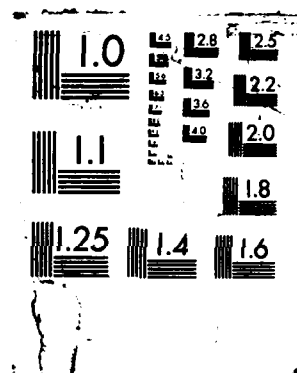
DEPT OF PHYSICS C P SAUNDERS 30 SEP 87 EOAD-TR-87-10

UNCLASSIFIED

AFOSR-85-0282

F/G 20/3

NL



DTIC

DTIC FILE COPY

(2)

ELECTE

DEC 28 1987

AD-A189 490

SECURITY CLASSIFICATION OF THIS PAGE

D

REPORT DOCUMENTATION PAGE

1a. REPORT SECURITY CLASSIFICATION UNCLASSIFIED		1b. RESTRICTIVE MARKINGS	
2a. SECURITY CLASSIFICATION AUTHORITY		3. DISTRIBUTION/AVAILABILITY OF REPORT Approved for public release; distribution unlimited	
2b. DECLASSIFICATION/DOWNGRADING SCHEDULE		5. MONITORING ORGANIZATION REPORT NUMBER(S) AD-TR-87-110	
4. PERFORMING ORGANIZATION REPORT NUMBER(S)		7a. NAME OF MONITORING ORGANIZATION EDARD	
6a. NAME OF PERFORMING ORGANIZATION Department of Physics UMIST	6b. OFFICE SYMBOL (if applicable) UMIST	7b. ADDRESS (City, State, and ZIP Code) 223/231 Old Marylebone Road London NW1 5TH U.K.	
8a. NAME OF FUNDING/SPONSORING ORGANIZATION EDARD	8b. OFFICE SYMBOL (if applicable) EDARD	9. PROCUREMENT INSTRUMENT IDENTIFICATION NUMBER AFOSR 85-0282	
8c. ADDRESS (City, State, and ZIP Code) 223/231 Old Marylebone Road London NW1 5TH U.K.		10. SOURCE OF FUNDING NUMBERS PROGRAM ELEMENT NO. 61102F PROJECT NO. 2301 TASK NO. D1 WORK UNIT ACCESSION NO. 193	
11. TITLE (Include Security Classification) Ice Particle Charge Transfer Studies (Unlimited)			
12. PERSONAL AUTHOR(S) Saunders C P R			
13a. TYPE OF REPORT Final	13b. TIME COVERED FROM Aug 85 to Jul 87	14. DATE OF REPORT (Year, Month, Day) 87-9-30	15. PAGE COUNT
16. SUPPLEMENTARY NOTATION			
17. COSATI CODES FIELD GROUP SUB-GROUP		18. SUBJECT TERMS (Continue on reverse if necessary and identify by block number) Thunderstorms, Electrification, Charge Transfer Ice Crystals, Rime ice, Cold Chamber, Aircraft Charging	
19. ABSTRACT (Continue on reverse if necessary and identify by block number) Electric charge transfer between ice crystals and an ice target has been measured under a range of environmental conditions which simulate the environment of a thunderstorm. The charge transfer is very dependent on ice crystal size and a cold chamber which permits long growth times has been used to determine charge/size relationships for crystal sizes up to 800 μ m. Also, a new hot-wire device has been developed to measure liquid water content. The collection efficiencies of a rimed target for water droplets and ice crystals have been determined. High velocity crystal/target impacts up to 100 m s ⁻¹ show a maximum charge transfer at 25 m s ⁻¹ .			
20. DISTRIBUTION/AVAILABILITY OF ABSTRACT <input type="checkbox"/> UNCLASSIFIED/UNLIMITED <input type="checkbox"/> SAME AS RPT <input type="checkbox"/> DTIC USERS		21. ABSTRACT SECURITY CLASSIFICATION	
22a. NAME OF RESPONSIBLE INDIVIDUAL C P R Saunders		22b. TELEPHONE (Include Area Code) 061-236 3311 (ext. 2710)	22c. OFFICE SYMBOL

DD FORM 1473, 84 MAR

83 APR edition may be used until exhausted.
All other editions are obsolete.

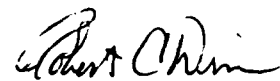
SECURITY CLASSIFICATION OF THIS PAGE

87 12 14 112

EOARD-TR-87-10

This report has been reviewed by the EOARD Information Office and is releasable to the National Technical Information Service (NTIS). At NTIS it will be releasable to the general public, including foreign nations.

This technical report has been reviewed and is approved for publication.

for 
OWEN R. COTE
Chief, Geophysics and Space


ROBERT C. WINN, Lt Col, USAF
Chief Scientist

GRANT No. AFOSR-85-0282

ICE PARTICLE CHARGE TRANSFER STUDIES

C P R Saunders

Physics Department
University of Manchester Institute of Science and Technology
Manchester M60 1QD
England

30 September 1987

Final Scientific Report

1 August 1985 - 31 July 1987

Approved for public release; distribution unlimited.

Prepared for:

United States Air Force
Air Force Office of Scientific Research
Building 410
Bolling AFB, DC 20332

and,

European Office of Aerospace and Development
London, England.

CONTENTS

Section 1	Introduction	Page 1
Section 2	Instrumentation	4
Section 3	A new hot-wire for measuring cloud liquid water content	11
Section 4	The collection efficiency of a rime covered target	20
Section 5	The collection efficiency of a cylindrical target for ice crystals	31
Section 6	The charging of a simulated soft-hailstone by large ice crystals	39
Section 7	Discussion, Conclusion and future work	53
Appendix I	The replication of cloud particles	59
Appendix II	Measurements of the surface temperature of a riming hailstone	61
Appendix III	The growth rate of hydrometeors	63
Appendix IV	The event probability of a cylindrical target	66

REFERENCES



Accession For	
NTIS CRA31	<input checked="" type="checkbox"/>
DTIC TAB	<input type="checkbox"/>
Unannounced	<input type="checkbox"/>
Justification	
By	
Distribution	
Availability Codes	
Date	Accession Number
A-1	

SECTION 1

INTRODUCTION

This report deals with research performed at UMIST into the electric charge that is transferred when vapor-grown ice crystals collide and separate from ice particles. The objective is to understand the electrification of thunderstorms in which it is now generally accepted that the electric dipole is set-up by charges on cloud particles. Our laboratory work is performed inside a cold-room, in which a water droplet and ice crystal cloud may be grown to simulate conditions inside a thunderstorm. A target acts like a graupel pellet (a soft-hailstone) which, in a thunderstorm, falls through the cloud and collides with super-cooled water droplets and ice crystals. This ice-coated target may be on a rotating frame which sweeps out the cloud, or it may be stationary, in which case the cloud is drawn past the target.

Previous work in UMIST has shown that at cold temperatures the target, simulating a graupel pellet, charges negatively with the crystals removing the equal and opposite positive charge. In thunderstorms, the graupel pellets fall and lead to the negative charge center, while the ice crystals are carried in the updraft to form the upper positive charge of the thunderstorm. This upper-positive lower-negative configuration has been well established as being typical of summer-type thunderstorms throughout the world. The laboratory work has also shown that at temperatures warmer than typically -20°C , the graupel pellets charge positively and fall to form a lower positive charge region, which has also been observed in the base of thunderstorms. In this case, the crystals are carried in the updraft and reinforce the negative charge region formed from the falling graupel particles.

The laboratory work has shown that the temperature at which the charge transfer changes sign is a function of the liquid water in the cloud.

Prior to the present work, our laboratory experiments had shown that the charge transfer was a sensitive function of the interaction speed between the two particles. Also, the ice crystal size was important in that the charge transfer depended on size to the fourth power. This strong dependence was used in extrapolations of the laboratory results to thunderstorms, in an attempt to account for the total charge transfer observed in the real situation. However, the laboratory cloud was limited in extent, and it was possible only to grow crystals of 100 μ m diameter; whereas, in nature, crystals have time to grow several hundred microns. Another conclusion was that the magnitude of the charge transfer was affected by the presence of liquid water in the cloud. With a cloud that consisted of ice crystals alone, the charge transfer was weak and inadequate to explain thunderstorm electrification; whereas, when water was present, substantial charge was transferred.

The present work extends the previous studies, thanks to the provision of a new cold-chamber with greater height. Inside this chamber, crystals of several hundred microns have now been grown, and these have been used in a series of experiments which have provided some surprising new results.

In addition to the thunderstorm experiments, some high speed experiments have been performed to determine whether the charge/velocity results obtained previously may be extrapolated to high velocities. These studies will have some relevance to the impact of cloud particles with airplanes which may lead to the build-up of static charges on the airplane skin, possibly leading to a

lightning strike.

This report is divided into sections dealing with various aspects of the work. The basic experimental set-up is described in Section 2, together with details of some of the experimental techniques used. Additional information is located in the appendices. Section 3 deals with a novel method of measuring the liquid water content in the laboratory cloud, which may have application to measurements in the natural environment. Section 4 investigates the enhanced collection efficiency of a rime-coated target, simulating a graupel pellet, for super-cooled water droplets. The non-uniform rime deposits disturb the air-flow around the collector leading to enhanced collection. Section 5 covers measurements of the collection efficiency of graupel for ice crystals. The theory of this topic is difficult and very few laboratory measurements have been made. The results are important to the electrification work, as electric charge is transferred only when ice crystals separate from an ice pellet. Section 6 covers the charge transfer experiments themselves. Section 7 discusses the results, draws conclusions and covers the future objectives for the continuation of these studies.

SECTION 2

INSTRUMENTATION

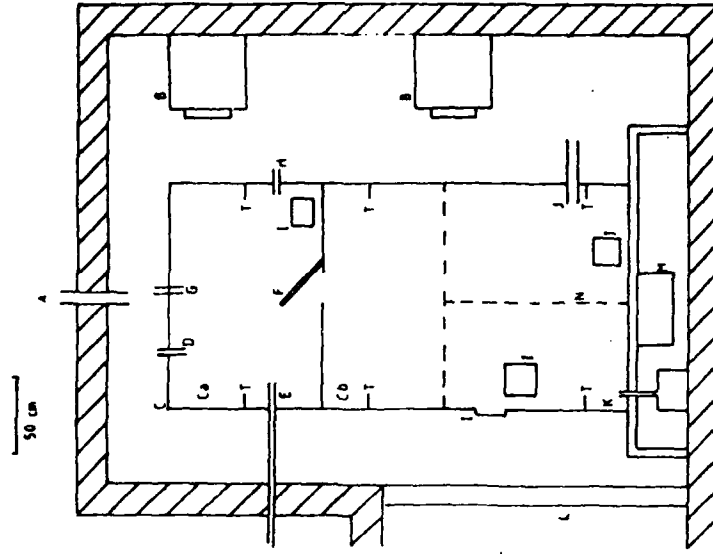
The charge transfer experiments were performed in a cloud chamber situated within a large cold-room. The cold-room has dimensions of 3m x 2m x 4m and has an effective operating temperature of 0°C to -37°C. The refrigeration equipment has a total cooling power of 5.6 kW. The cloud chamber consists of a large metal box divided into two smaller chambers, as shown in Figure 1. The size of the lower chamber is 0.94m x 1.5m x 2m and the upper chamber has dimensions 0.9m x 1.5m x 1m. The two chambers, which are connected by a trapdoor situated in the floor of the upper chamber, remain essentially independent of one another. The two chambers have a number of observation windows which are shielded to prevent any build-up of charges affecting the experimental apparatus. Figure 1 also shows the positions of the six thermocouples which were used to monitor the chamber temperature. The cloud chamber was earthed to prevent the apparatus from being affected by radio frequency noise. The two chambers were not quite air-tight so that air from the cold-room could replace air that was removed during the experimental runs.

The cloud was formed by introducing steam from a boiler through a hole in the floor of the lower chamber. The droplet cloud in the upper chamber was produced by an ultrasonic nebuliser situated on a shelf outside the cold-room. The power to the kettle could be controlled from outside the cold-room, thus enabling control of the liquid water content of the cloud which was measured with the hot-wire device described in Section 3. The accuracy of this device was approximately 0.02 g m^{-3} and was insensitive to the presence of ice crystals. As noted by Mossop

Figure 1

The cloud chamber and the
position of the
thermocouples

- A : Access port
- B : Cooling fans
- C : Cloud chamber; Ca - upper chamber
Cb - lower chamber
- D : Steam inlet - upper chamber
- E : Nebuliser inlet
- F : Trapdoor
- G : Levitation inlet
- H : Access Port
- I : Window
- J : Cloud sampling tube
- K : Steam inlet - lower chamber
- L : Cold room door
- M : Motor
- N : Cloud chamber door
- T : Thermocouple



(1984) the drop size distribution could be modified by changing the size of the water vapor inlet nozzle. The nozzle diameter used here was 25 mm; at a liquid water content of 1 g m^{-3} the drop size distribution had a maximum size of $33 \text{ }\mu\text{m}$ and a modal diameter of $12 \text{ }\mu\text{m}$. When the cloud liquid water content was about 2 g m^{-3} there was a vertical temperature gradient of 1°C m^{-1} in the lower chamber.

The ice crystals were produced by seeding the cloud with a wire which had been dipped in liquid nitrogen. The wire was introduced quickly into the cloud chamber, which nucleated the cloud and, as the environment was supersaturated with respect to ice, the ice crystals grew at the expense of the water droplets and could be seen as 'dust' in a light beam. The maximum crystal size which could be produced in this was about $130 \text{ }\mu\text{m}$. Larger ice crystals, $>600 \text{ }\mu\text{m}$, were produced using a slightly different method. The droplet cloud was formed in both chambers; in the upper by the nebuliser and in the lower by the steam generator. As the nebuliser produced droplets by ultrasonic vibration and not boiling, a cloud was formed in the upper chamber without any subsequent rise in the environment temperature which lead to the upper chamber being about 2°C colder than the lower. The upper cloud was seeded using the method described above, and a suction pump connected via a tube to the top of the chamber provided an updraft which countered the terminal fall velocity of the growing crystals. The droplet supply was maintained and the crystals grew to about $150\text{--}200 \text{ }\mu\text{m}$ in diameter. After about two minutes, the suction pump was switched off and the trapdoor connecting the two chambers was opened. The crystals fell through into the supersaturated environment of the lower chamber and continued to grow. About 30 seconds later, the

crystals, now approximately 300 μm in diameter, appeared in a light beam at the floor of the lower chamber. The crystals were slowly lost to the walls and floor of the chamber, and lasted only for a further two minutes. At this time the crystal size reached about 600 μm . The final size and number concentration of the ice crystals was controlled by the number produced in the upper chamber. An initial high concentration led to a high concentration of smaller crystals. Conversely, a low number led to a low number of larger crystals; the largest diameter obtained was over 700 μm .

The nature of the cloud particles in the experiments was determined by the continuous formvar replicator which is described in Appendix I. The cloud particles are drawn past a film covered with 2% formvar in chloroform, the particles stick, and the solution dries to leave a plastic replica of the particle. The replicator had collection efficiencies of unity for droplets and ice crystals greater in diameter than 10 and 20 microns respectively. The film was marked with water resistant ink to provide time marks throughout the cloud development. The replicator could not collect ice crystals greater than 150 μm in diameter at the flow speeds used. As the crystals fell near the replicator orifice they experienced a horizontal force due to the air being drawn into the orifice. However, due to the inertia and drag of the large crystals, they were only displaced slightly towards the orifice in the time taken to fall through the flow. Hallett collected 1mm diameter ice crystals with such a replicator, but at aircraft velocities. These speeds are not practicable in the laboratory, as the film becomes clogged with water droplets. In order to collect the large crystals, a special method was developed following the work of Schaefer (1962), van

den Hage (1969) and Saunders and Wahab (1973). The cloud particles were collected on specially prepared microscope slides, which were exposed to the cloud for a known time. The slides were prepared in the laboratory using the following method. A 4% solution of formvar in chloroform was made in the usual way. The slides were then dipped into the formvar, the excess solution was drained off and the slides were placed in a desiccator and allowed to dry. The desiccator prevents contamination of the slides by water droplets condensing on the formvar by evaporative cooling. When the slides were required, they were placed in another desiccator in the cold-room and cooled to the ambient temperature. A tube of diameter 5 cm, which is connected to a vacuum pump, protrudes into the cloud-chamber at the same at the same height as the targets. When the pump is switched on, the cold dry slide is inserted into the tube perpendicular to the flow and is exposed to the flow for five seconds and then removed from the tube. The slide is then sprayed with a fine mist of chloroform from an atomiser (kept at the ambient cold-room temperature) to activate the dry formvar and then replaced in the cold-room desiccator to dry. The slide could be removed from the cold-room for analysis under a microscope after about three minutes. Crystals $>800\text{ }\mu\text{m}$ have been successfully replicated with these slides. Previous methods have required that the formvar solution is kept at about -5°C , which means that the bulk solution is very susceptible to corruption by water vapour. If this occurs, the formvar solution is useless, as hair-like growth occurs on the crystals as the water vapor in the solution diffuses to the crystal and freezes. The method described above ensures that no water vapor enters the solution, and thus clean formvar slides with clear ice crystal replicas can be produced

every time. The ice crystal and droplet concentrations were calculated using the equations described in Appendix I.

The charge transfer experiments were performed by moving targets of length 14 cm through a mixed cloud of water droplets and ice crystals. In the large ice crystal experiments the target diameters were 5 mm and 0.5 mm. The targets were mounted vertically on a frame attached to a central shaft as shown in Figure 2. The shaft could be rotated so that the targets moved with their axes normal to the direction of motion and riming occurred on the leading edge of the targets. The rod speeds used were in the range $2\text{--}4\text{ m s}^{-1}$ but some experiments were performed at a speed of 10 m s^{-1} . Shielding cups, 6 cm high, were placed at both ends of the target to prevent a rime bridge from forming and linking the targets to earth. The shielding cups, Figure 2, were grounded to remove any charges acquired during an experimental run.

The targets were connected to earth via a sensitive charge amplifier. The circuit is shown in Figure 3. The amplifier power and output leads were taken out through slip rings positioned at the bottom of the shaft under the cloud chamber. The 555 timer converts the positive supply voltage to a negative supply voltage which is regulated by the 79105 voltage regulator. The charge amplifier is a CA3140S chip which will operate down to temperatures of -55°C . Both positive and negative supply rails are required so that the amplifier can respond to an input current of either polarity. The background noise level of the charge amplifiers was about 1 mV so the charge acquired by the target was measurable if the charging rate was greater than 0.1 pC s^{-1} . The supply voltage was fused at 5 volts. The amplifier has a sensitivity of $1\text{ mV} \equiv 10^{-13}\text{ A}$; charge flowed to earth with

Figure 2

The experimental apparatus

- A : Main shaft
- B : Support arms
- C : Fixing nut
- D : Shielding cup
- E : Access hole to locking nut
- F : Thin wire
- G : Charge amplifier
- H : Simulated hailstone target
- I : Bearing
- J : Base plate
- K : Slip rings
- L : Drive wheel
- M : Drive belt
- N : Shielding plate
- O : Main drive wheel
- P : Motor
- Q : Motor housing

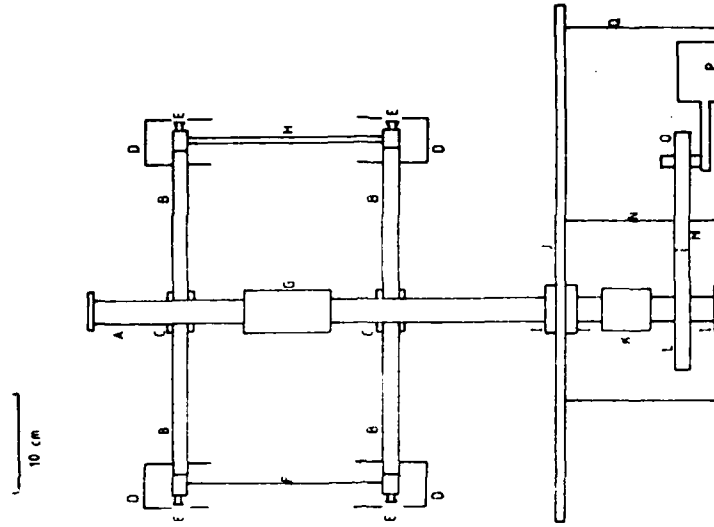


Figure 3

The charge amplifier

R1 : 3.3 k

R2 : 10 k

R3 : 100 M

R4 : 82 k

R5 : 020

Cl : 10 nF

C2 : 1 up

C3 : 100 uF

C4 : 10 nP

C5 : 10 nF

C6 : 2.2 uF

10.0 : 1.3

CS : 2.2

63 : 100 hr

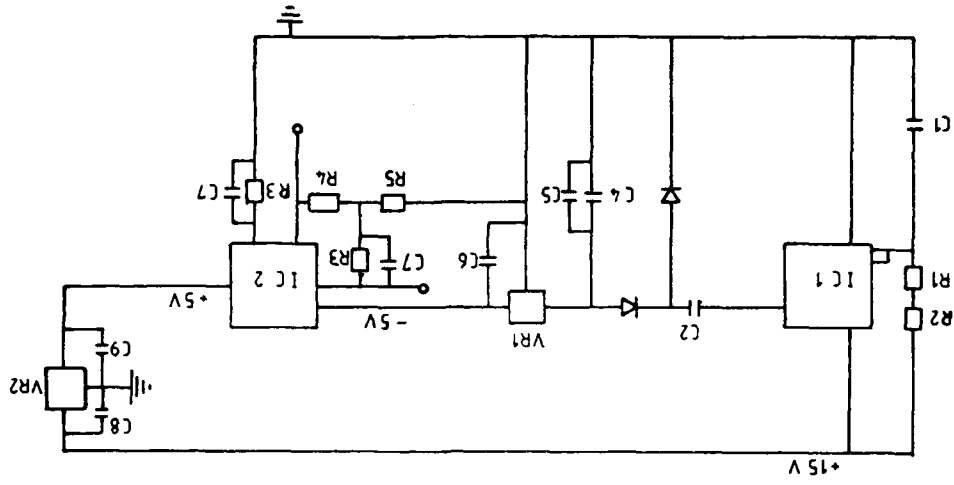
DI : IN4148

VR1 : 78L05

VR2 : 79L05

IC1 : 555 timer

IC2 : CA3140S



a time constant of 1 second. Chart recorders were used to record the charging currents from the two targets. In addition, the rotating frame carried two other probes for measuring the liquid water content of the cloud and the rime accretion rate of a 5 mm target.

The rime accretion rate, RAR, is the amount of rime collected by the target per unit time per unit area, Jarayatne and Saunders (1985), and was found to be an important parameter in controlling the charge transfer. As the droplets freeze, the rime surface is warmed due to the release of latent heat. This rise in temperature above ambient was measured with an accuracy of 0.13°C by a platinum resistance temperature sensor of diameter 5 mm which thus experienced the same liquid water content as the 5 mm target. By using the equations of Ludlam (1951) and Macklin and Payne (1967, which are described in Appendix II, the effective liquid water content, E_w , which is made up from the cloud droplets large enough to hit the target, may be calculated from the temperature elevation of the rime. Hence the rime accretion rate can be determined. There is no error in the measurement introduced by the presence of ice crystals in the cloud, as they do not release latent heat on striking the target. The rotating frame also carried a heated wire which was used to measure the total liquid water content of the cloud.

In conjunction with the rotating targets, there was also a stationary target connected to a charge amplifier. The target, of length 2 cm, was situated inside a tube of diameter 2 cm which protruded a short distance into the cloud chamber. A regenerative pump drew the cloud past the target at speeds of up to 110 m s^{-1} , which is typical of some aircraft speeds. Three separate sets of experiments were performed with a clean metal target, a

rimed target and a riming target.

Thus during each experimental run the charging current to two targets, the rime accretion rate and the liquid water content of the cloud could be measured simultaneously.

SECTION 3

A NEW HOT-WIRE FOR MEASURING CLOUD LIQUID WATER CONTENT

Introduction

The measurement of wind velocity by monitoring the power dissipation in a hot-wire was first suggested by Kennelly (1909) and tested experimentally by Morris (1912). King (1914) detailed extensively the convection of heat from small cylinders in a fluid flow, using Boussinesq's (1905) equation for heat loss to a stream of fluid. He suggested that there were applications for 'hot-wire anemometry'.

Merceret and Schricker (1975), from the work of Wynngaard and Lumley (1967), adapted a hot-wire anemometer for measuring the liquid water content, l.w.c, of a cloud. They found that the constant temperature hot-wire nimbiometer was far superior to the constant current hot-wire devices such as the Johnson-Williams instruments. The J-W instruments will only respond accurately to droplets $< 30 \mu\text{m}$ and have a high power consumption, difficult calibration and a time constant longer than one second. Merceret and Schricker found a relationship between the power used and the mass of water intercepted by the wire with time. With their analysis they did not need to supply heat of vaporisation as the droplets were not evaporated due to their low operating temperature. They calculated the proportion of wire that is wet at any instant in time, and so only needed to 'cut' the droplets rather than evaporate them, and hence there will be little spectral filtering over a wide range of droplet sizes.

King, Parkin and Handsworth (1978) also preferred the constant temperature device for use on an aircraft. They used a coil of 1.7 mm diameter and length 34 mm. They found that slave

coils on either end were necessary to maintain a fairly constant temperature along the master coil. The slave coils are 17 mm in length and 1.7 mm in diameter and do not form part of the sensing probe. They used a simple control circuit to maintain a constant temperature. An analysis of a similar control circuit was presented by Freymuth (1977). Various operating temperatures for the wire were tried, ranging from 76°C to 178°C in both wind tunnel and cold-room. An operating temperature in the region of 80-90°C was recommended for two reasons:

- (a) At some altitudes the boiling point of water can be as low as 90°C.
- (b) If the temperature is in excess of 100°C then evaporation can take longer due to the formation of an insulating layer between the droplets and the wire.

Later, however, King et al. (1981) state that the wire temperature can be as high as 160°C before any nucleate boiling of the drops is observed. This is due to a 30 μ thick covering of epoxy resin on the wire which has a surface temperature of 75°C for a wire temperature of 160°C. King et al. (1984) state that with an epoxy covered wire the wire had to be at least 60°C warmer than the unshielded wire in order to achieve the same response. They also state that the optimum operating temperature of the unshielded probe is about 180-200°C, and therefore the shielded version would operate at about 240°C, but this leads to failure of the device. At a temperature of 220°C the response of the shielded probe is about 0.9 that of the unshielded probe. Bradley and King (1980) and King et al. (1981, 1984) showed the frequency response of the electronic circuit and presented details of extensive wind tunnel and cold-room tests performed on

the probe.

The following sections outline the principles behind the operation of a hot-wire device and the calibration of such a device.

General Operating Principles of a Hot-Wire Device

If a hot object is placed in a colder fluid flow, then it will lose heat until it is in temperature equilibrium with the fluid. If, however, a current is supplied to the object, in this case a metal wire, then a constant temperature can be maintained and the power supplied gives an indication of the fluid velocity in the case of hot-wire anemometry, or cloud liquid water content, l.w.c., in the case of hot-wire nimbiometry.

King's law, after L V King (1914), states that for small cylinders the general heat transfer law is:

$$P = (A + BU^N) (T_w - T_a)$$

where: P is the rate of cooling of the object and has the dimensions of power, A, B, N are the 'King's law constants', U is the velocity of the fluid, T_w, T_a are the wire and air temperatures respectively.

King et al. (1978), however, state that the power necessary to maintain the probe wire at a particular temperature can be determined by the dimensions of the probe, and is given by:

$$P = ldvw[L + c(T_w - T_a)] + lk(T_w - T_a)Nu$$

where: l is the wire length, d is the wire diameter, v is the air velocity, w is the liquid water content, L, c are the latent and specific heat of water respectively, T_w, T_a are the wire and air temperatures respectively, k is the thermal conductivity of air, and Nu is the Nusselt number for the heat transferred from the wire. The first term is known as the 'wet' term, and is the heat

required to warm the supercooled water droplets from temperature T_A to T_W and then to evaporate them. The second or 'dry' term represents the heat transferred to the cooler air flowing over the wire.

There were two possible approaches to the problem of positioning the probes: (a) a rotating probe or (b) a stationary probe with the cloud being drawn past it. The nature and calibration of both probes and the electronic control circuitry are detailed in the following sections.

The Electronic Control Circuit

The novel control circuit, shown in Figure 4, uses a switching signal to regulate the operating temperature, whereas other workers have used a linear circuit to perform this function. The wire is heated by applying to it a chain of fixed voltage pulses whose mark-space ratio is varied to control the mean electrical power dissipation in the wire. As the loading on the wire increases due to an increase in cloud liquid water content, or a decrease in air temperature, the mark-space ratio increases.

The 555 timer, IC1, is running as an astable multivibrator which produces a square wave output with a high time of 0.7 ms. The 4027, IC2, is a J-K Flip-Flop which changes from a low state output of 0 V to a high state output of 12 V on pin 2. When pin 4 is high, pin 2 is high, and vice-versa. The 4027 triggers the transistor which in turn applies the rail voltage of 12 V across the bridge formed by R_7 , R_9 , R_{10} and the wire (R_8). The wire is heated until the bridge reaches a balance. The voltage comparator, IC3, monitors the voltage across the two arms of the bridge and, when balance is reached, it resets IC2 which turns TR1 off.

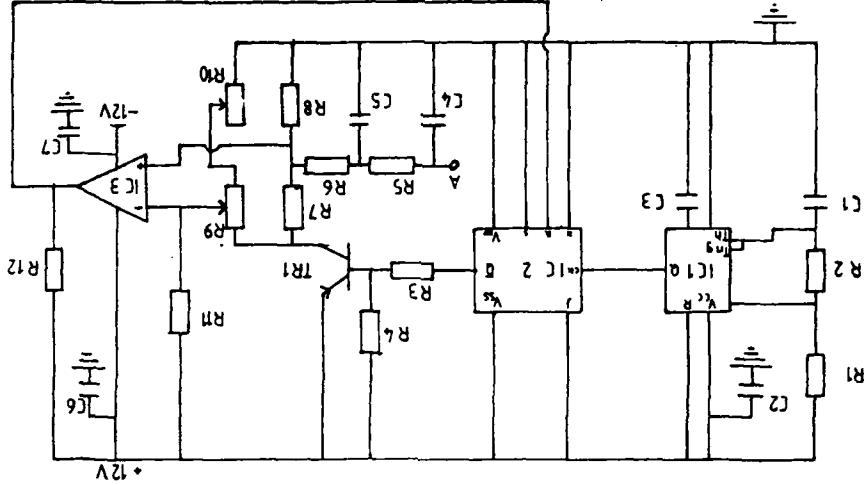
Figure 4

The electronic control circuit

- | | |
|---------------|---------|
| R1 : 10 K | |
| R2 : 100 K | |
| R3 : 4.7 K | |
| R4 : 10 K | |
| R5 : 1 K | |
| R6 : 1 K | |
| R7 : 5 | 25 Watt |
| R8 : Hot-Wire | |
| R9 : 10 k | pot |
| R10 : 1 k | pot |
| R11 : 22 k | |
| R12 : 10 k | |

All resistors 1/4 Watt, except as noted

- C1,C3 : 0.1 uF
C4,C5 : 0.1 uF, disc ceramic
C2,C6,C7 : 470 uF, 16V
- IC1 : 555 CMOS timer
IC2 : 4027 J-K Flip-Flop
IC3 : 311 Comparator
- TRI : TIP 146 pnp



This sequence occurs for every cycle of the 555 timer. The frequency is set sufficiently high so that the cycle time is short compared with the thermal response time of the wire. This short cycle time ensures that the fall in the wire temperature is small, compared to its operating temperature during the off time of the transistor.

The coupling capacitors across pins 1 and 8 (555), pins 1 and 8, and 1 and 4 (311) are simply to smooth out any irregularities in the power supply. When the circuit is initially switched on there needs to be an offset of a few millivolts on pin 3 of the 311 to send the 311 output high and subsequently turn the 4027 on.

The transistor TR1, TIP 146, is a pnp type transistor. A pnp is used in preference to a npn type due to the inverted signal from pin 2 of the 4027, and so when the 4027 switches off there is less heat dissipation in the transistor due to the reversal in base current when the 4027 switches off.

The voltage across R8 (wire) is a square wave signal; the 'on' time increasing as air or water droplets are blown across the wire. The actual output is at point A, after the filter circuit which effectively removes the square wave. There is a voltage noise on the signal of approximately 15 mV, which is primarily due to noise from the slip-rings.

To set the operating temperature of the wire, two potentiometers are used; the first to turn on the 4027 and heat the wire to almost the correct temperature, and the second, 1k, is used to set accurately the temperature due to its greater sensitivity. At the required operating temperature, the wire resistance is R_w . The voltage applied across the wire, V_w , during the on time of the transistor is:

$$V_w = R_w V_s / (R_w + R_7) \quad (1)$$

where V_s is the supply voltage

The power dissipated in the wire during this time is:

$$P_w = V_w^2 / R_w = R_w V_s^2 / (R_w + R_7)^2 \quad (2)$$

If the on time is of duration t_{on} and the total cycle is t , then

the average power, P_w , dissipated in the wire is:

$$\overline{P}_w = P_w t_{on} / t = R_w V_s^2 t_{on} / (R_w + R_7)^2 t \quad (3)$$

The mean voltage across the wire, \overline{V}_w , is:

$$\overline{V}_w = V_w t_{on} / t = R_w V_s t_{on} / (R_w + R_7) t \quad (4)$$

In practice \overline{V}_w is derived via a low pass filter at point A. Thus from equations 3 and 4

$$\overline{P}_w = V_s \overline{V}_w / (R_w + R_7) \quad (5)$$

Thus there is a linear relationship between V_w and the power dissipation. Therefore, the fractional changes in V_w are equal to the fractional changes in power dissipation, that is:

$$d\overline{V}_w / \overline{V}_w = d\overline{P}_w / \overline{P}_w \quad (6)$$

In the conventional circuits used by King and others, the power dissipation is given by:

$$P_w = V_w^2 / R_w \quad (7)$$

therefore:

$$dV_w / V_w = 0.5 dP_w / P_w \quad (8)$$

From equations 6 and 8 it can be seen that the pulse width modulated control provides an output which has twice the sensitivity to power dissipation changes of a conventional circuit. Also, there is a reduction of dissipation in the controlling transistor which leads to reduced overall power and instrument weight. As indicated by King, conventional circuits require adjustment of the frequency compensation to optimise performance and avoid instability. This is not required with pulse width modulated control.

In order to maintain a constant temperature across the probe, King et al.(1978) had to use slave coils on both ends of the probe. The coils were not part of the sensing circuit. However, in this case, the wire is of a very small diameter and of relatively short length, and so the temperature gradient losses that King encountered can be ignored.

Calibration and Results

The probe was operated at a wire temperature of 76°C. The reason being that at higher wire temperatures there occurs film boiling at the surface of the wire causing an insulating layer of vapor between the droplet and the wire. The responses at 76°C and 98°C are $7.27 \text{ g m}^{-3} \text{ V}^{-1}$ and $9.33 \text{ g m}^{-3} \text{ V}^{-1}$ respectively, indicating that there is a better response at the lower operating temperature. At still lower temperatures, 56°C and 36°C, there was evidence of the wire becoming saturated with water droplets leading to a longer evaporation time. Located on the opposite arm to the probe was a collecting rod of length 100 mm and diameter 1.5875 mm. The LWC of a cloud was deduced from the weight of rime accreted on the rod after it had been rotated for a time (Macklin,1962). The LWC values achieved using this method were corrected for the collision efficiency of the rod. The droplet spectra (obtained with a Knollenberg optical probe) for two different clouds were used to average the collision efficiency (CE) of the rod over all droplet sizes by using the equation:

$$CE = (\sum N_d E_d) / N_{tot} \quad (9)$$

where N_{tot} is the total number of droplets/cm³, N_d is the number of droplets in size range Δd and E_d is the collision efficiency of the rod for droplets of diameter $d \text{ } \mu\text{m}$ (Ranz and Wong, 1952).

By using this analysis the mean efficiency of the rod, 57%,

agreed within 1% for the two different clouds. All of the clouds were produced by a nebuliser, and they had a broad spectrum of droplet sizes with a mean droplet diameter of 12 μm .

The initial tests were performed at a temperature of -9°C and then repeated at -3°C and 14°C . These results are shown in Figure 5, and it can be seen that the instrument gives a linear response dependent on the LWC of the cloud and its ambient air temperature. The lines have an equation:

$$\text{LWC} = 7.27V + 0.1575T. \quad (10)$$

As the lines are parallel, it is possible to use just one line and introduce a temperature factor such that

$$V_{\text{cal}} = \Delta V + 0.022\Delta T \quad (11)$$

where V_{cal} is the voltage on the calibration line, ΔV is the recorded output above 1.5V and ΔT is the temperature difference from -9°C . (Warmer than -9°C is positive and colder than -9°C is negative).

The calibration remained unchanged if a new wire of the same specification and length was used. The calibration could be checked very easily by rotating the probe in clean air at a known temperature while monitoring the output and comparing this with the original calibration.

Figure 6 shows the clear air output, V_a against the output V_c , obtained when the probe is rotated in a crystal cloud. It was important that the cloud consisted purely of ice crystals, as the presence of a few droplets, even 10 cm^{-3} , can give rise to considerable errors. This experiment was repeated at different air temperatures and with different sized crystals which were obtained by different methods of seeding a supercooled cloud by introducing into it a thin rod which had been dipped in liquid nitrogen. Small crystals were obtained by leaving the rod in the

Figure 5
The output vs temperature graphs
for three temperatures

- 1 -3°C
- 2 -9°C
- 3 -14°C

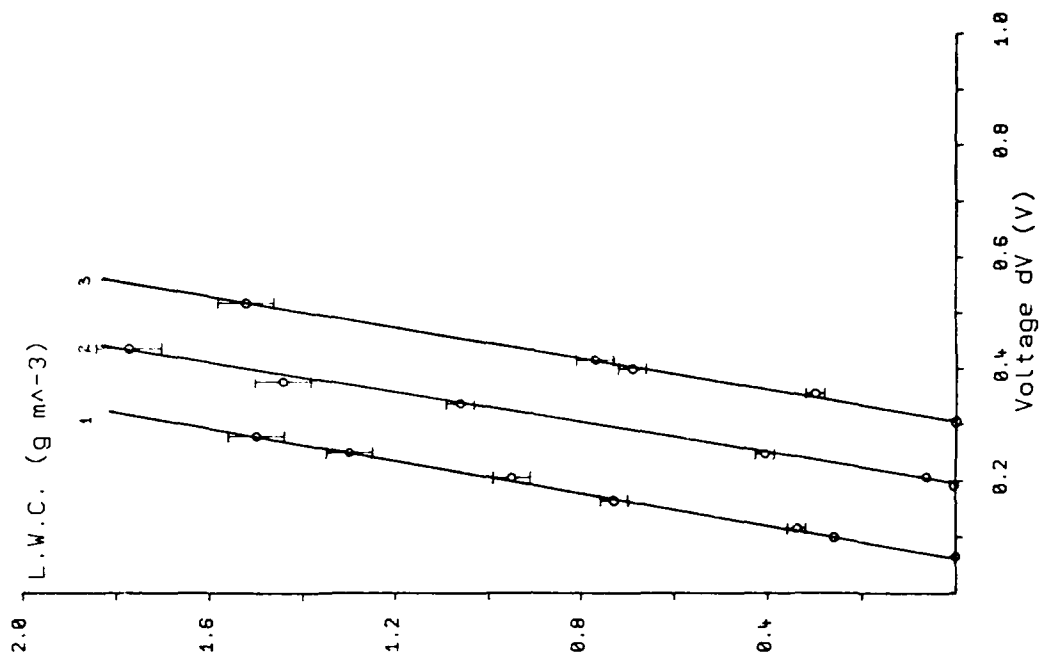
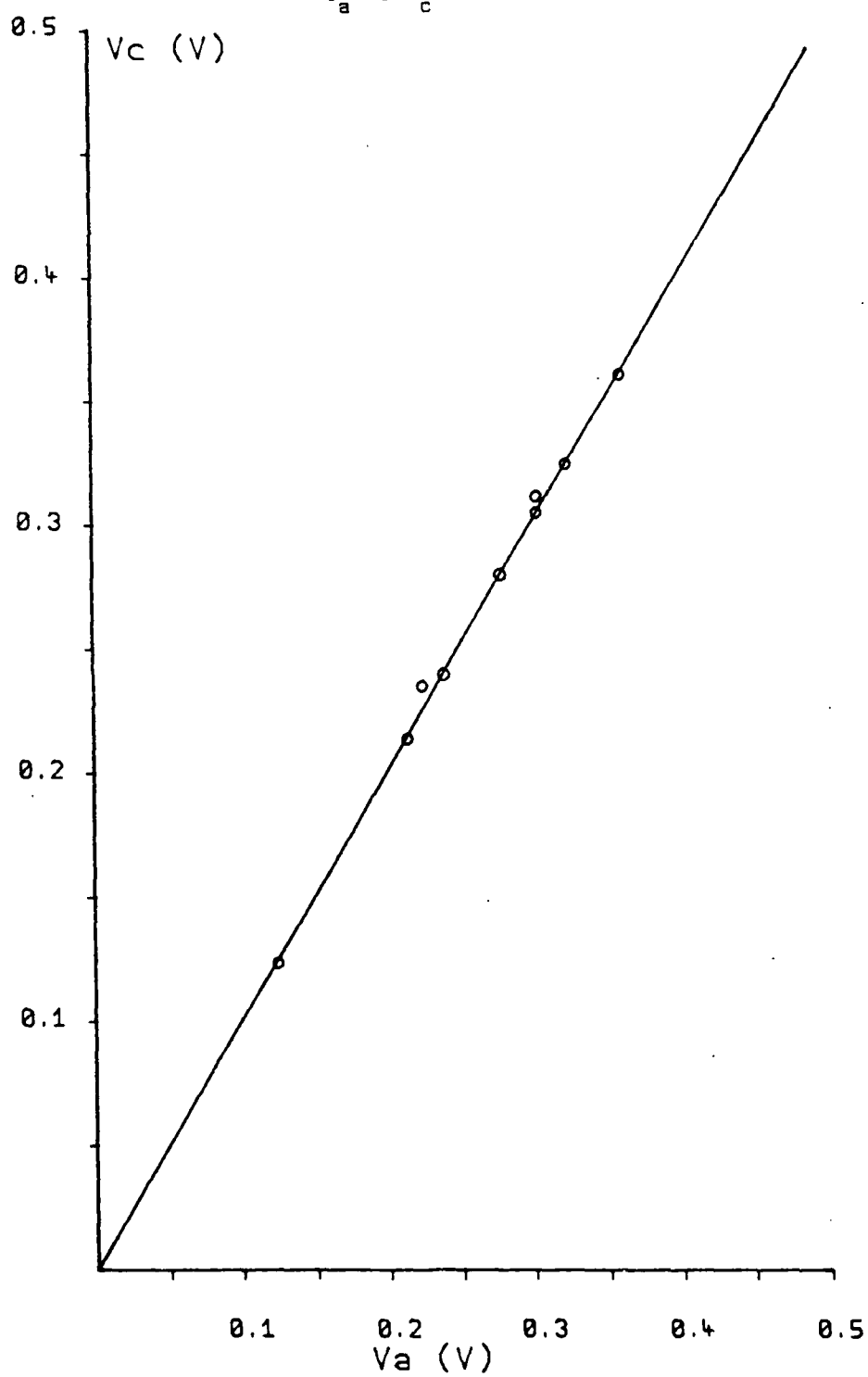


Figure 6

V_a vs V_c for the Rotating Probe



cloud for a relatively long time of around 4 s. In the majority of these experiments the cloud output, V_c , equalled the clear air output, V_a , giving a 1:1 correlation. In the worst case, there was an output of 5 mV above the value of V_a which corresponds to a LWC of 0.01 g m^{-3} which is well within the accuracy of the device. This means that in a mixed cloud of ice crystals and supercooled water droplets the crystals will be ignored and the recorded output will be a true measure of the LWC, with no error introduced by the presence of the crystals irrespective of the crystal diameter.

Conclusion

This hot-wire device is suitable for use in the laboratory, as it needs only a simple calibration and the data may be presented in the form of a voltage-time graph. The probe itself is robust, easy to construct and inexpensive. The total error was determined by taking the square root of the sum of the square of the individual errors. The source of these errors were: the mass of rime collected, the diameter and velocity of the collecting rod and the collection time. The most significant error was in the mass of accreted rime. The instrument has a response time of less than 0.5 s and is accurate to 4% at 1.0 g m^{-3} , 4.6% at 0.5 g m^{-3} and 13.2% at 0.06 g m^{-3} .

SECTION 4

THE COLLECTION EFFICIENCY OF A RIME COVERED TARGET

Introduction

It is the purpose of this part of the study to investigate whether soft-hailstones have an increased collection efficiency for water droplets due to the presence of rime feathers. The study also investigates the dependence of the collection efficiency on temperature and impact velocity.

The accretion of supercooled water droplets upon cloud particles is known as riming, and is the dominant growth process for large hydrometeors. It is important to know the values of the collection efficiency of growing soft-hailstones for supercooled water droplets through which they fall, because the charge transfer due to ice crystal collisions appears to be affected by the presence of liquid water on the riming target.

Ranz and Wong (1952) modelled theoretically the collision efficiency of a smooth cylindrical target for smoke particles of a known diameter. Many workers, including Jayaratne et al. (1983), have used their results to determine the growth rate of a soft-hailstone when it moves through a cloud of supercooled water droplets of known drop size distribution and number concentration. The collision efficiency is assumed to be the same as the collection efficiency for this case, because the droplets freeze and stick on impact with the collector. Jayaratne et al. simulated thunderstorm conditions in the laboratory, and drew ice crystals and supercooled droplets past a rimed target which represented a soft-hailstone of 5mm diameter falling at 3 m s^{-1} , for this case, according to Ranz and Wong, the target does not collect any droplets small than $6 \mu\text{m}$ diameter.

The liquid water content, w , of a supercooled cloud can be measured from the amount of rime which is accreted on a moving target in a given time, as shown by Brun et al. (1955), Rogers et al. (1983), Saunders et al. (1984), and in this report. The method is only possible if the drop size distribution of the cloud and, also, the collection efficiency of the target for the droplets is known accurately. The density of rime grown in this way was investigated by Macklin (1962), and Saunders and Zhang (1987). In both cases, the targets were exposed to a stream of water droplets which froze on impact and formed the rime. From the geometrical dimensions and weight, the rime density was calculated. This method provided a measure of the effective liquid water content in the cloud, Ew , where E is the collection efficiency. Measurements of the density of rime are only concerned with the amount of water that collides with the target, and so this method removes the need to calculate E accurately. The results of Saunders and Zhang compared favorably with those of Macklin. At low impact speeds and temperatures, the growth of rime 'feathers' is enhanced. The term 'feathers' was used by Macklin to describe the rime appearance following the freezing of individual droplets on top of one another, so that the rime deposit grew out from the ice surface. Under these conditions, a riming target will not be of uniform cross section, and the collision efficiency theory of Ranz and Wong may not be strictly applicable.

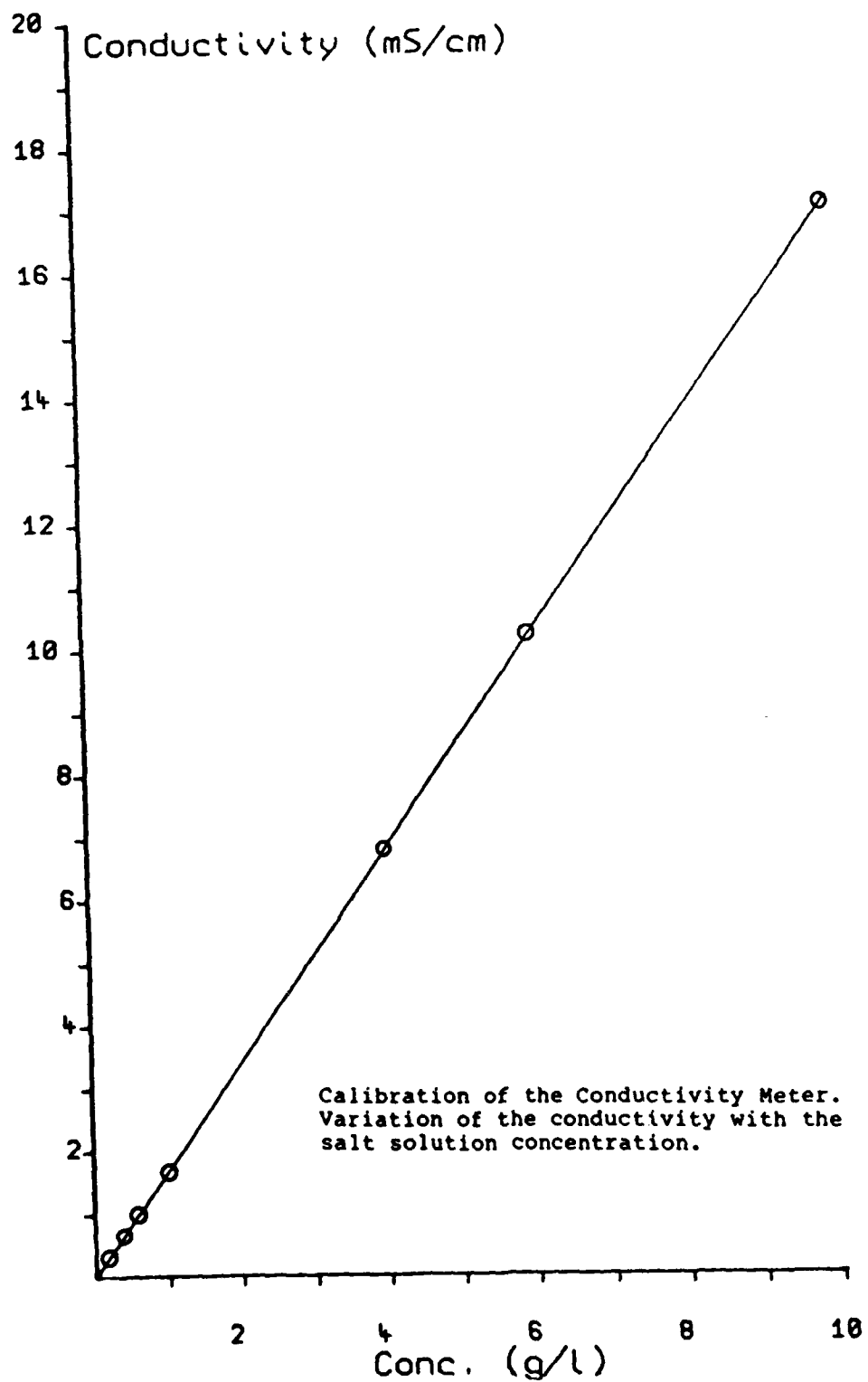
Experimental Method

The experiments were performed in a transparent chamber situated within the large cold-room. The aim of the experiments was to determine whether small droplets are collected by rime feathers.

In order to achieve this, the droplets were formed from a strong salt solution and then drawn past a previously rimed target of length 53mm. The target diameter was 5mm, which is the same size as that used in the charging experiments. A plastic target was used in preference to a metal one, because rime scraped from a metal target contained tiny metal shavings which subsequently contaminated the rime solution. The target material did not affect the nature of the riming.

The presence of the salt droplets in the rime was detected by a Kent conductivity meter. If the droplets hit the rime feathers, then the pre-existing pure rime became contaminated with the salt solution. As contamination increased due to increasing exposure to the salt droplet cloud or increasing collection efficiency with feather development, the rime conductivity also increased. The conductivity meter was first calibrated with known concentrations of NaCl solution. The results, presented in Figure 7, show that the meter has a linear response with increasing salt solution concentration. This linearity continues up to 100 g l^{-1} , at which point the solution starts to become supersaturated with salt. The response of the instrument was $0.05 \mu\text{S cm}^{-1}$, which corresponds to a change of $0.006 \mu\text{l}$ in the amount collected. The salt solutions were made up with NaCl and deionised distilled water, so as to minimise the effect of any impurities, and to ensure that the solutions were of a consistent conductivity. New standard salt solutions were used every day because the concentration of the solution increased due to evaporation of the water. The concentration used was 10 g l^{-1} ; a concentration of 1 g l^{-1} was tried but the contamination of the rime was below the threshold of detectability of the conductivity meter. The meter was checked periodical-

Figure 7



ly; however, there was no change in the calibration.

The pure water droplet cloud was produced using the method of Jayaratne et al., Mossop (1984), and others. A boiler introduced water vapor into the cloud chamber at a constant rate to produce droplets which subsequently cooled to the ambient temperature. The cloud had a modal drop size of $12\text{ }\mu\text{m}$ and the liquid water content was typically between $1\text{--}2\text{ g m}^{-3}$. The experiments were performed at temperatures in the range -5 to -20°C with impact speeds of 3 and 5 m s^{-1} . The cloud was drawn past the target at a constant rate for 5 minutes, which was found to be sufficient time for the rime feathers to grow. The rimed target was then exposed to the salt droplet cloud produced by a small Unicorn nebuliser. This cloud was drawn past the target for 5 minutes, at the same velocity as that used in the pure riming part of the experiment. All the contaminated rime was then removed from the target and diluted with 20 ml of deionised distilled water.

The drop size distribution of the salt cloud was analysed by a Knollenberg Forward Scattering Spectrometer Probe (FSSP). The modal diameter was about $10\text{ }\mu\text{m}$, and a typical drop size distribution is shown in Figure 8. As can be seen, there were some droplets larger than $20\text{ }\mu\text{m}$ which were not desirable but were unavoidable. The presence of these droplets was accounted for in the analysis of the data.

The theoretical collection efficiencies, shown in Figure 9, were calculated from the equations of Löffler and Muhr (1972), for a smooth collector of diameter 5 mm , cloud temperature of -10°C , with air velocities of 3 and 5 m s^{-1} . The Ranz and Wong efficiencies used by Jayaratne et al. over-estimated the collection efficiency for small droplets by about 10%, compared with

the Löffler and Muhr equations. The collection efficiency increases slightly with decreasing temperature, due to the lower viscosity of air at lower temperatures. For the 3 m s^{-1} air velocity, it can be seen that the collection efficiency for droplets of diameter between 5 and $8 \text{ }\mu\text{m}$ is less than 1.0%. These theoretical collection efficiencies are for smooth collectors, and do not take into account any turbulence due to the roughness of the surface.

The total volume of salt water droplets collected by the soft-hailstone target can be calculated from the following formula.

$$V_d = (X_L)(V_c + V_d + 20 \times 10^{-3}) / (X_N) \quad (1)$$

where X_N is the concentration of salt solution in the nebuliser, (g/l), X_L is the concentration of salt solution in the rime plus 20ml of water, (g/l); V_d is the total volume of salt solution droplets which collide with the target, (l); V_c is the volume of pure rime on the target, (l).

Now, $(V_c + V_d)$ is much less than 20ml, so from (1)

$$V_d = 20 \times 10^{-3} X_L / (X_N) \quad (2)$$

Thus from the salt concentration of the rime liquid and the initial salt solution, the volume of salt cloud which hits the rime target can be calculated. From the Löffler and Muhr formula and the measured droplet size distribution, the total volume of salt droplets that can collide with the target is V_D . So, if $V_d > V_D$ then the difference is made up from the extra droplets that collide which are not accounted for by the collection efficiency formula for smooth targets.

Figure 3

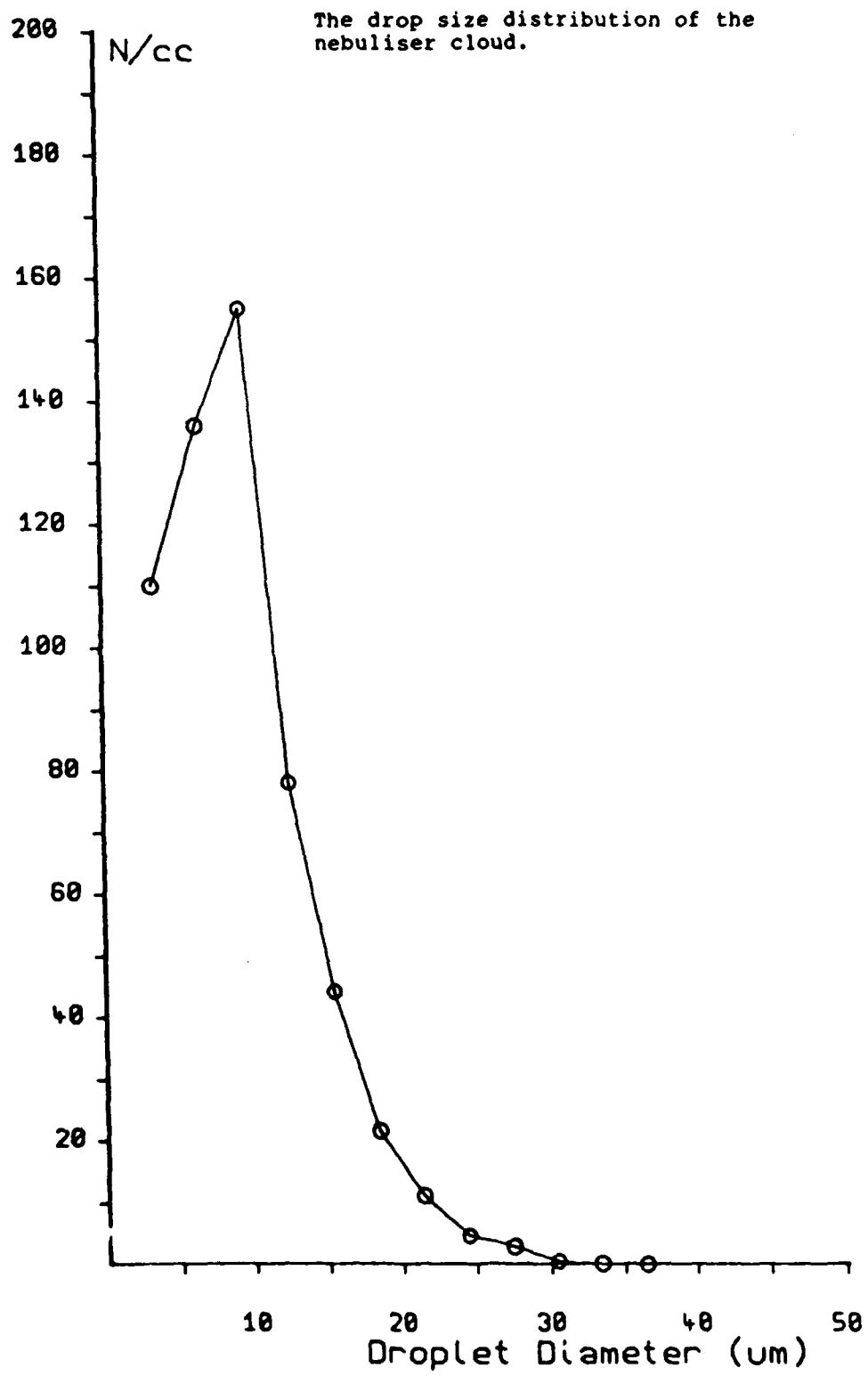
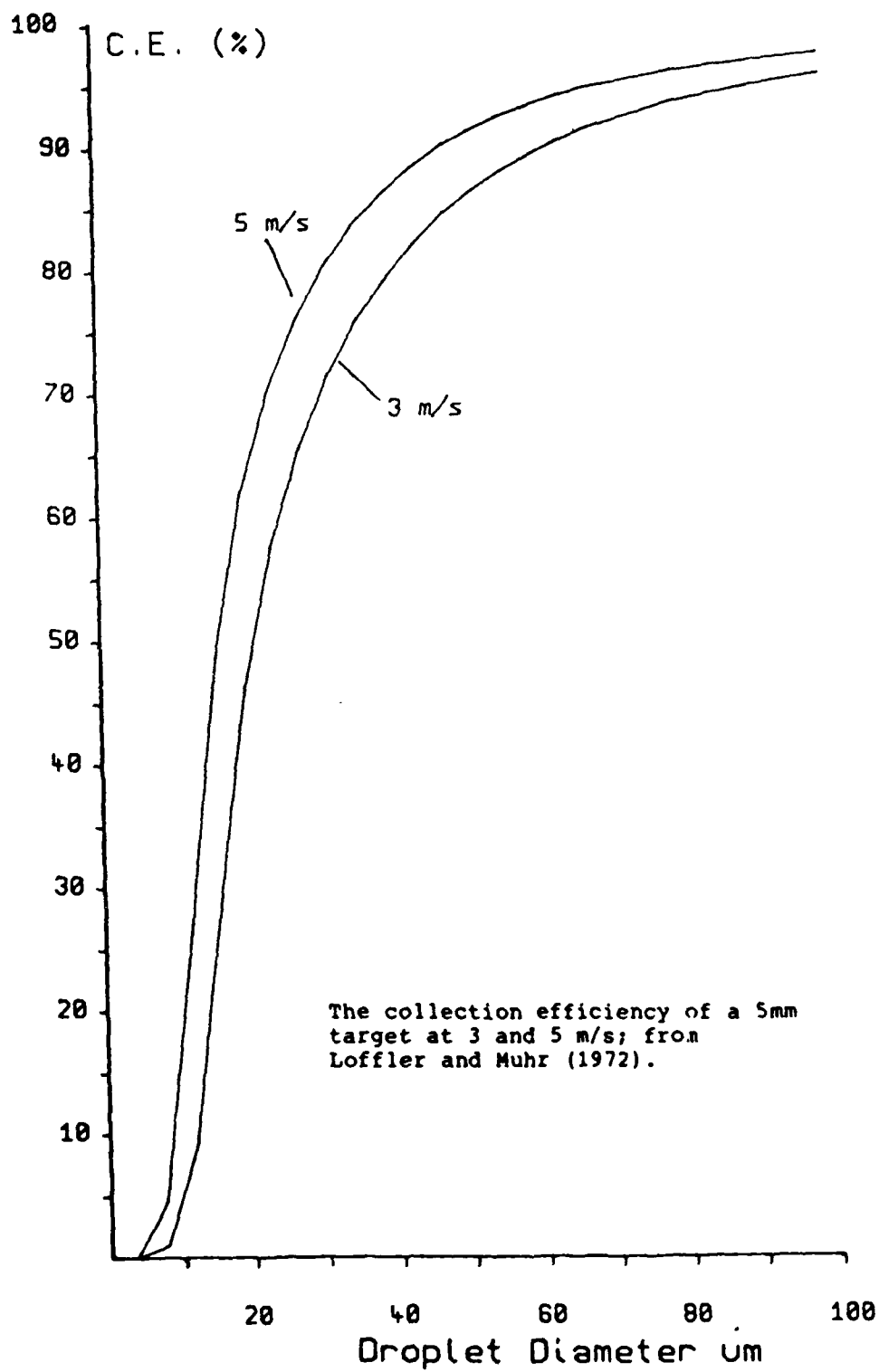


Figure 9



Results

The experiments were performed at different temperatures between -5 and -20°C at a constant air velocity of 3 m s^{-1} . The pure droplet cloud was drawn past the target for 5 minutes before being exposed to the salt droplets for 5 minutes. The validity of the equations described in the previous section was confirmed by varying the concentration, X_N , of the nebuliser solution. Figure 10 shows that the volume collected is approximately the same for all values of X_N . The only limits on the solution concentration were of detectability at low values and of supersaturation at high values.

Figure 11 shows the volume of salt droplets collected by the rime against cloud temperature. At -5°C the volume collected is around $28.9\text{ }\mu\text{l}$ increasing to $37.1\text{ }\mu\text{l}$ at a temperature of -20°C .

The time of exposure of the target to the pure droplet cloud was varied from 2 to 7 minutes at a temperature of -10°C . The subsequent increase in the collection efficiency of the target for the salt droplets is reflected in the volume of the salt droplets collected in 5 minutes, Figure 12. As the exposure time increased, the number and size of the rime feathers also increased for the first 6 minutes of collection. Beyond this time the collection efficiency remains approximately constant, indicating no further increase in feather concentration.

In further experiments, performed under the same conditions as above, the pure droplet cloud was drawn past the target at a velocity of 5 m s^{-1} for 5 minutes. The rime acquired the kernel appearance described by Macklin (1962) but the rime feathers were not as visible as in the above case. Figure 13 shows the salt droplet volume collected in 5 minutes against temperature. At

Figure 10

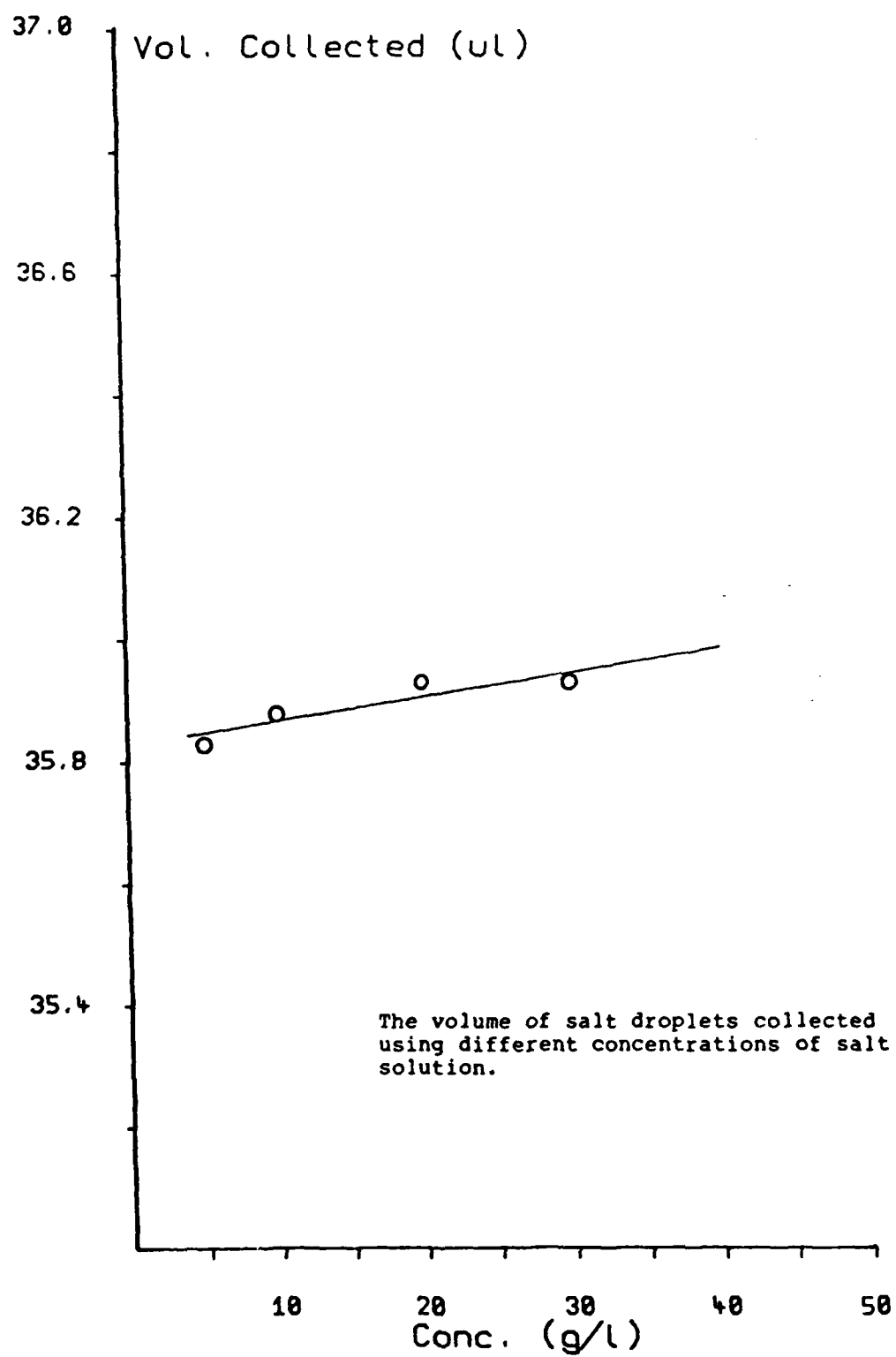


Figure 11

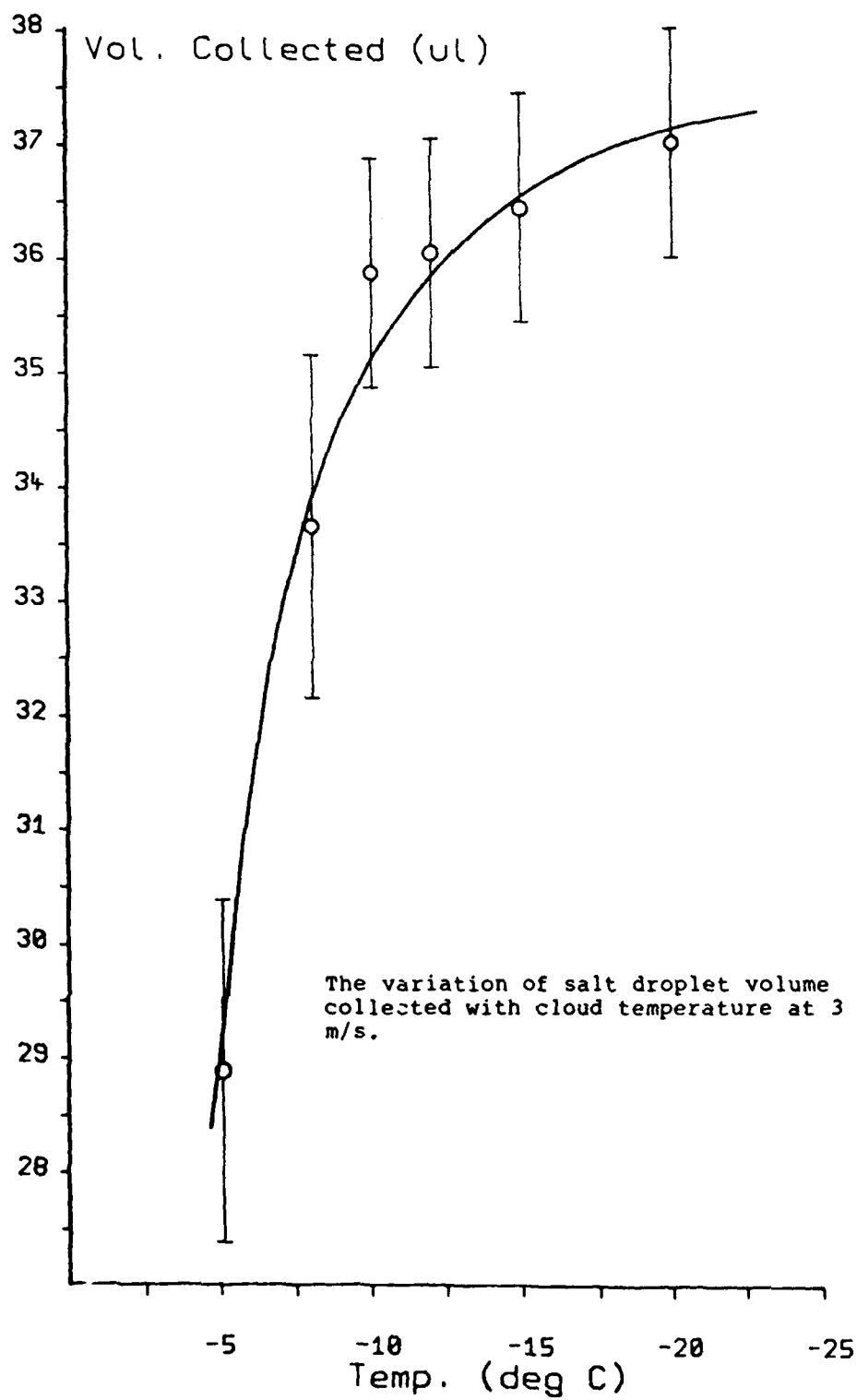


Figure 12

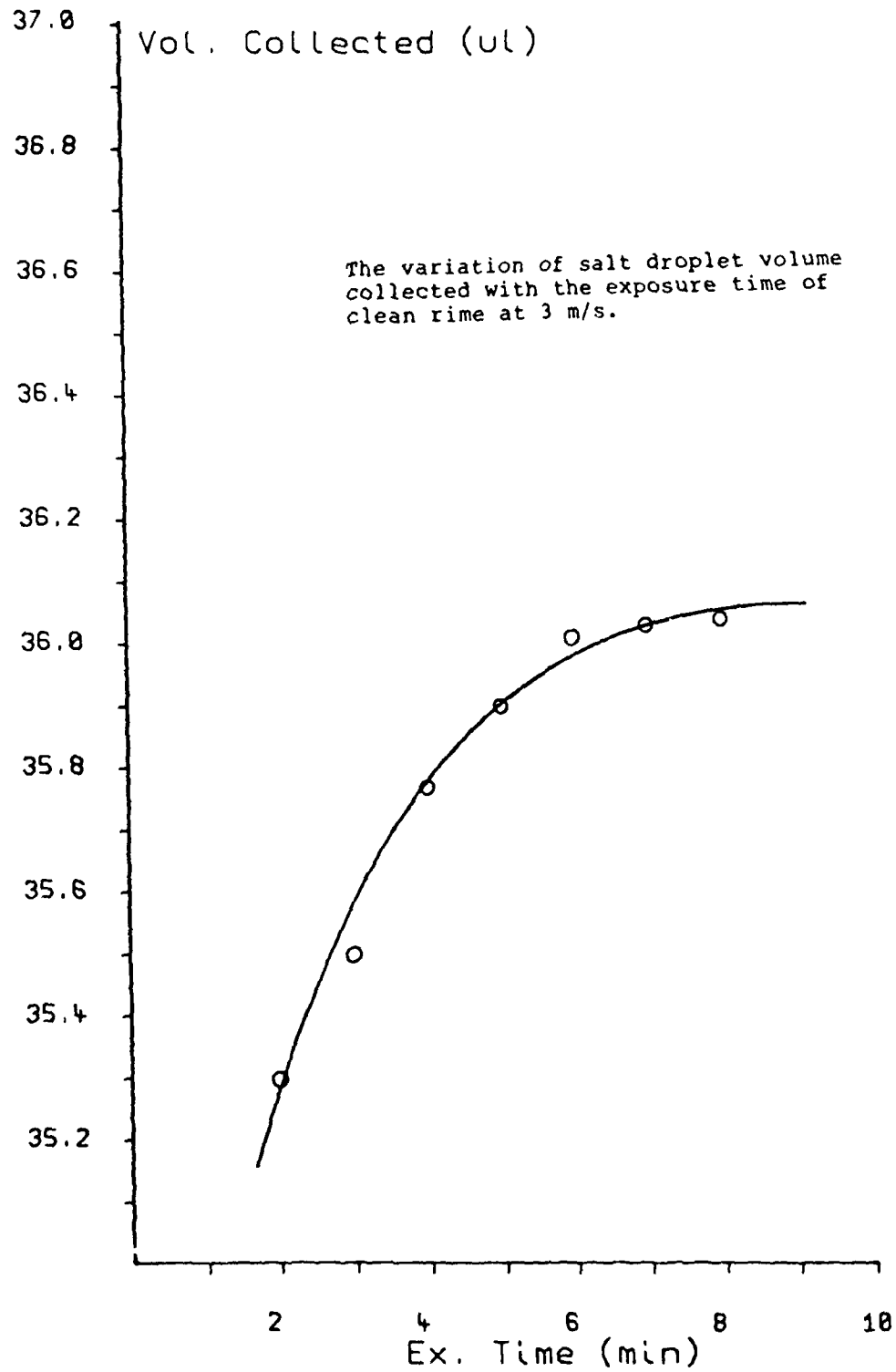
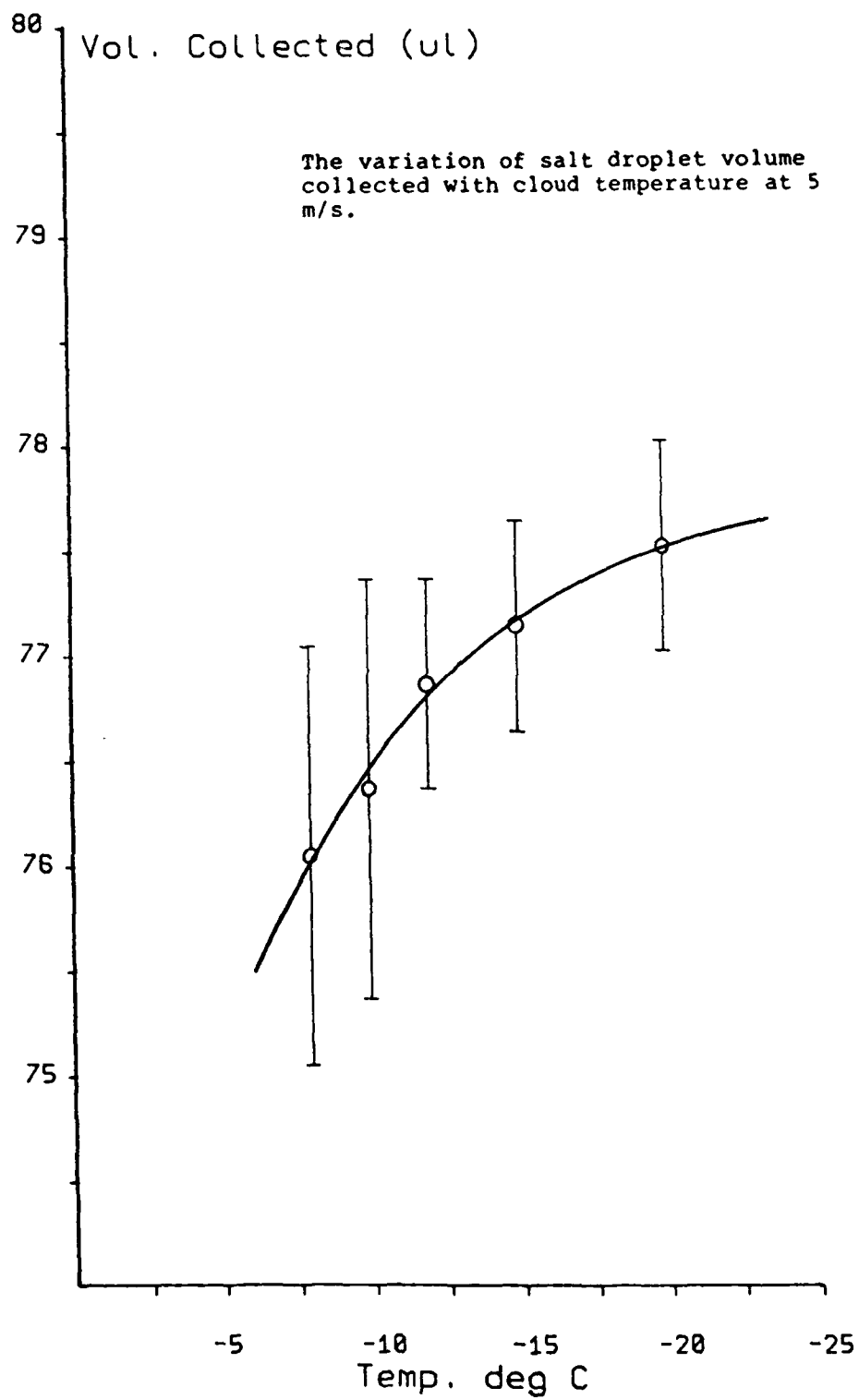


Figure 13



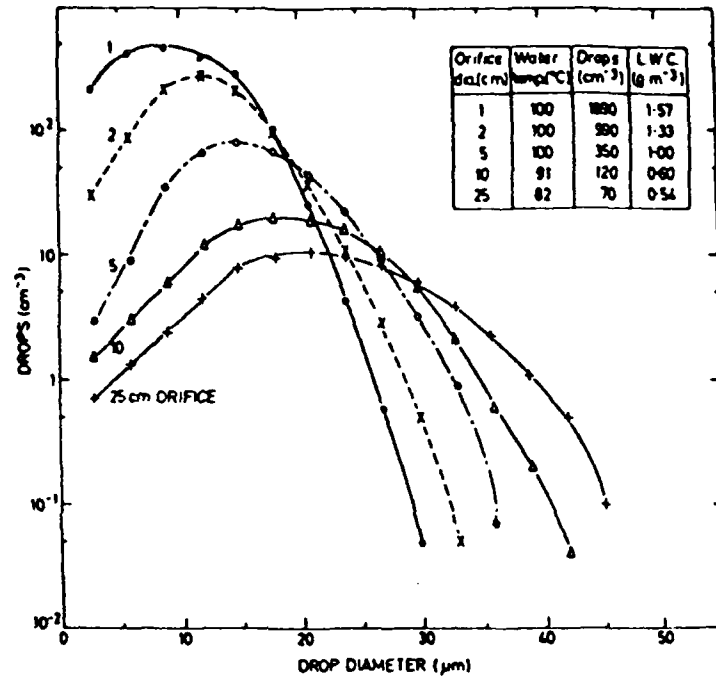
this higher impact velocity, the increase in the amount collected with decreasing temperature is less than at 3 m s^{-1} . The reasons for this will be discussed in the following section.

Discussion

It has been hypothesised by previous workers, Macklin (1962), and Dong and Hallett (1986), that as a hailstone grows due to the accretion of water droplets, the collection efficiency for those droplets increases due to the formation of rime feathers.

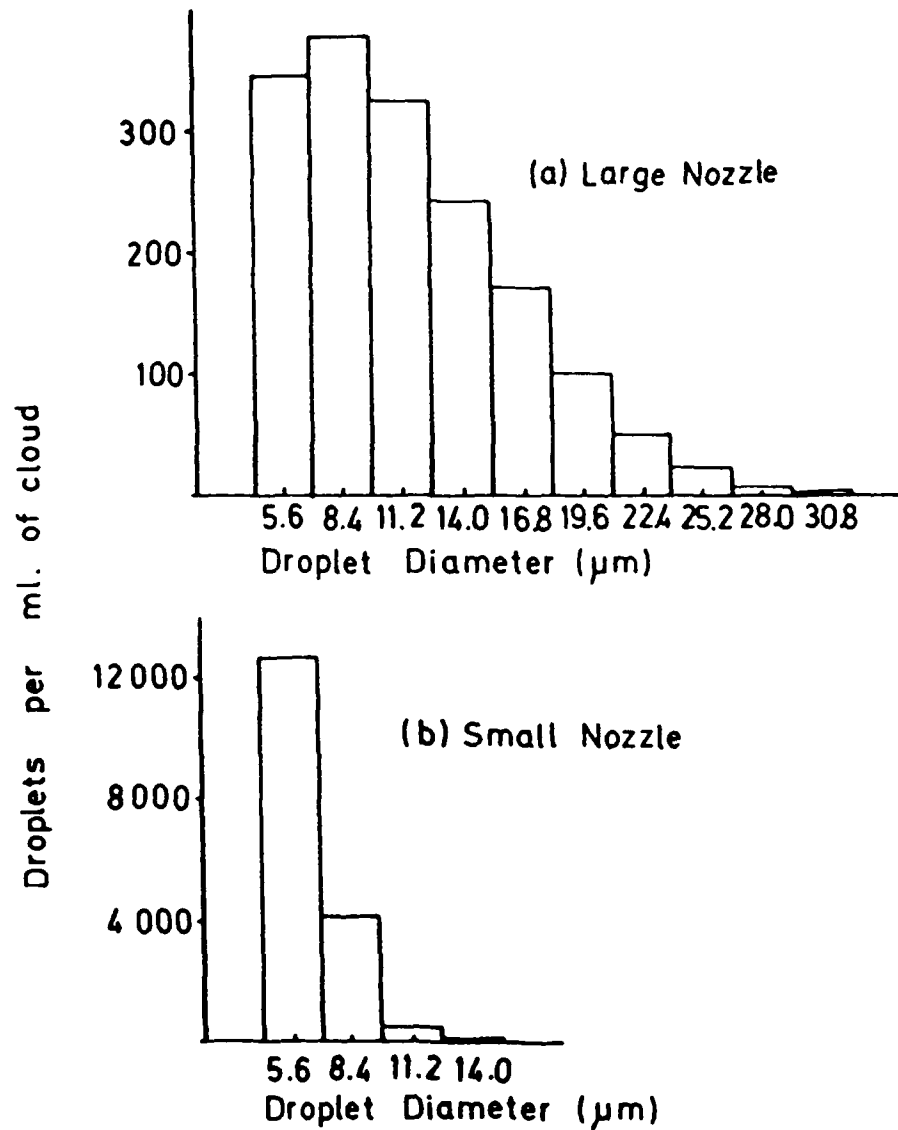
Mossop (1984) showed that in the production of laboratory clouds the drop size distribution is affected by the size of the water vapor inlet nozzle. It can be seen from Figure 14a that as the nozzle size decreases the drop size distribution shifts to a higher concentration of smaller droplets. This was confirmed by Jayaratne and Saunders (1985), Figure 14b, when they showed that the charging of a hailstone due to the collision and separation of ice crystals is dramatically affected by the drop size distribution present in the cloud. Figure 15a shows the charging which occurs with a large nozzle of diameter 32 mm at -10° , whereas Figure 15b shows the charging under similar conditions but with the small droplet cloud produced by the small nozzle of diameter 5 mm. In the second case, when negative charging occurs, the ice crystals have grown at the expense of the droplets which have a maximum size of $6\mu\text{m}$, and so are too small to strike the target according to the theory of Ranz and Wong. Jayaratne and Saunders (1985), and Baker et al. (1987), concluded from these experiments that it is the surface properties of the interactants which are important in controlling the sign of the charge transfer. Charging is positive if the hailstone is growing faster than the ice crystals, and negative if growing more slowly. The results

Figure 14a

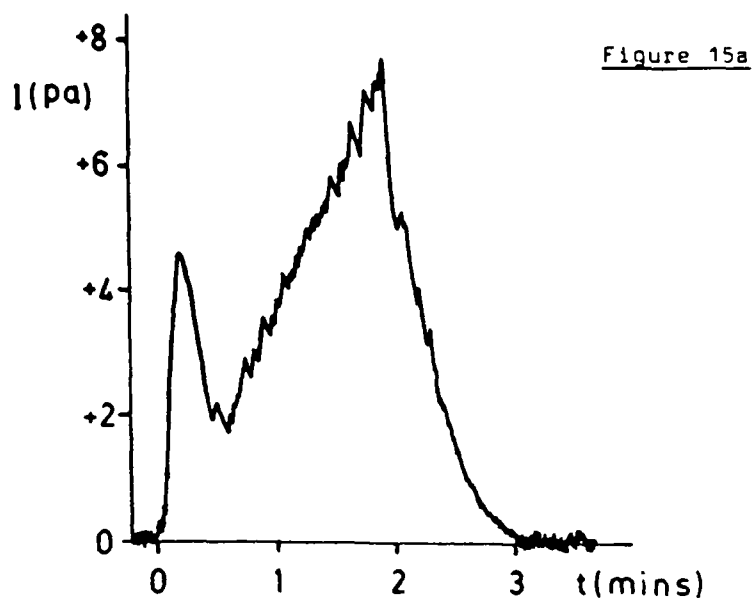


The effect of nozzle diameter on the cloud drop size distribution; from Mossop (1984).

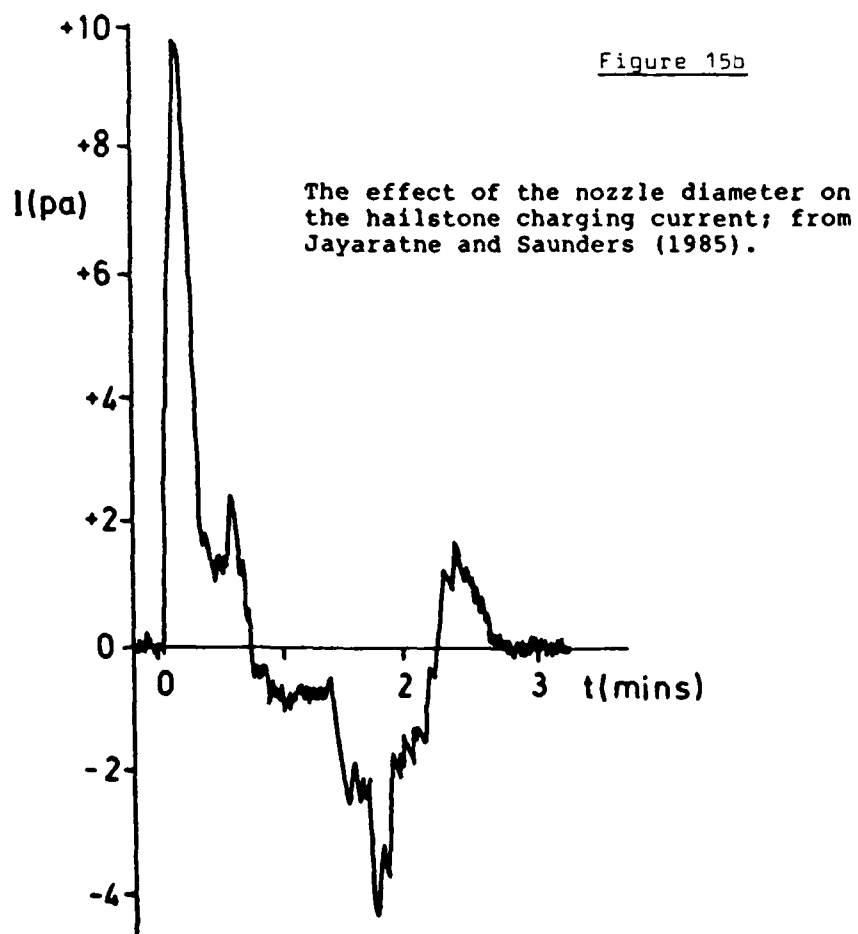
Figure 14b



The effect of nozzle diameter on the cloud drop size distribution; from Jayaratne and Saunders (1985).



(a) Large Nozzle



(b) Small Nozzle

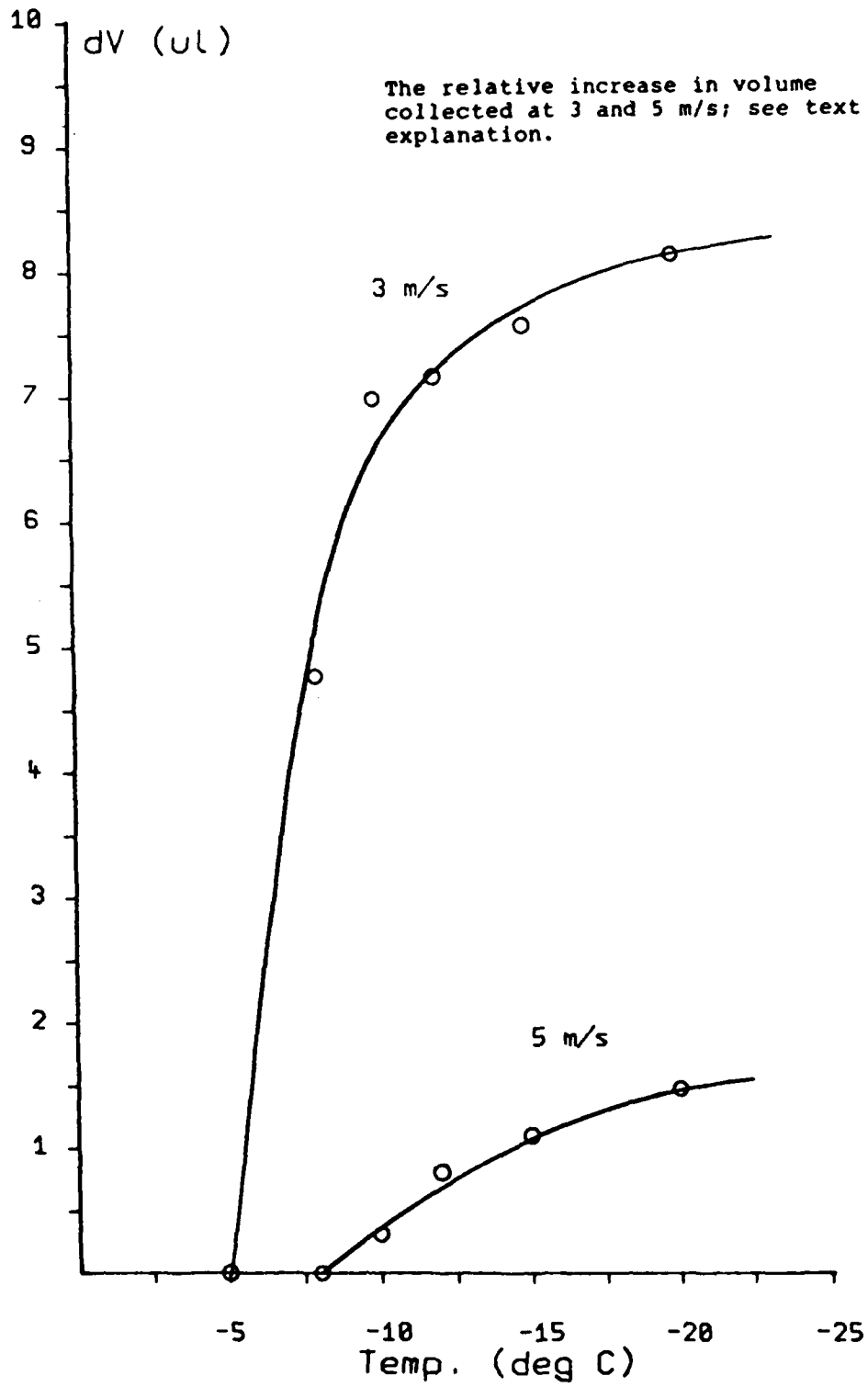
of the present study show that some riming due to the small droplets may occur due to the presence of rime feathers on the target, and this brings the charge sign hypothesis into question. It can be shown, however, by using the formulae of Baker et al., that the amount of water accreted by the hailstone is insufficient to increase the hailstone growth rate above that of the ice crystals, and so the sign of the charging is unaffected. A detailed account of the relative growth rates of the cloud particles is given in Appendix III.

The appearance of the rimed surface under varying conditions has been described in detail by Macklin (1962), Stallabrass (1978) and Lowaski (1983). At low temperatures and low impact velocities, the droplets freeze without significant flattening which enhances the growth of the rime feathers. At higher temperatures, the rime appears as smooth clear ice. As the droplets freeze they release latent heat of fusion which warms the rime surface above the ambient cloud temperature. Using the results of Ludlam (1951), it can be shown that if a cloud of temperature -5°C and liquid water content 1 g m^{-3} is drawn past a 5mm diameter target at 5 m s^{-1} then the surface temperature of the rime increases to -2.9°C . Under similar conditions, but with a cloud temperature of -8°C , the rime surface temperature will be -5.9°C . Thus, conditions of wet growth are not achieved in these experiments. However, the droplet freezing time is temperature dependent, with longer freezing times at higher temperatures giving time for the freezing droplets to flow over the surface, leading to a smooth ice surface. Löffler and Muhr assumed that the collector is smooth, and thus their theory and the present experimental results agree, with a near zero target collection efficiency at temperatures above -8°C . In the case of a smooth

collector, the theoretical collection efficiency increases with increasing air velocity. However, if the collector is rough then the experiments show that the increase in the volume collected due to the roughness decreases with increasing air velocity, as indicated in Figure 16. The volume collected at -5°C (3 m s^{-1}) and -8°C (5 m s^{-1}) is taken as zero, and the relative increase in volume collected due to the presence of the rime feathers is shown as a function of temperature. It can be seen that at low speeds where feather growth is enhanced, the volume collected increases substantially at lower temperatures. At a flow speed of 5 m s^{-1} the feather growth is inhibited, and thus the collector surface is essentially smooth. Macklin noted that with an increase in impact velocity the rime surface appearance changed from a 'feathery' to a 'kernel' type due to gaps in the rime being filled-in by subsequent droplets impacting at the higher velocity. This change will occur at lower temperatures for higher values of liquid water content. For instance, at a temperature of -15°C where rime feather growth is prominent, the surface temperature would rise to -10°C if the liquid water content was increased to 3 g m^{-1} . The growth of rime feathers would then be inhibited and the collection efficiency of the target would decrease.

The equivalent collector diameter is defined as that smooth collector diameter which would theoretically (Löffler and Muhr) collect the same volume of droplets as in the experiment. At low air speeds (3 m s^{-1}), where feather growth occurs, this diameter is 3.2mm; whereas, at 5 m s^{-1} the equivalent collector diameter is 4.8mm. The presence of rime on the collector increases the collection efficiency for all droplet sizes. At 3 m s^{-1} the collection efficiency for $5 \mu\text{m}$ droplets has increased from 0.06%

Figure 16



for a smooth 5mm collector to 0.21% for a rough surface with an equivalent collector diameter of 3.2mm. Table 1 shows the collection efficiency for a 5 mm and a 3.2 mm diameter collector at air speeds of 3 and 5 m s⁻¹. As shown in Appendix III, this increase is insufficient to have any effect on the significance of the Jayaratne and Saunders small droplet charging experiments.

The results presented here are for a certain set of experimental parameters such as collector diameter, cloud droplet spectrum and impact speeds. The net contribution of the rime feathers to the increase in collection efficiency must be obtained in order that the results can be applied to a different experimental situation. Table 2 shows the proportion of the droplets caught to the total number in the air flow for both the smooth and the rough collectors. At a flow speed of 3 m s⁻¹ the ratio increases as the temperature falls, due to the enhanced growth of the rime feathers at lower temperatures. Thus the volume of droplets collected by a rimed collector may be increased by 50% above that predicted by the Löffler and Muhr equations for a smooth collector. However, at 5 m s⁻¹, the ratio for the rough collector is about the same as that of the smooth collector. This is due to the feather growth being inhibited at higher impact speeds as discussed earlier.

Collection

The collection efficiencies given by Löffler and Muhr are only valid for smooth collectors. When the target is covered with rime, the collection efficiency of the target for small droplets does increase, particularly at low temperatures. It does not, however, increase with the velocity because feather growth is inhibited when the rime density increases with increase

TABLE 1

Collection efficiency (%) given by Löffler and Muhr for
a collector diameter of 5 and 3.2 mm at a flow speed of
 3 m s^{-1}

Droplet Diameter μm	5 mm	3.2 mm
2.5	0.00	0.00
5.0	0.06	0.21
7.5	0.66	2.37
10.0	3.56	10.94
12.5	11.28	26.16
15.0	23.38	40.94
17.5	35.84	51.92
20.0	46.05	59.81
22.5	53.87	65.72
25.0	59.91	70.36
27.5	64.73	74.11
30.0	68.68	77.21
32.5	74.81	82.00

TABLE 2

Ratio of theoretical volume and actual volume collected
to total volume in flow.

Temp.	3 m s^{-1}		5 m s^{-1}	
	Smooth	Rough	Smooth	Rough
-5	0.300	0.369	-	-
-8	0.303	0.430	0.447	0.450
-10	0.304	0.463	0.448	0.452
-12	0.306	0.468	0.451	0.455
-15	0.308	0.474	0.453	0.460
-20	0.313	0.482	0.457	0.468

in the droplet impact velocity. The collection efficiency also increases, up to a certain limit, with increasing amounts of rime on the target. The collection of small droplets is insufficient to modify the soft-hail stone growth rate, and hence to influence the conclusions of Jayaratne and Saunders (1985) concerning the sign of the charge transferred when ice crystals bounce off a soft-hailstone.

SECTION 5

THE COLLECTION EFFICIENCY OF A CYLINDRICAL TARGET FOR ICE CRYSTALS

Introduction

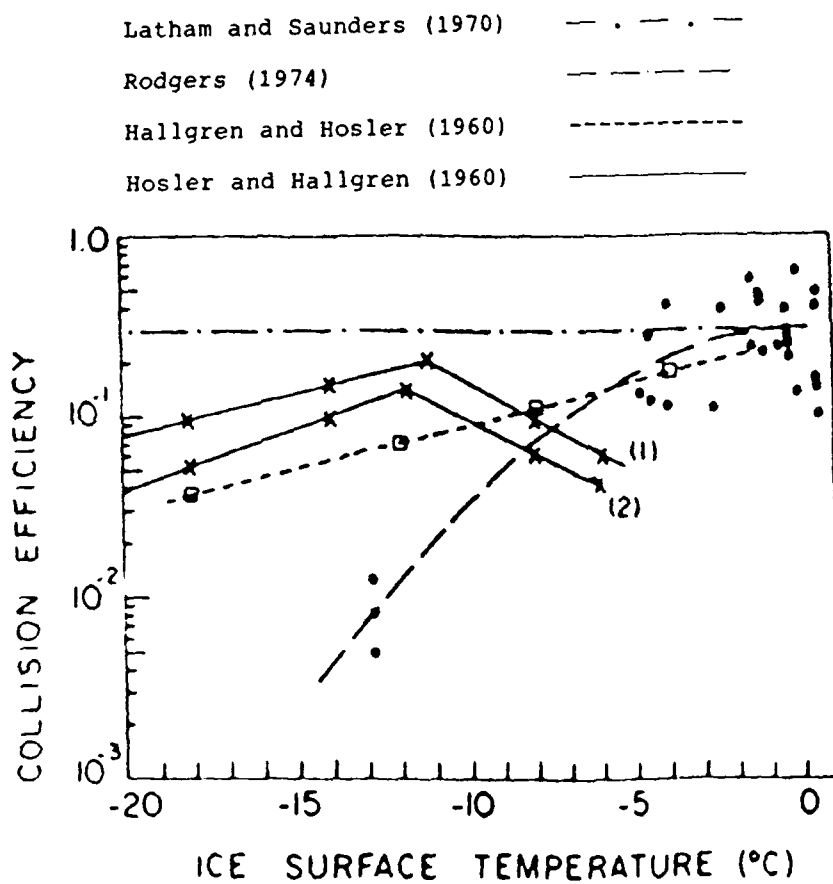
The collection efficiency of an ice sphere for very small ice crystals has been investigated by only a few workers, including Hosler and Hallgren (1960), Hallgren and Hosler (1960), Latham and Saunders (1970) and Rogers (1974). There have been no theoretical studies, owing to the complexity of modelling the movement of an ice crystal through a fluid.

Apart from Latham and Saunders, all the previous studies have found that the collection efficiency has a temperature dependence; the collection efficiency increases as the temperature of the target approaches 0°C due to the formation, on the surface, of a pseudo-liquid layer which enhances the adhesion efficiency. Figure 17 summarises their results; it can be seen that the collection efficiency is less than unity in all cases. Rogers, and Latham and Saunders, used only small plate crystals at all temperatures, whereas Hosler and Hallgren dealt with the crystal types which occur at the temperature at which the experiments were performed. Hosler and Hallgren found that the collection efficiency was a maximum of about 0.2 at about -10°C, decreasing to 0.05 at -5°C. They suggested that this change in collection efficiency was due to the change with temperature of ice crystal habit from plates to prisms.

Latham and Saunders (1970) measured the collection efficiency of an ice sphere of diameter 2mm for plate ice crystals of diameter 5 μm at an impact speed of 3 m s^{-1} . The collection efficiency was calculated from the mass of ice

Figure 17

Summary of previous collision
efficiency work



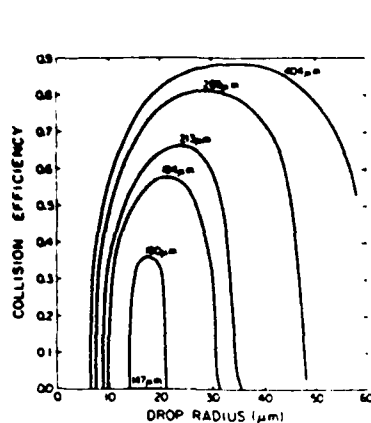
crystals collected by the sphere in a known time. The collection efficiency was about 0.3 at all temperatures in a zero electric field. When an electric field of about 1500 V cm^{-1} was applied, the collection efficiency increased to 0.8. They state, however, that the increase is due to an increase in the aggregation efficiency, and not in the collection efficiency.

Jayaratne (1981) found that the continuous formvar replicator, (Appendix I), has a collection efficiency of unity for ice crystals greater than $20 \mu\text{m}$ in diameter at an impact speed of 4.7 m s^{-1} . The cross-sectional shape of this flow was a rectangular jet, and so the collection efficiency for a $20 \mu\text{m}$ crystal may not be unity for a cylindrical target. Jayaratne et al. (1983) calculated the Event Probability (the collision efficiency times the separation probability) by comparing the charging current to two targets of different diameter (see Appendix IV). The event probability of the thinner target was assumed to be unity and so a maximum value of the event probability, due to the collision efficiency not being known at that time, could be calculated for the thick target. The charge per event results were not corrected for the collision efficiency of the target, and so will tend to underestimate the charge per event for the smaller ice crystals.

The collection efficiency of an ice crystal for water droplets has been investigated extensively by such workers as Ono (1969), Wilkins and Auer (1970), Harimaya (1975) and Pitter (1977). A summary of this work is shown in Figure 18. The collection efficiency for a large droplet of about $40 \mu\text{m}$ diameter may be close to zero, as a consequence of the relative velocity of the two particles being close to zero. This section describes the work performed to determine the collection efficiency of a

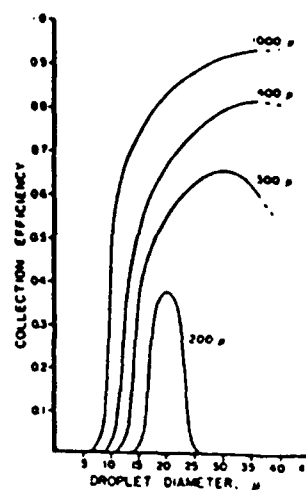
Figure 13

The collection efficiency of an ice crystal for water drops



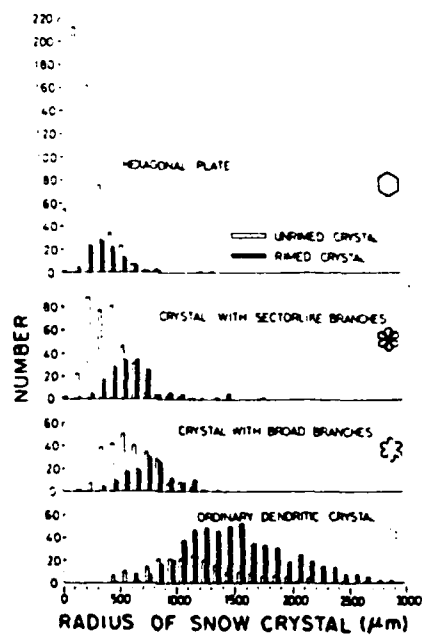
a

from Pitter (1977)



c

from Wilkins & Auer
1970



b

from Harimaya (1975)

cylindrical target for ice crystals of different types. Experiments were also performed to determine the event probability of a cylindrical target.

Experimental Procedure

The method used was to compare the ice crystal number concentration in the cloud to the concentration found on the cylindrical target. The ratio of the two concentrations is equivalent to the target collection efficiency and will increase with increasing flow speeds or with decreasing target diameter. The experiments were performed in the cloud chamber in the cold-room. The cloud was formed by nucleating a water droplet cloud in the usual way. The size and number concentration of the ice crystals formed was determined from formvar covered microscope slides past which the cloud was drawn.

The cylindrical target was a formvar covered glass rod of known diameter. These coated rods were prepared in the same way as the microscope slides. However, before exposure to the crystal cloud, the rod was dipped in cold chloroform to activate the formvar. The reason for this is that the ice crystals have a finite probability of bouncing off the target (see Appendix II), and so the ice crystal concentration would be underestimated. The wet formvar ensures that the target has a sticking efficiency of unity, and that all ice crystals that collide with the target are captured. Thus the collection efficiency is the same as the collision efficiency. The target diameters used were 3, 4, 5 and 6mm, and the airflow speeds used were 3, 4 and 5 m s⁻¹. The airflow speed used for the microscope slide was 7 m s⁻¹, so the collection efficiency of the slide was assumed to be unity for all but the smallest (< 19 μm) ice crystals.

The habit of ice crystals fall into three distinct types; columns, plates and dendrites. These types occur at around -6, -10 and -15°C respectively. However, small dendrites less than 80 μm in diameter approximate to small hexagonal plates as the dendritic arms are not very pronounced at this size. Thus the experiments were performed at -6 and -11°C, with ice crystals corresponding to columns and hexagonal plates. The ice crystal number concentration varied from 10^4 to 10^7 m^{-3} and the ice crystal diameter ranged from 10 μm to 140 μm .

Experiments were also performed with wet and dry formvar covered glass rods. The dry target simulates a hailstone in that the sticking efficiency is less than unity and ice crystals can collide with and separate from the target. The calculated number concentration was again compared with that in the cloud, to give the event probability. The event probability could be compared with that previously calculated from the charging currents of two simulated hailstones of different diameters, as described in Appendix IV.

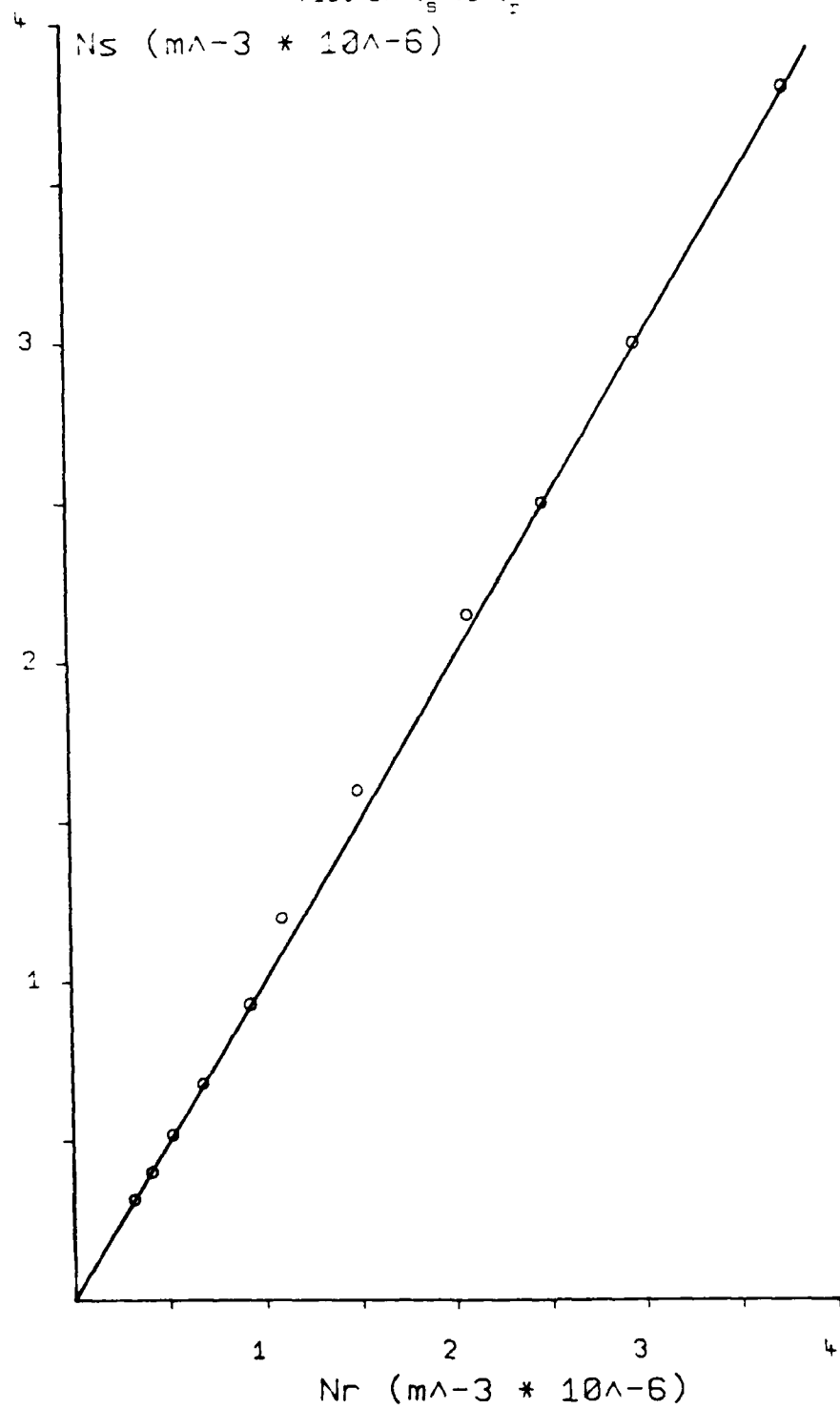
Measurement of the Collision Efficiency

The validity of the assumption that the microscope slide has a collection efficiency of unity was confirmed by comparing the number concentration on the 5mm rod to that on the slide for an airflow of 7 m s^{-1} . Figure 19 shows the slide number concentration, N_s , the rod number concentration N_r , and the ice crystal diameter.

As can be seen, there is a 1:1 correlation between the two concentrations for crystal sizes over 30 μm . The number concentration on a dry slide and a wet slide, and on a wet rod and dry rod were also compared. Again, there was a 1:1

Figure 19

Plot of N_s vs N_r



relationship between the results.

The following experiments were performed with wet formvar targets to ensure that the sticking efficiency was unity.

These experiments were performed at an air speed of 3 m s^{-1} for rod diameters of 3, 4, 5 and 6mm, and for column and plate type crystals of different sizes. Figures 20 and 21 show the collision efficiencies against ice crystal diameter for the different rod diameters, for plates and columns respectively. The collision efficiency of the 3mm rod is nearly unity for all crystal sizes. It can be seen that the collision efficiency is unity for all rods, when the plate diameter is greater than $80 \mu\text{m}$ for columns of length $100 \mu\text{m}$.

The air speed was varied between 3 and 7 m s^{-1} for the 5mm rod. The collision efficiency increases with increasing air speed, until it is unity for all crystal diameters examined at 7 m s^{-1} ; Figures 22 and 23 are for plates and columns. Again, the collision efficiency for a column type crystal is lower than that of a plate type crystal of the same size.

Measurement of the Event Probability

In these experiments, a comparison between the number concentration for wet and dry rods was made in order to obtain the sticking efficiency. The dry rod simulates a hailstone whose sticking efficiency is less than unity. The 5mm rod was used so that these results could be directly compared with those from the charging experiments. Experiments with the 3mm rod were also performed to investigate the effect on the event probability of a smaller target diameter. The event probability was calculated from the product of collision efficiency and one minus the sticking efficiency.

Figure 20

Collision efficiency of different planimeter rods
for plate crystals

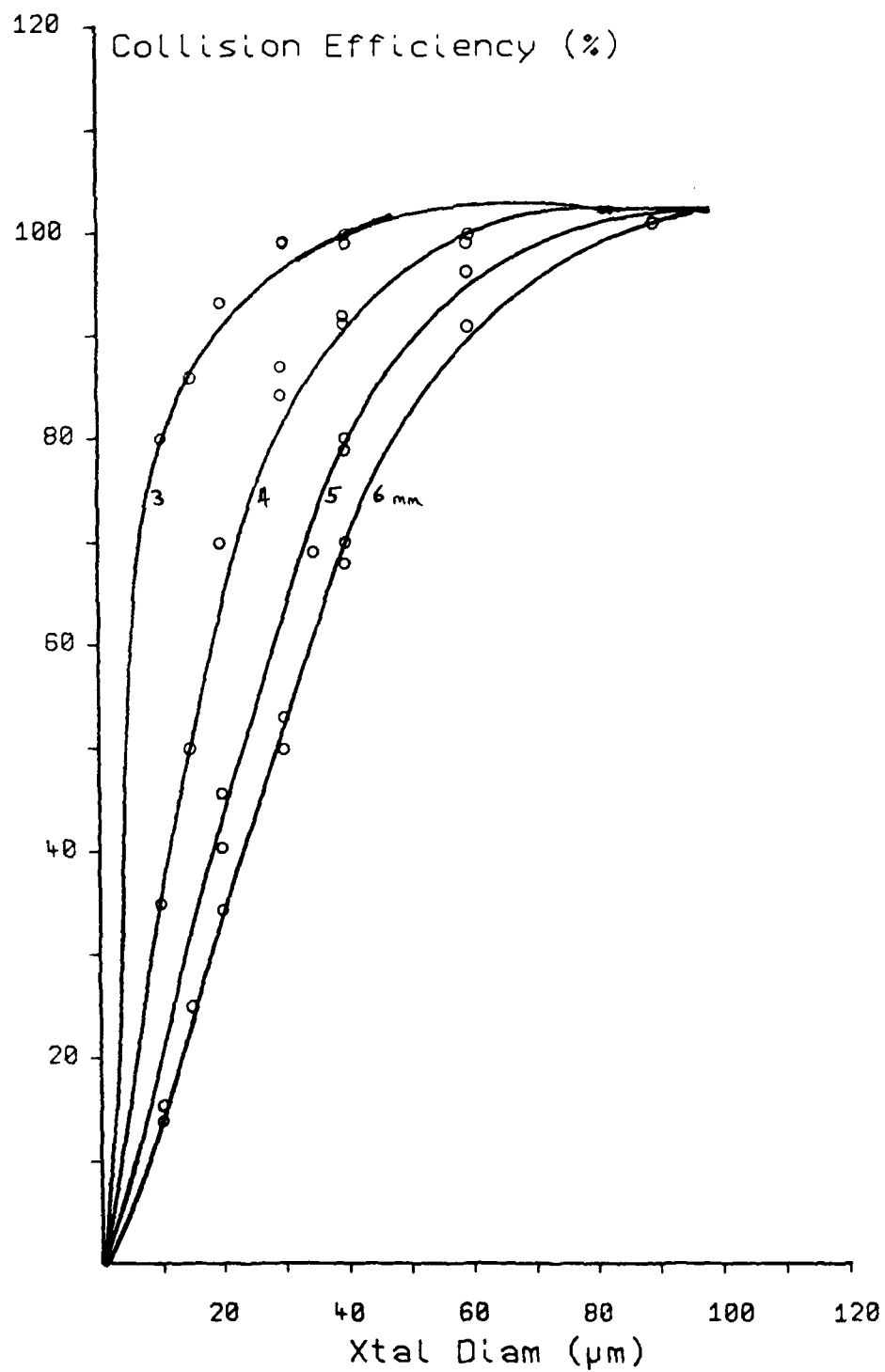


Figure 21
Collision efficiency of different
diameter rods for column crystals

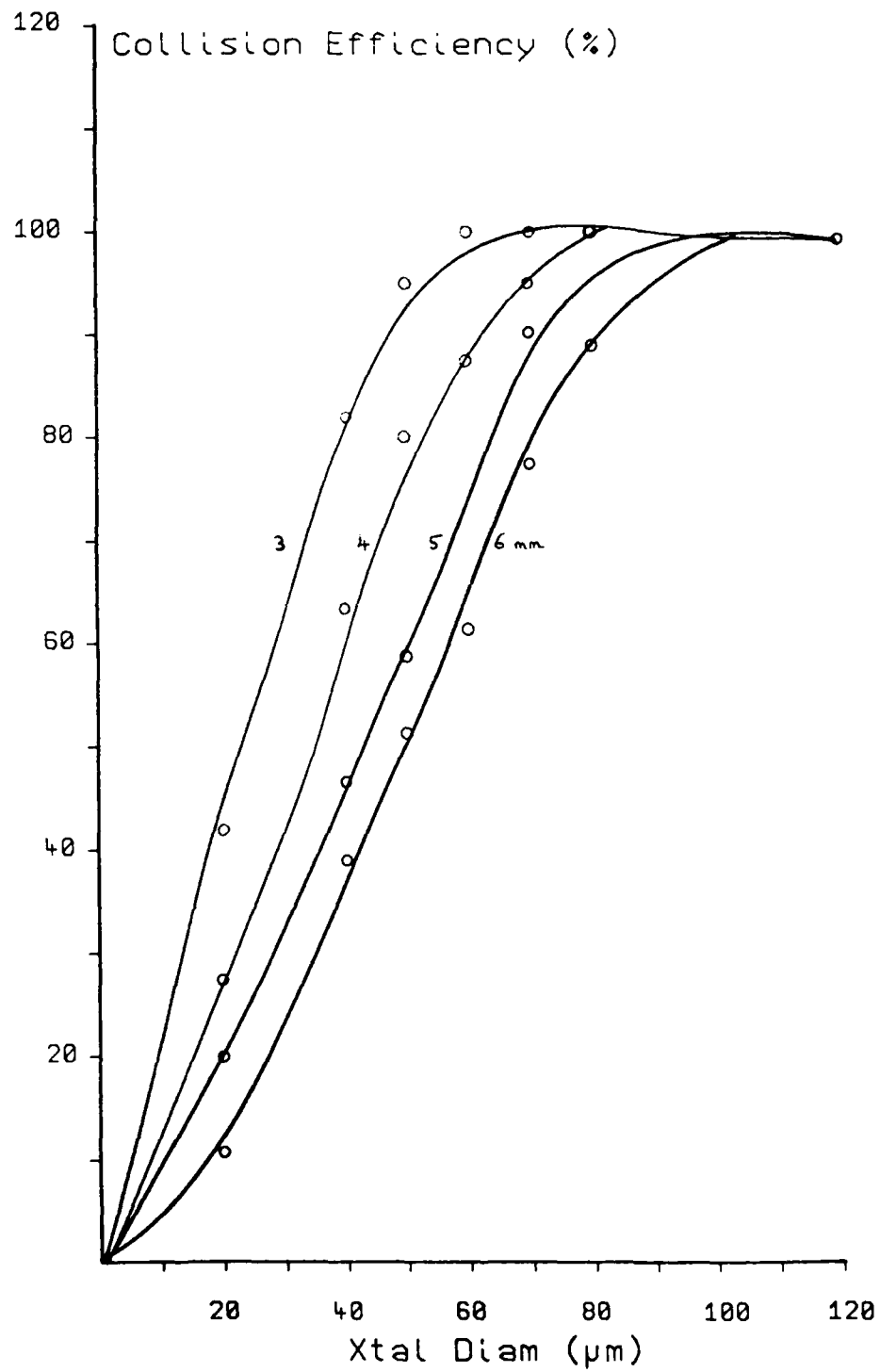


Figure 12

Collision efficiency of 5 μm rod for
plate crystals at different velocities

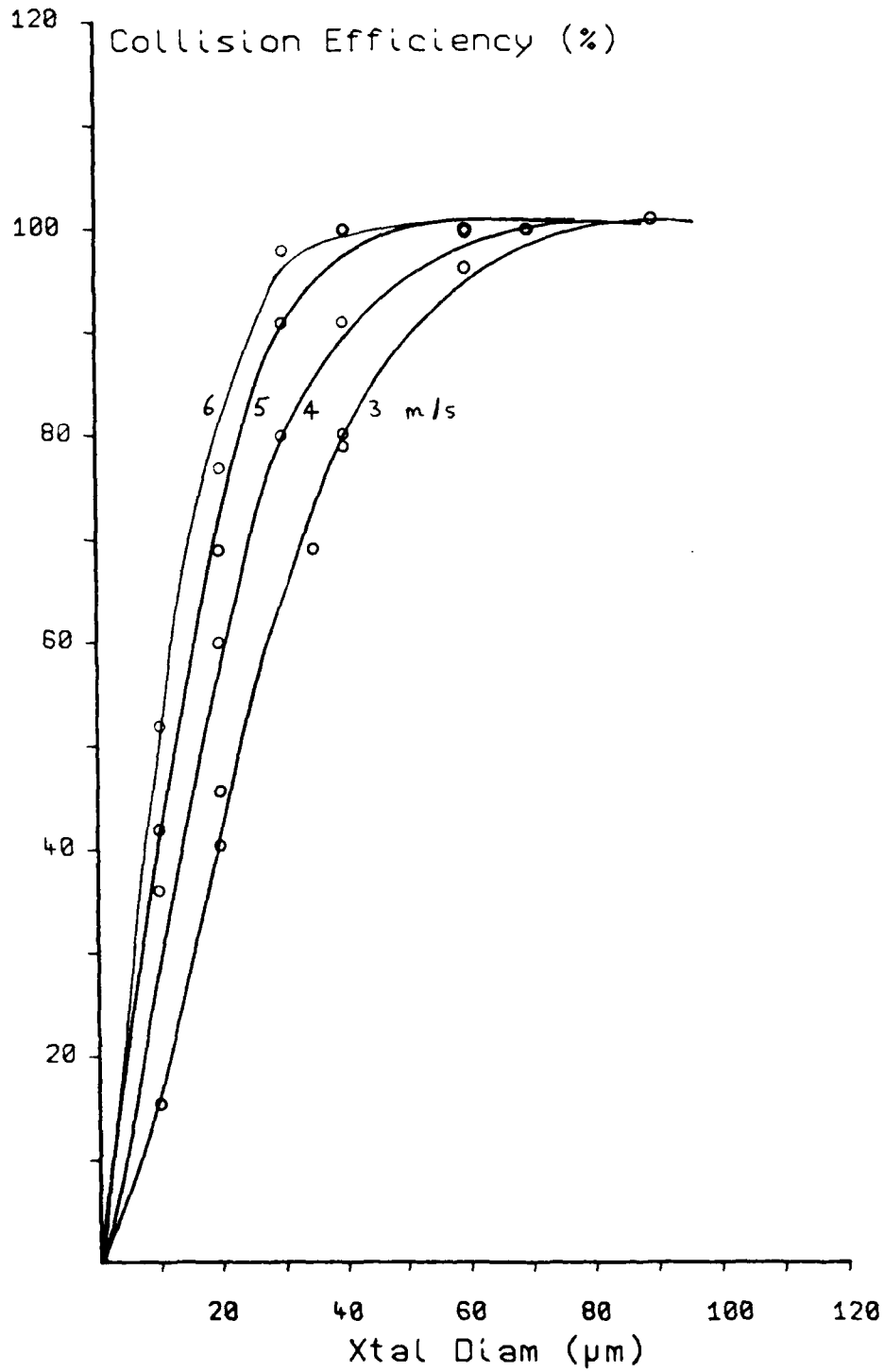


Figure 23

Collision efficiency of 5 mm rod for
column crystals at different velocities

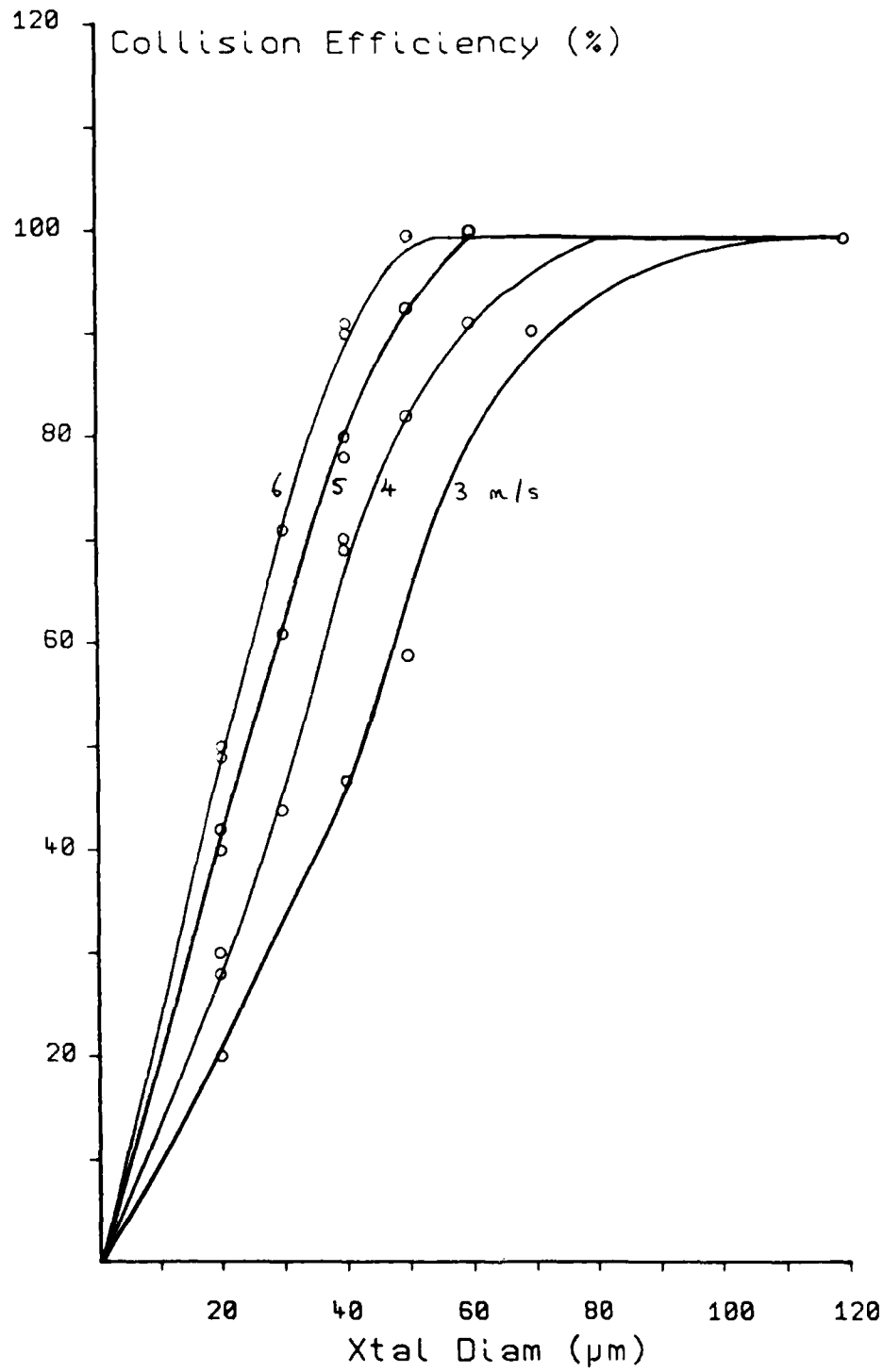


Figure 24 shows the event probability against ice crystal diameter for both rods at -10°C an air speed of 3 m s^{-1} . The 5mm target has a lower event probability than the 3 mm target for a particular crystal diameter. The event probability of the larger target varies from 0.1 to 0.35 for the crystal diameter range 10 to $500 \mu\text{m}$, whereas for the smaller target the event probability varies from 0.25 to 0.55 over the same range. The event probability is insensitive to crystal type; the smaller crystals were columns, plates and sectors, whilst the larger crystals ($>200 \mu\text{m}$) were sectors and dendrites. The event probability is also insensitive to cloud and target temperature but is very sensitive to impact speed.

Figure 25 shows the event probability for both targets against crystal diameter for an air speed of 7 m s^{-1} . The event probability of the 5 mm target for a $100 \mu\text{m}$ crystal increases from 0.1 at 3 m s^{-1} to 0.3 at 7 m s^{-1} . Thus there is a higher proportion of the ice crystals bouncing off the target at higher impact speeds.

Discussion

The work presented here shows that the collision efficiency of a cylindrical target for ice crystals is less than unity if the crystal diameter is less than $100 \mu\text{m}$. Figures 19 to 23 show that the collision efficiency is dependent on crystal diameter, D_x , speed, v , and target diameter, D_c . These parameters can be related by the following equation:

$$\psi = 10vD_x/D_c$$

The graph of ψ against collision efficiency for plates and columns is shown in Figure 26a and b. The collision efficiency of a target for plates and columns cannot be related directly in

Figure 24

Event probability of 5 and 3 mm rod at 3 m/s

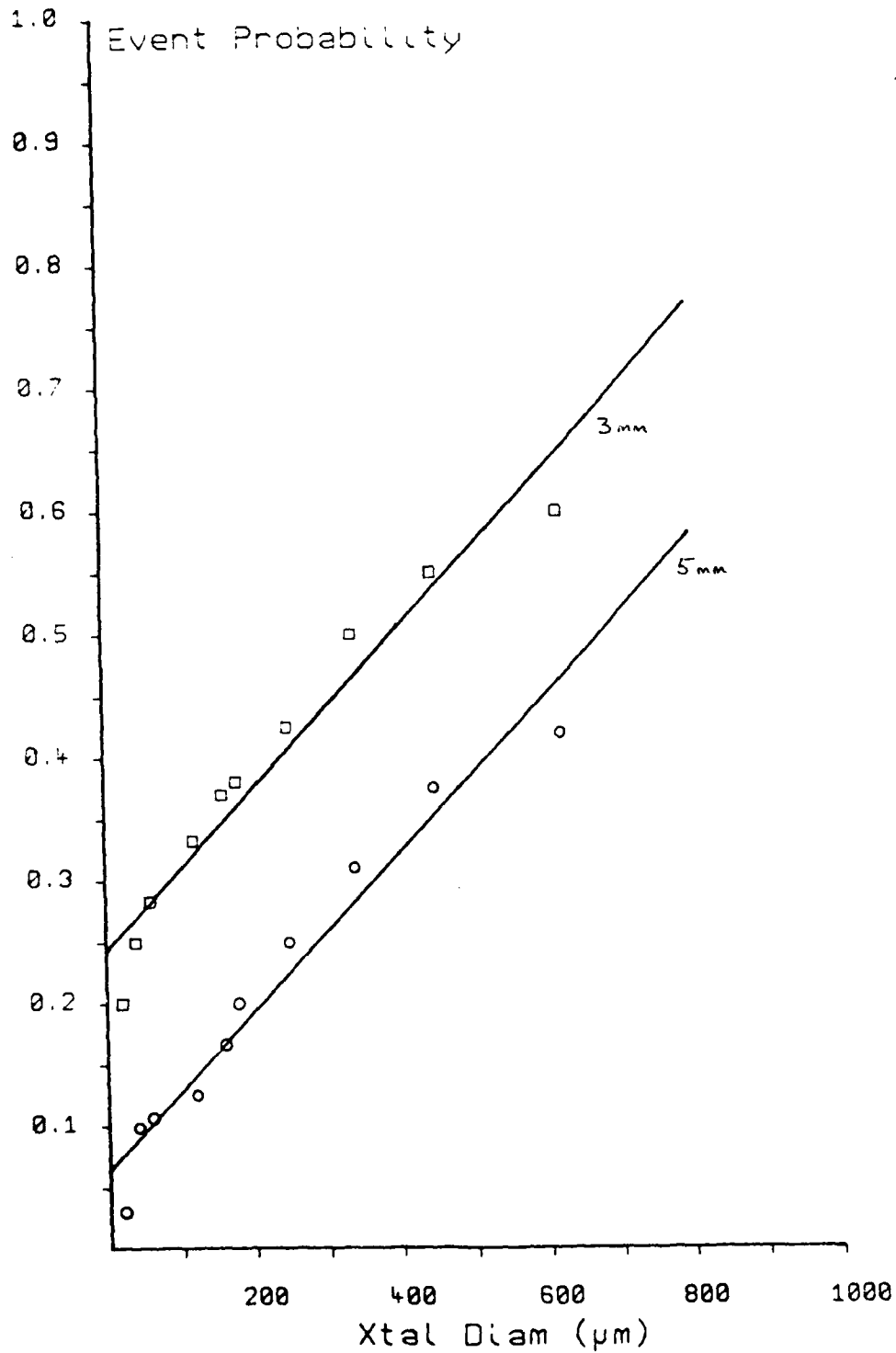


Figure 25

Event probability of 5 and 3 mm rod at 7 m/s

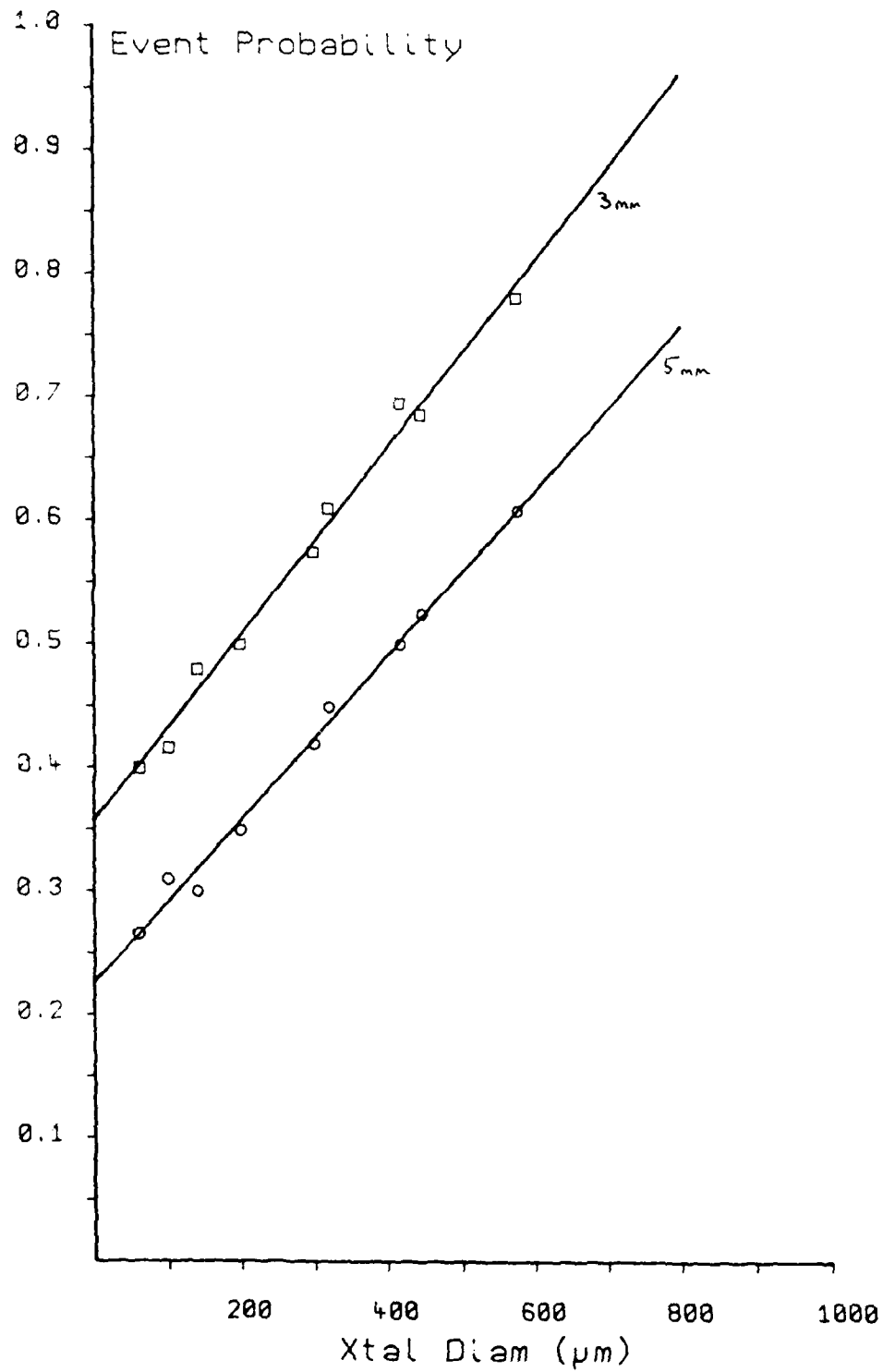
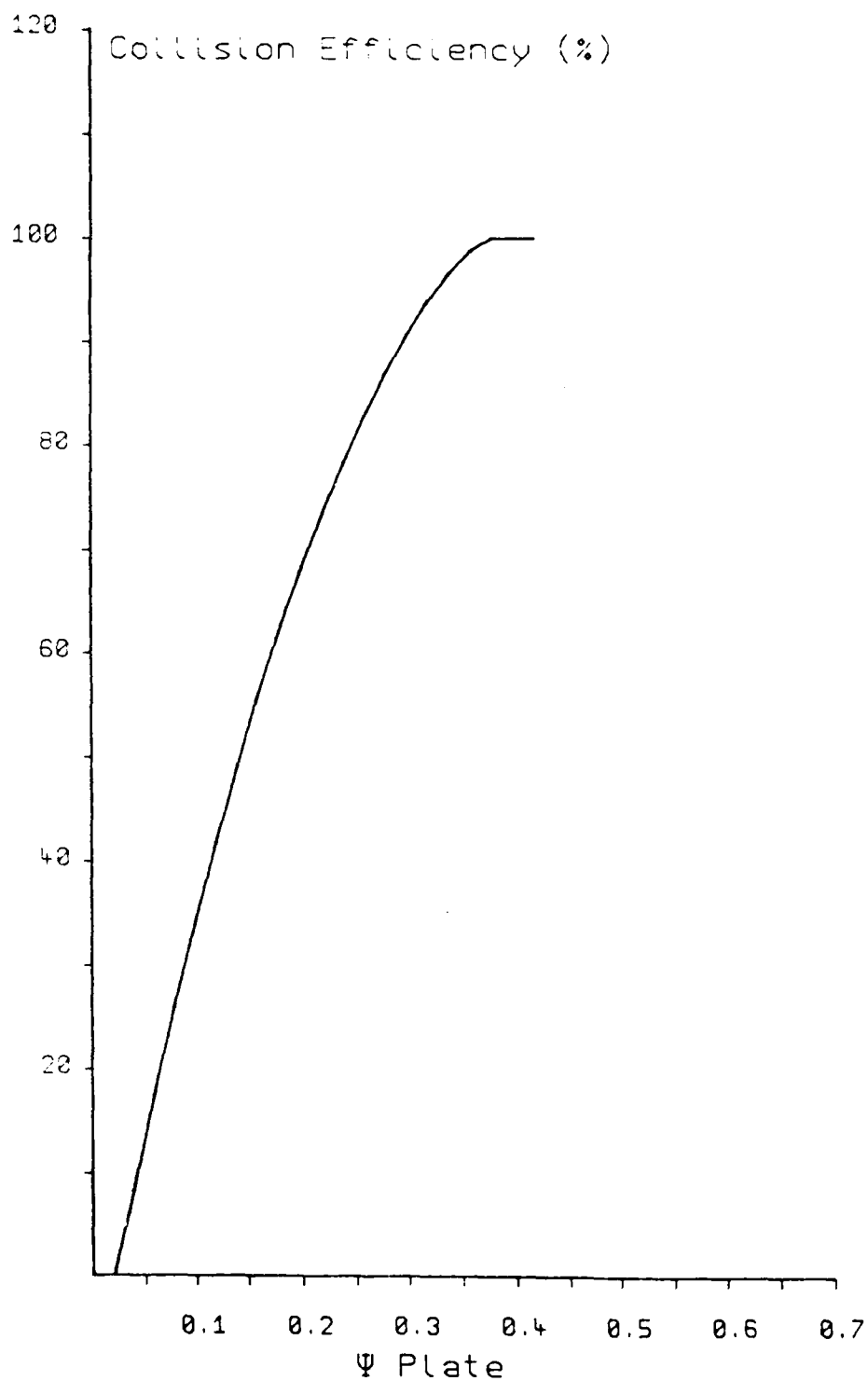
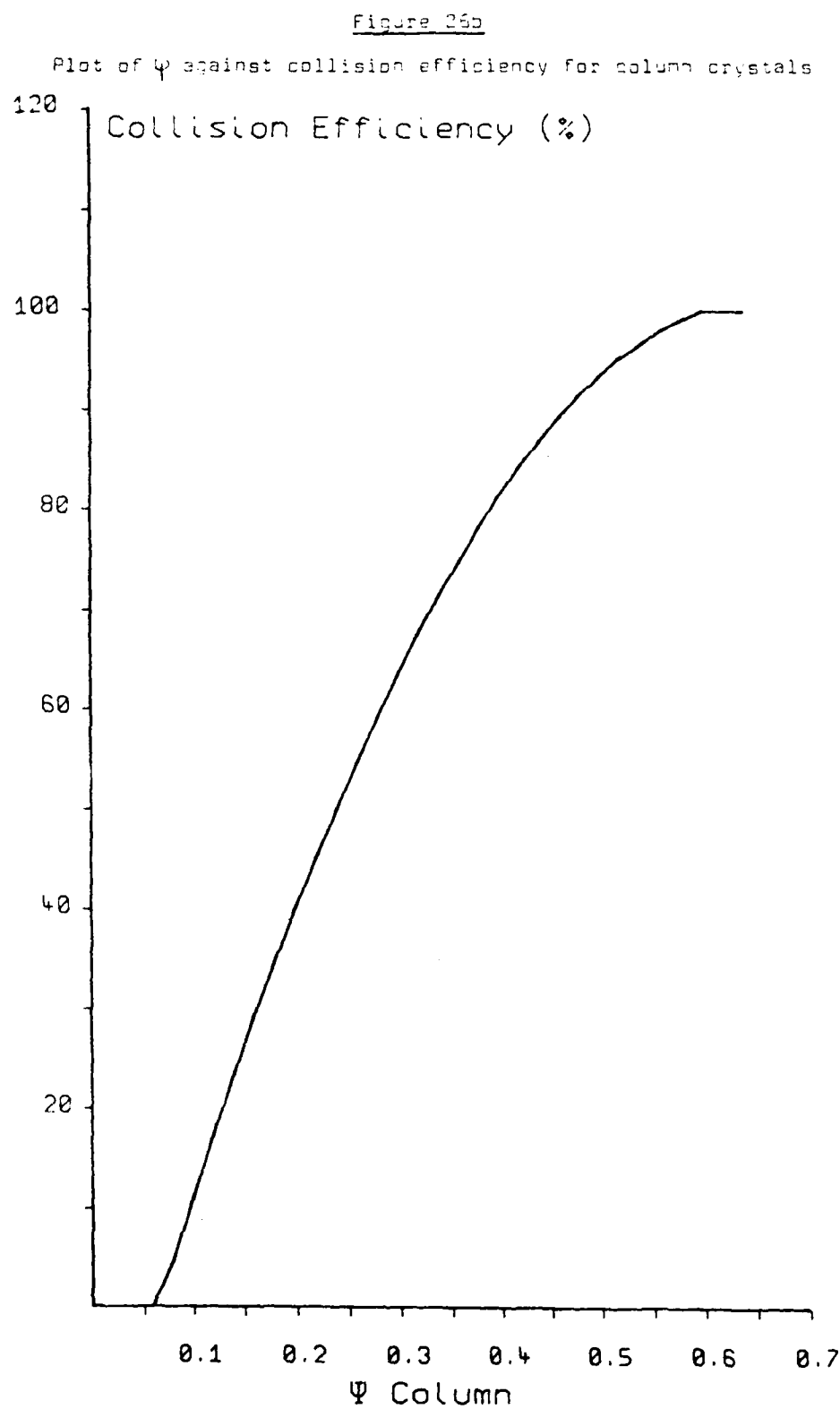


Figure 36a

Plot of ψ against collision efficiency for plate crystals





one equation, due to the different dependence on crystal shape. The collision efficiency cannot be related to the equations of Ranz and Wong (1952) or those of Löffler and Mühr (1977) as their equations dealt with a spherical droplet, and the results presented here show that a hexagonal plate or column crystal cannot be idealised to a sphere as assumed by Takahashi (1978).

The above relationship was used to calculate the collision efficiency from the results of Latham and Saunders (1970). Their results gave a collection efficiency of 0.3 and the equation gives 0.22, which is in fairly good agreement. When the equation was applied to the results of Hosler and Hallgren, it gave a collection efficiency of 0.5 as opposed to 0.1. However, surprisingly, they found that the collection efficiency increased when the collector diameter increased from 0.127mm to 0.36mm, and so the low collection efficiency could be a consequence of the very small collector diameters they used.

The values of event probability calculated here are in good agreement with those values calculated from the charging experiments. The charging determined event probability against collection efficiency determined event probability is shown in Figure 27. These results presented here for a dry target will tend to overestimate the event probability slightly at warm temperatures $> -10^{\circ}\text{C}$, due to the high adhesion efficiency of a riming hailstone.

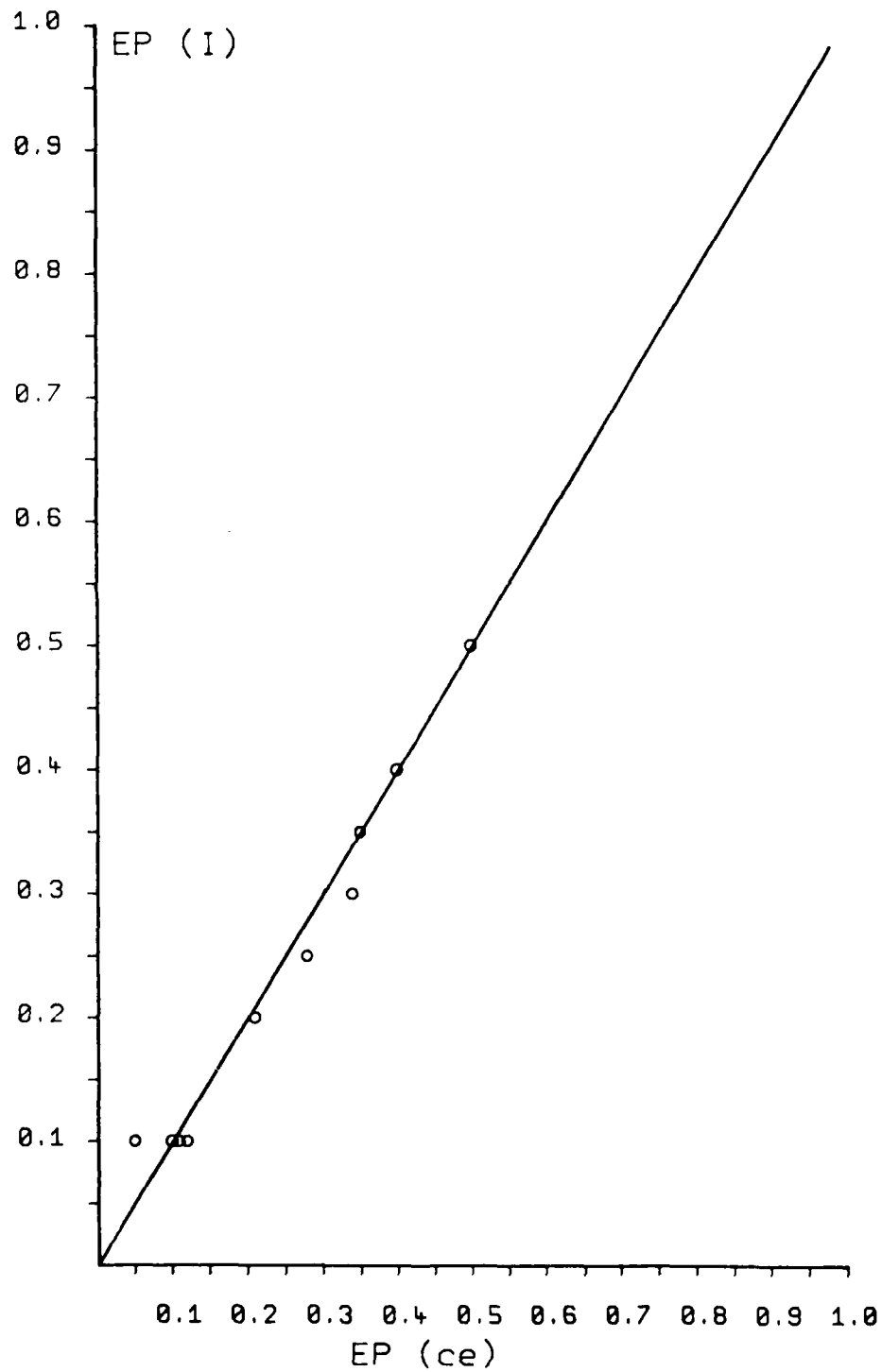
Conclusion

The collision efficiency of a target for ice crystals varies with impact speed, crystal diameter and rod diameter. The collision efficiency is unity for all crystal sizes greater than 100 μm . The results presented here are in fairly good agreement

Figure 27

Event probability from the two wire experiments
compared with the slide method

EP_I vs EP_{ce}



with those of previous workers, even though the experimental procedure was radically different. The event probability also varies with these parameters, with the probability increasing with increasing impact speed and crystal diameter.

SECTION 6
THE CHARGING OF A SIMULATED SOFT-HAILSTONE BY
LARGE ICE CRYSTALS

Introduction

The purpose of this study was to investigate the charging of a simulated hailstone under a range of cloud conditions with large ice crystals greater than 200 μm in diameter. The maximum size achieved by Jayaratne et al. (1983) was 130 μm , and the present work is designed to extend the charge per event-crystal diameter dependence and the velocity-crystal diameter dependence, determined by Jayaratne et al. to larger crystal sizes. Also the charging of aircraft was simulated by impacting ice crystals on a rimed and an unrimed target at high speeds of around 100 m s^{-1} .

The pioneering work of Reynolds, Brook and Gourley (1957) proved conclusively that a soft hailstone can become electrified when ice crystals bounce off it. They rotated a metal sphere through a cloud consisting of supercooled water droplets and ice crystals at -27°C , and measured the charge acquired by the sphere. They detected negative charge at high liquid water contents, and positive at low. Subsequent work by Saunders et al. (1984) showed that the positive charging was anomalous, being due to the high rotational forces present in their experimental set-up. The typical liquid water content was about 2 g m^{-3} , and the crystals were produced in concentrations of 10^7 m^{-3} by seeding the cloud with dry ice. The spheres were rotated at a high speed of about 8 m s^{-1} . At these values, they measured a charge of -160 fC per crystal collision. However, their estimates of crystal concentration may have been in error. They did not detect any charging when the sphere was rotated in water

droplets alone.

Church (1966), in a similar set of high speed experiments, found that a hailstone would charge positively if the cloud temperature was warmer than -20°C . The hailstone charged negatively if the vapour supply was cut off during a run. He measured a maximum charge per event of 1.6 fC.

Takahashi (1978) also repeated the Reynolds experiments at high speed, and measured negative charge at high liquid water contents below -10°C and positive at low values of liquid water content. The charge per collision ranged from -16 fC to +30 fC for a 100 μm diameter crystal.

Jayarathne et al. (1983) provided the first comprehensive investigation into the charging of a soft hailstone by the collision of ice crystals at velocities appropriate to those found in thunderstorms. When they rotated a target through a cloud of supercooled water droplets, riming occurred on the leading edge but no charging to the hailstone was detected. The cloud was then seeded with a wire which had been cooled to liquid nitrogen temperature, and ice crystals grew in the supersaturated environment. Strong positive charging was detected at a temperature of about -18°C for liquid water contents greater than 0.3 g m^{-3} ; negative charging was detected below this 'reversal' temperature, typically -18°C , unless the liquid water content was unrealistically high. The charge per event for a 125 μm diameter crystal was about +10 fC at an impact speed of 3 m s^{-1} at a temperature of -10°C . The present work extends these results to larger crystals and higher velocities.

Experimental Procedure

The low speed experiments were performed entirely within the cloud chamber in the cold-room. The targets were mounted on the rotating apparatus, and could be moved through the cloud with their axes normal to the direction of motion. The target speed was typically 3 m s^{-1} , and riming occurred on the leading edge. The target was connected to an electrometer which had a sensitivity of $1 \text{ mV} \equiv 10^{-13} \text{ A}$ which could detect the charge to the target if the charging rate was greater than 0.2 pC s^{-1} . The output was recorded on a chart recorder. Two targets were used; one of diameter 5mm and the other of diameter 0.5mm. They were placed at opposite arms of the apparatus, as shown in Figure 2. The event probability (see Appendix IV and Section 5) is assumed to be unity for the smaller target.

The cloud chamber consisted of a metal box divided into two parts; the upper was the initial growth chamber for the ice crystals, and the lower was the experimental chamber where the ice crystals interacted with the simulated hailstone. A supersaturated environment was maintained in both chambers; The cloud in the upper chamber was seeded, and the crystals grew to about $200 \text{ }\mu\text{m}$. At this point, the trapdoor was opened and the crystals fell through to the bottom chamber. After about 3 minutes, the crystals were about $600 \text{ }\mu\text{m}$ in diameter. The maximum growth rate occurred at -15°C with dendritic crystals; the maximum sized plate crystal was about $300 \text{ }\mu\text{m}$. There was an unavoidable temperature gradient of 1°C m^{-1} over the height of the cloud chamber but the region where the riming occurred was well mixed and so had uniform temperature.

The ice crystal number concentration was measured by drawing a sample of cloud past a dry formvar covered microscope slide at

7 m s^{-1} . The slide was then sprayed with cold chloroform and allowed to dry before being analysed under a microscope. The actual concentration was calculated from the equations described in Appendix I. The collision efficiency of the target for small ice crystals was taken into account, using the results presented in Section 5. The Rime Accretion Rate was determined from the elevation of the rime surface temperature above ambient, caused by the release of heat when the droplets collide with and freeze on the target, as detailed in Appendix II.

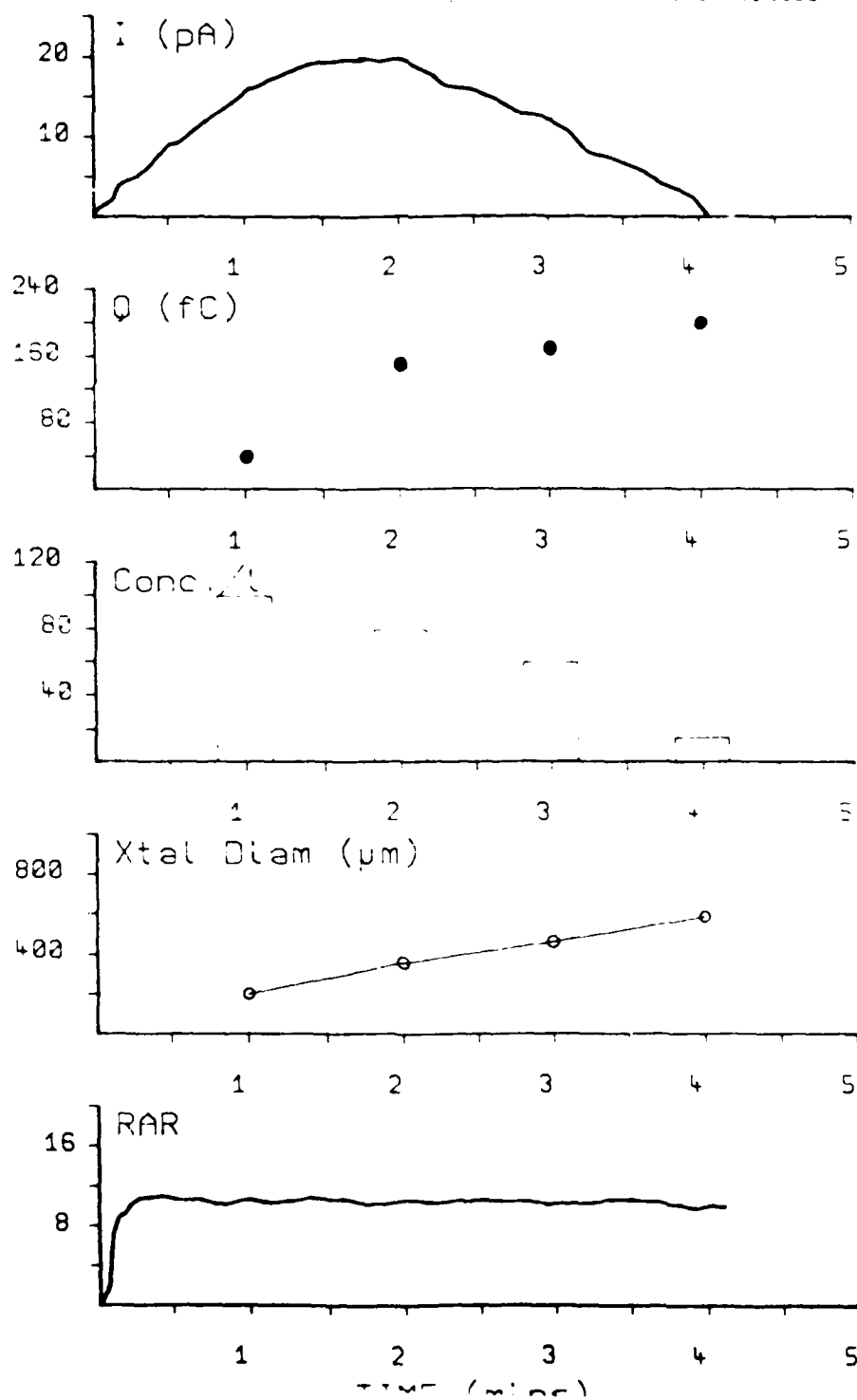
Thus, for each experimental run, the charging current to both simulated soft-hailstones, the rime accretion rate, the cloud temperature and the size and number concentration of the ice crystals could be measured.

Results

Charging in Mixed Cloud: The Positive Charging Regime

The result of Jayaratne et al. that the target becomes positively charged at temperatures above -18°C was confirmed. The majority of these experiments were performed at -15°C with dendrites up to $800 \mu\text{m}$ in diameter. Figure 28 shows a typical charging current to the target at a temperature of -15°C . The figure also shows the rime accretion rate, and the crystal size and number concentration sampled at intervals during the run. The rime accretion rate, which remains approximately constant, was calculated to be about 10 mg cm^{-1} from the rime surface temperature elevation of 1.5°C . The time $t=0$ corresponds to the time when the trapdoor was opened to allow the crystals to fall through to the lower chamber. The upper chamber cloud had been seeded between 1 and 2 minutes previously. Jayaratne et al. noted an initial positive peak when crystals first hit the riming

Typical run at -15°C showing variation of rim accretion rate and ice crystal size and concentration



target, which occurred irrespective of the cloud temperature. This was due to a high concentration of small ice crystals soon after seeding the cloud. In the present case, there was only a uniform cloud of larger crystals and so the positive peak was not detected. The positive peak could be reproduced if the cloud was seeded at the bottom of the chamber near the target apparatus. The shape of the charging current and the variation of the liquid water content with time was very similar to that of Jayaratne. The maximum diameter dendrite produced in the chamber was 800 μm , and the charge per event for this size of crystal was +220 fC.

The experiments were repeated at -6°C where the predominant ice crystal habit is columns and prisms. The rime surface temperature was around -5°C . The maximum reproducible column length was 380 μm which gave a charge per event of 100 fC. Figure 29 shows typical charging currents to both targets at this temperature. The event probability for this run with 300 μm columns was calculated to be 0.25, which is a slightly smaller value than at lower temperatures due to the higher adhesion efficiency at warmer temperatures. Figure 30 shows the variation with time of the ice crystal size and number concentration, and the rime accretion rate. The largest plate crystal obtainable was 300 μm , leading to a charge per event of 80 fC.

Figure 31 shows the charge per event against crystal diameter. Jayaratne et al. found a relationship between charge and size of the form $q \propto d^4$ for crystals up to about 120 μm in size. Their result was confirmed for small crystals and the d^4 line is shown in the figure. For crystals greater than 150 μm diameter, the charge per event is less than that predicted by extrapolating the d^4 relationship to larger crystal sizes. Above 450 μm there is only a slight increase in the charge transferred with an

Figure 29 shows the charging currents to the 5 and 0.5 mm targets at -10^3 C.

Figure 29

Charging currents to the 5 and 0.5 mm targets at -10^3 C

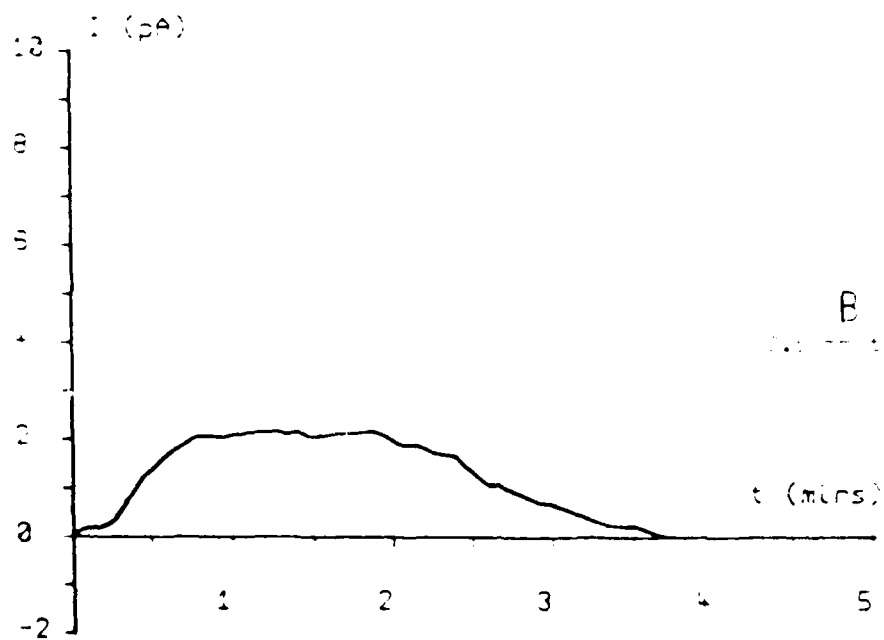
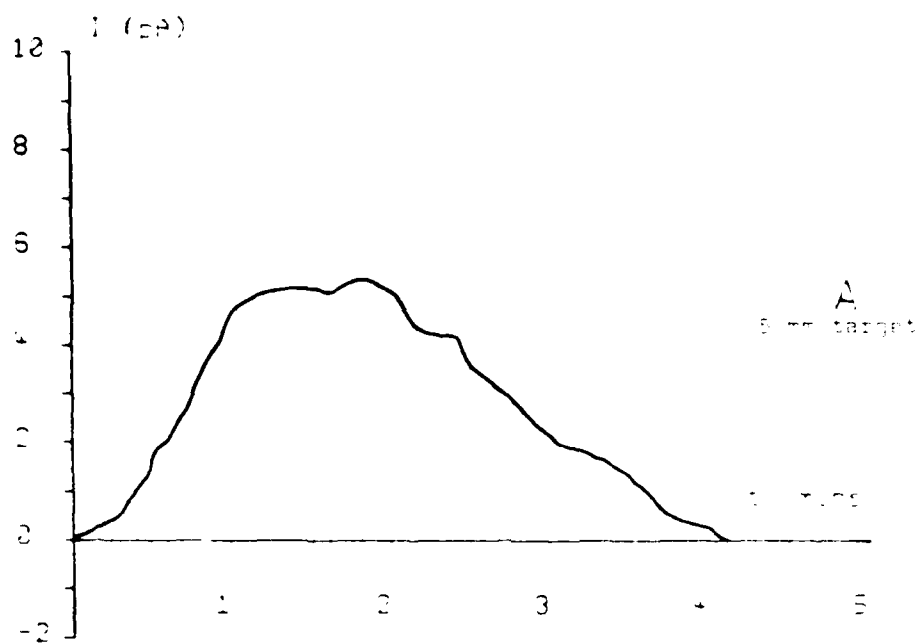


Figure 3C

Typical run at -4°C showing variation of ring accretion rate and ice crystal size and concentration

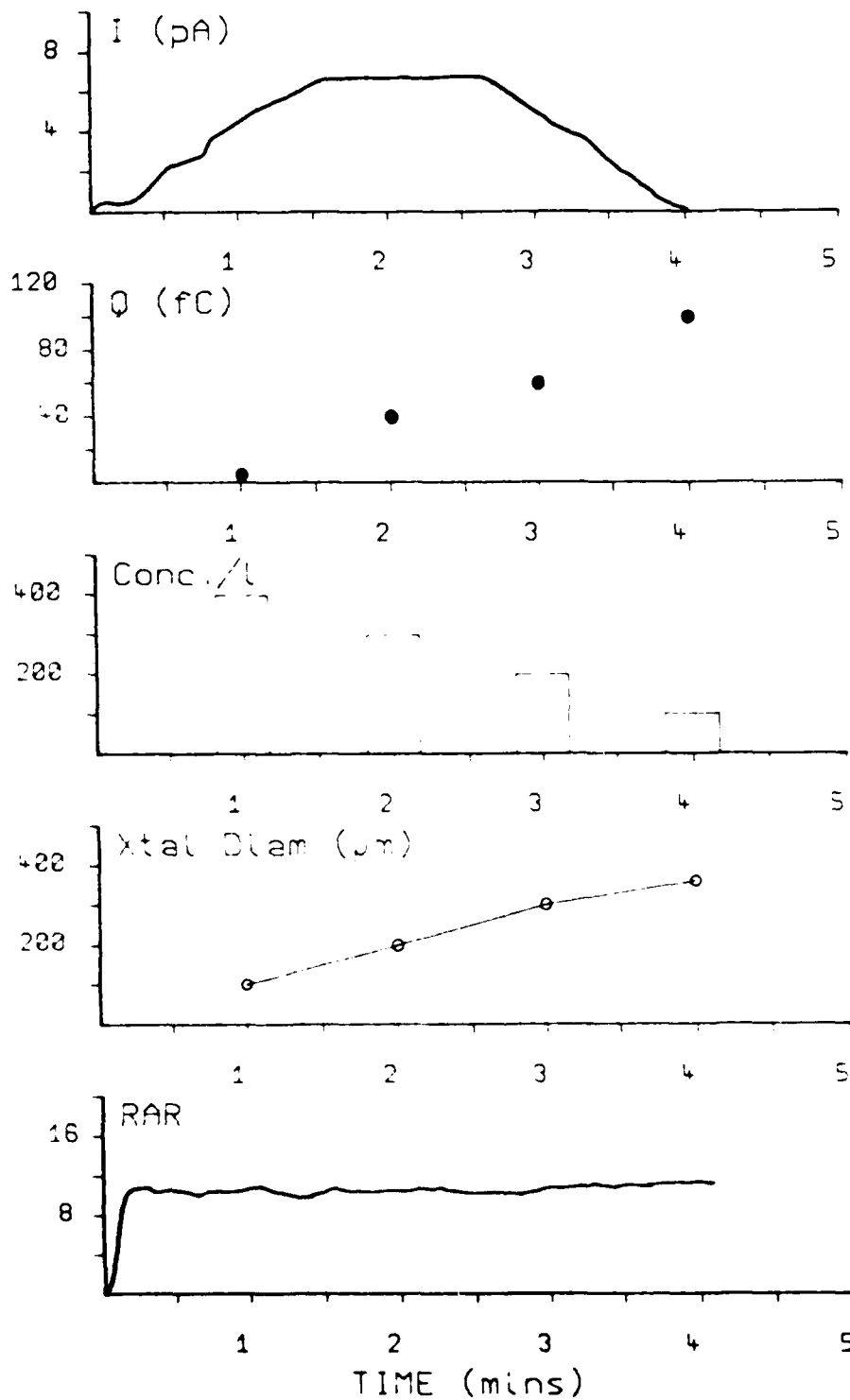
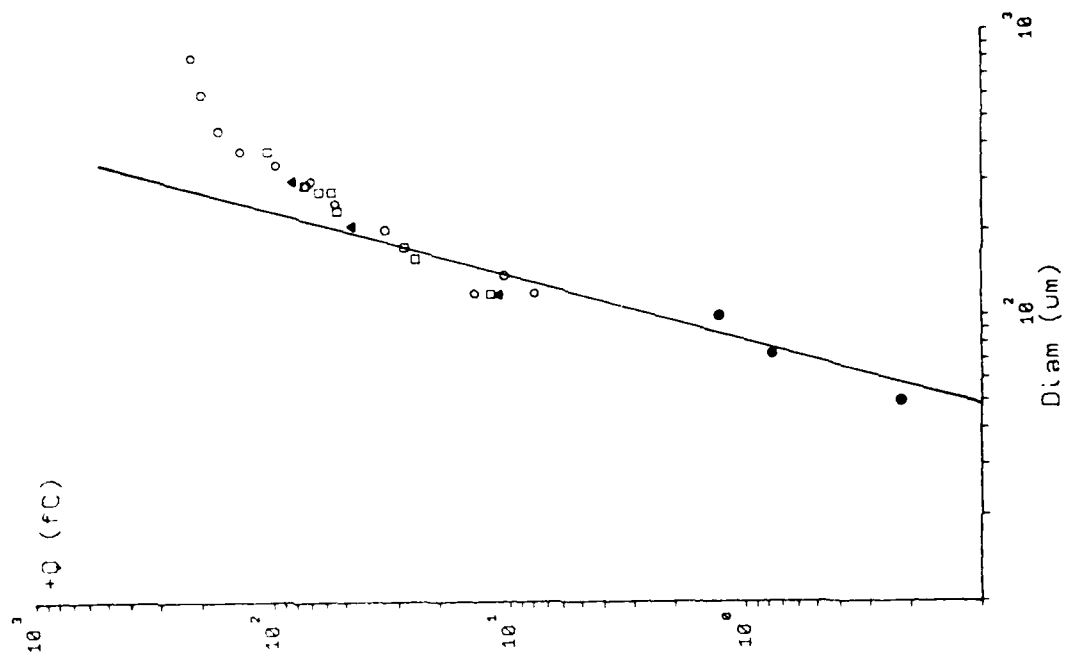


Figure 31

Charge per event vs ice crystal
diameter positive charging
regime

- : from Jayaratne et al (1983)
- : -15°C
- : -12°C
- ▲ : -6°C



increase in crystal diameter. The mean slope of the line for small crystals is 4.4; for medium sizes (between 150 and 450 μm) it is 1.8, while for large crystals it falls to about 0.3.

The Negative Charging Regime

At temperatures below the reversal temperature of -18°C , the charging to the target is predominantly negative. The main crystal habit is plates and bullets at these temperatures. Experiments were performed to measure the negative charge per event for large ice crystals.

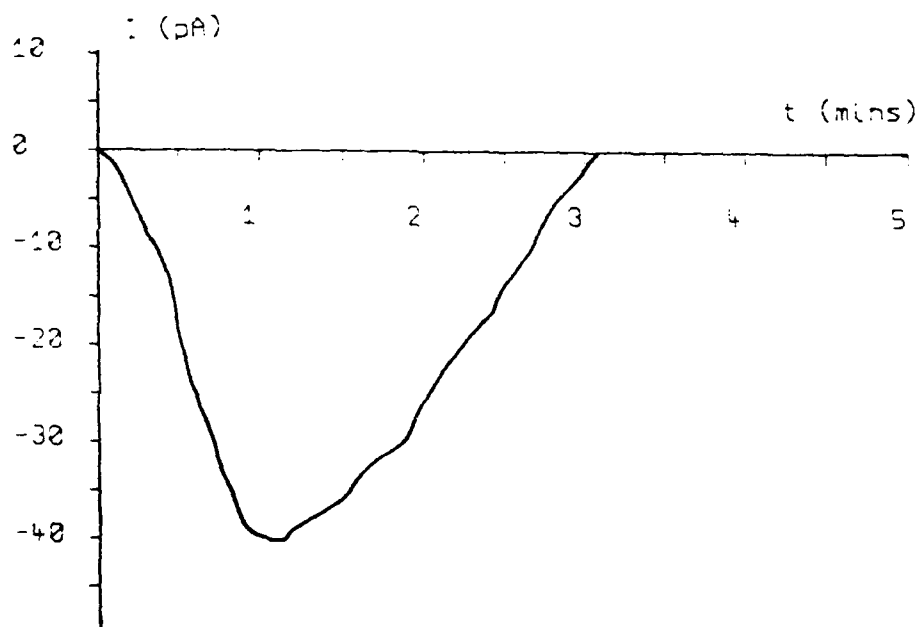
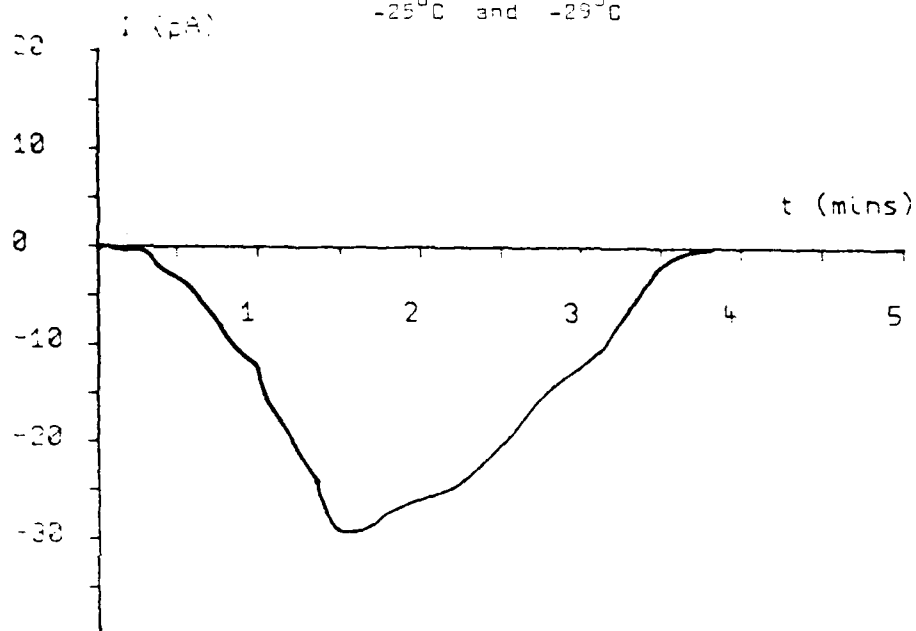
Figure 32 shows typical runs at -25°C and -29°C ; the charging is negative throughout the run. The predominant crystal type was bullet clusters, which separated more charge than a single crystal of the same size. This is reflected in the magnitude of the charging current. When they first appear at the target, the clusters are about 400 μm in diameter and reach about 1000 μm in diameter at the end of the run.

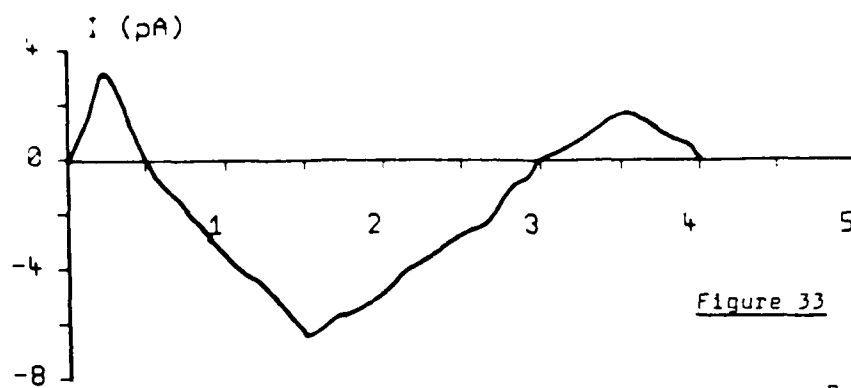
The results of Jayaratne et al. were confirmed by seeding the cloud in the lower chamber. The initial positive peak was observed, followed by negative charging during the rest of the run. Figure 33 shows such a run at -21°C ; the maximum crystal diameter was 140 μm . The figure also shows the crystal size and number concentration during the run. No bullet clusters were observed, only plates.

The values of charge per event from these experiments were similar to those found by Jayaratne for small crystals. Figure 4 shows the charge per event against crystal diameter; the line is about 10% from the Jayaratne line at a single crystal diameter of 100 μm . The bullet clusters separated more charge, as

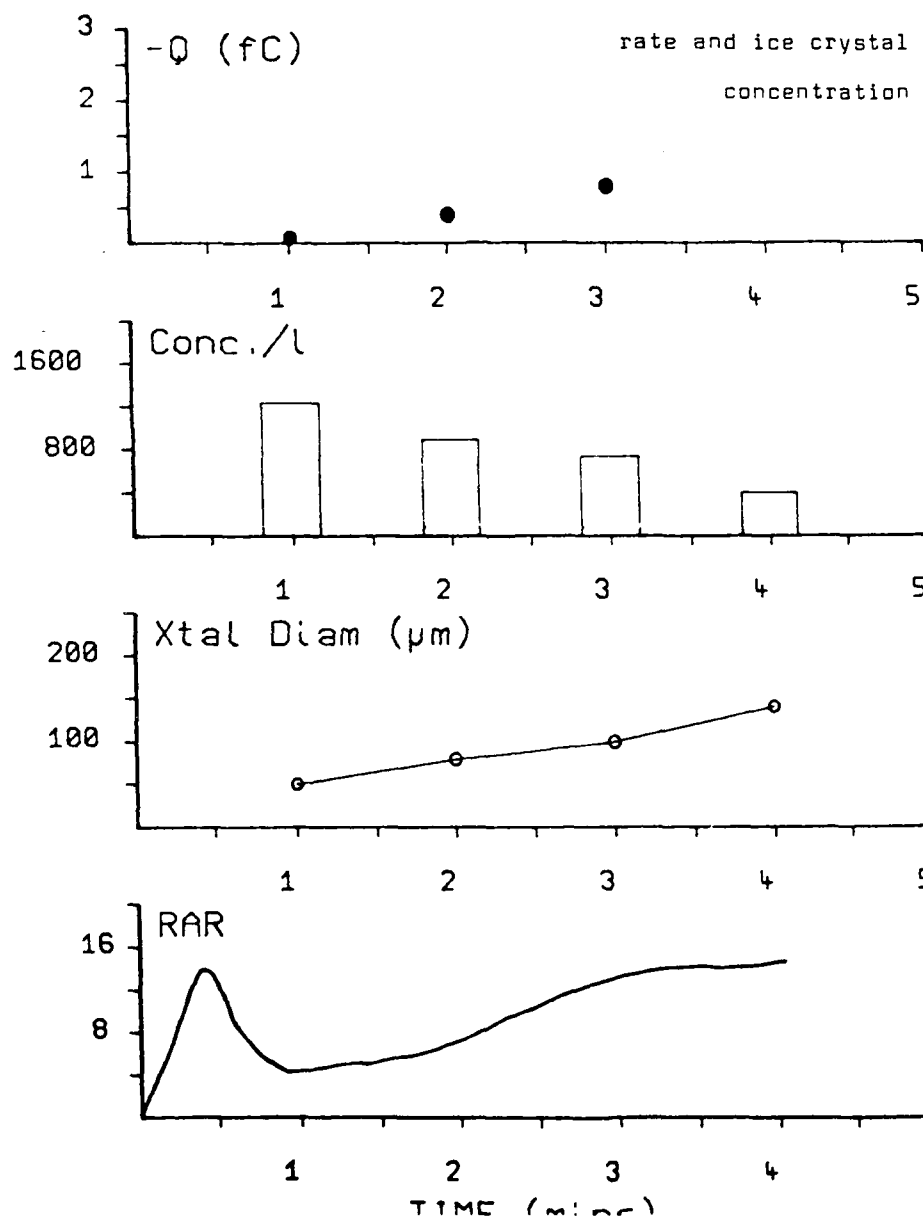
Figure 32

Charging current to 5 mm target at
-25°C and -29°C

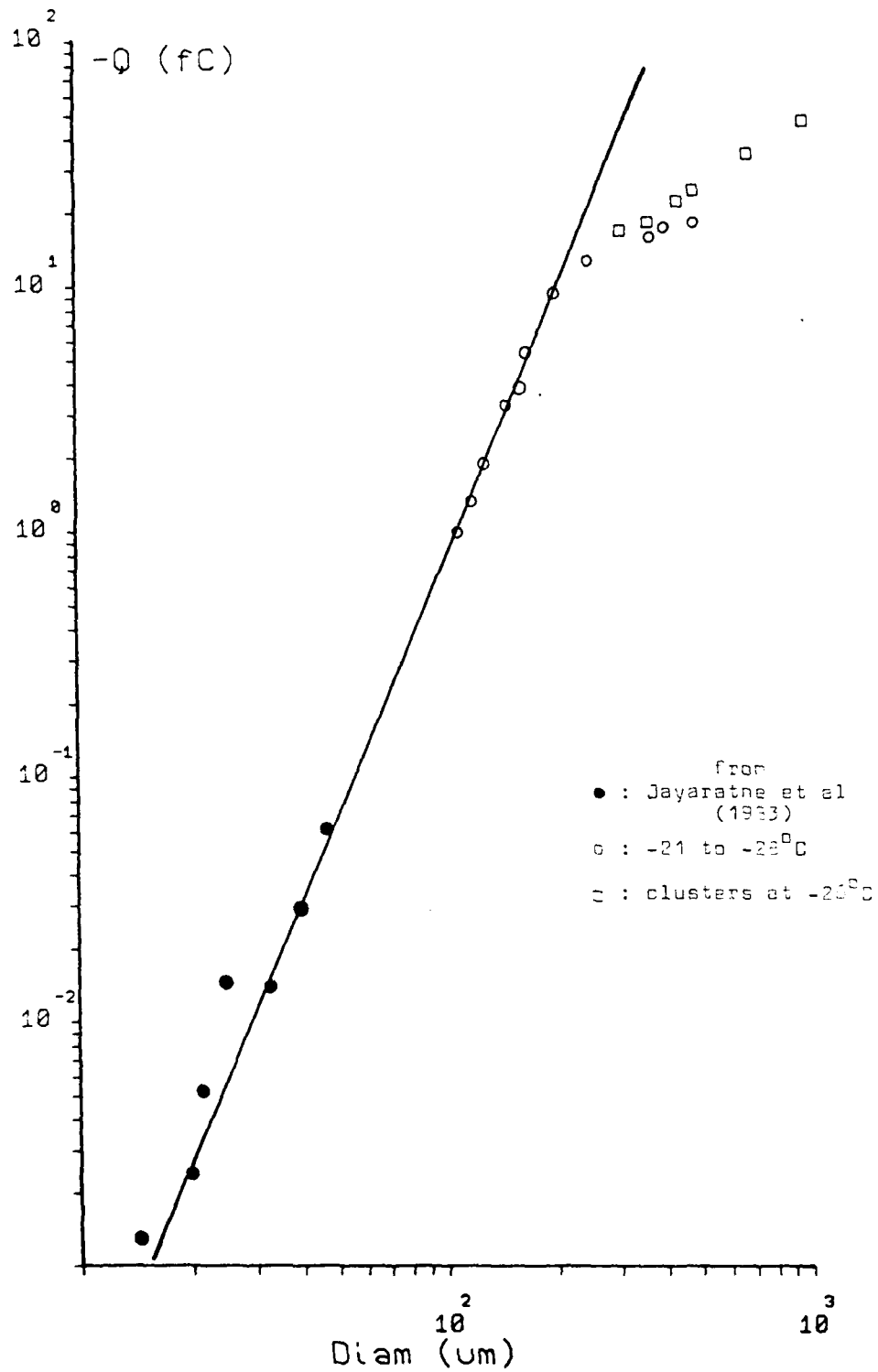




Typical run at -21°C showing
variation of rime accretion
rate and ice crystal size and
concentration



Charge per event vs ice crystal diameter relative charging regime



shown in the figure. A possible explanation for this is discussed later.

The Effect of the Rime Accretion Rate on the Charge per Event

A parameter which controls the sign and the magnitude of the charge per event is the rime accretion rate. At low values, the charging to the target is negative at all temperatures, whereas at high values the charging is positive. Jayaratne et al. found that the sign and magnitude of the charge per event was dependent on the cloud liquid water content, which can be calculated from the rime accretion rate if the droplet spectrum and the collection efficiencies of the target for the droplets is known. The method employed in this study was to measure the rime accretion rate, directly, from the temperature elevation of the target above ambient, which is caused by the freezing of the water droplets (see Appendix II). Thus the collection efficiencies and the droplet spectrum need not be known.

In the experiments presented here, the boiler power was varied so that the rime accretion rate varied from 0 to $25 \text{ mg cm}^{-2} \text{ min}^{-1}$ at different temperatures in different runs. The graph shown in Figure 35 illustrates the dependence of the sign of the charge per event on the rime accretion rate versus temperature. The dependence of the magnitude of the charge per event for a $150 \text{ }\mu\text{m}$ crystal on the rime accretion rate at -10°C is shown in Figure 36. At $3 \text{ mg cm}^{-2} \text{ min}^{-1}$ the charge per event is -2 fC rising to 70 fC at a rime accretion rate of $25 \text{ mg cm}^{-2} \text{ min}^{-1}$.

The Effect of Ice Crystal Growth Temperature

An attempt was made to grow large diameter single ice crystals for use at temperatures below -20°C in the presence of

Figure 35

Sign dependence on the rime accretion rate

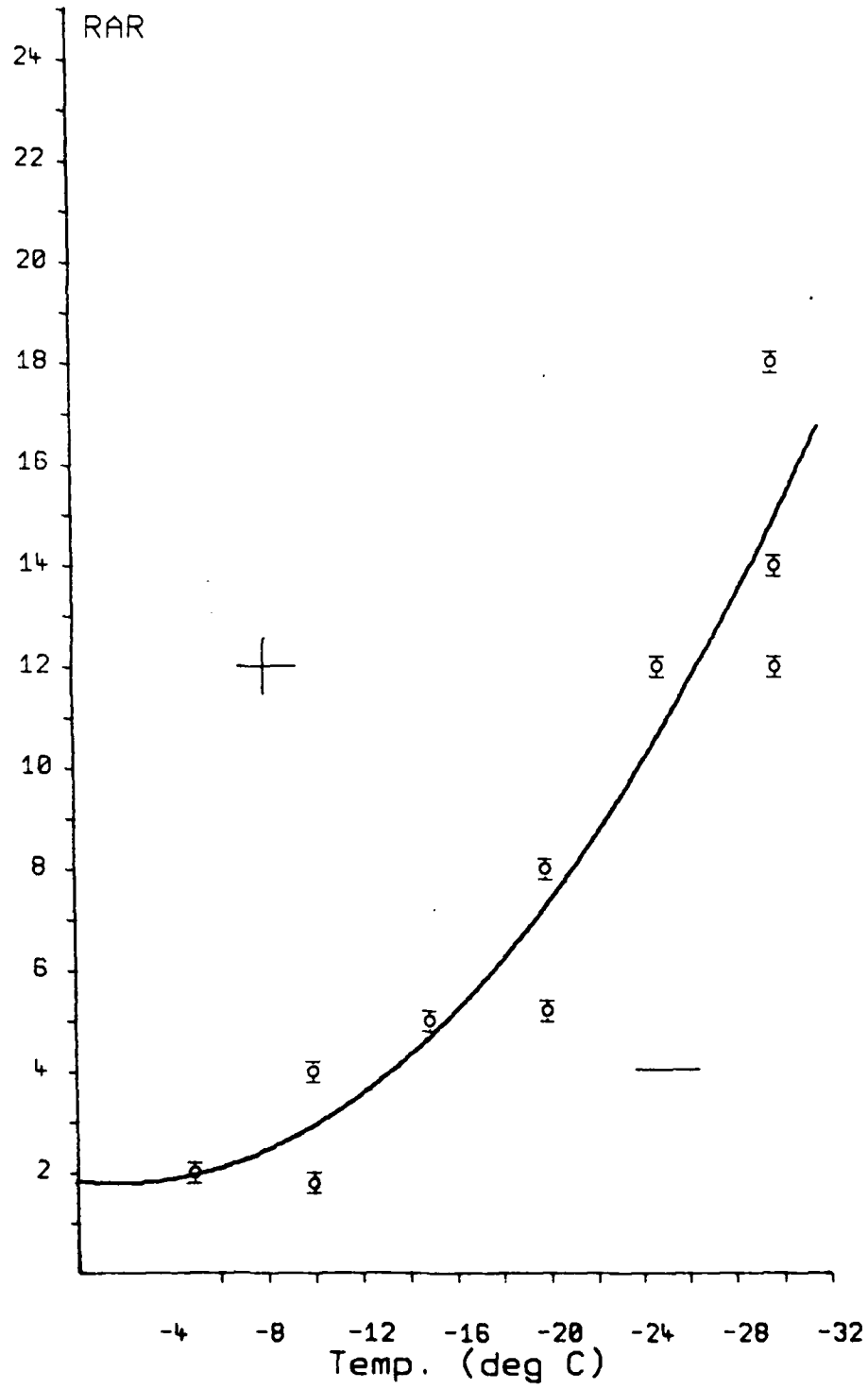
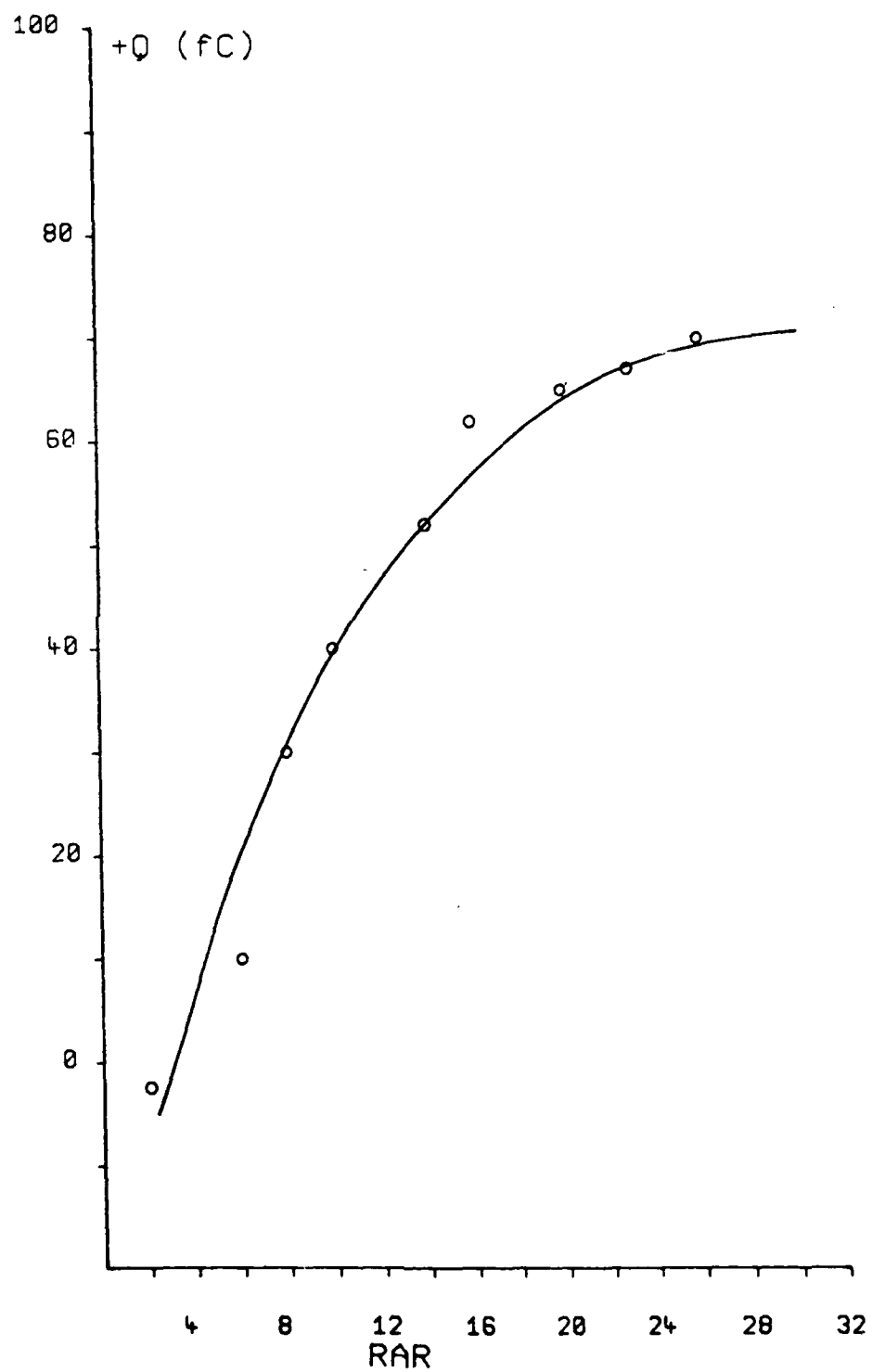


Figure 36

Effect of the rime accretion rate on the magnitude of the charge per event of a 150 μ m ice crystal



liquid water. The maximum growth rate occurs with dendritic crystals at -15°C and so the top chamber was warmed to -15°C whilst keeping the lower chamber well below the reversal temperature. Surprisingly, the resulting charge transfer to the target was positive, even though the lower chamber temperature was below -20°C . The sign of the charging is opposite to that normally obtained at these temperatures. Figure 37 shows two runs; one at -28°C with the upper chamber at -29°C and the other at -28°C , with the upper chamber temperature of -15°C . The two charging currents are of opposite sign, even though the air and rime surface temperatures of the two runs are the same. The rime accretion rate for both runs is also similar.

To investigate this unusual behaviour for crystals grown at -15°C but interacted at colder temperatures where negative target charging is expected, these experiments were repeated using stationary targets. Figure 38 shows the charging currents to the targets when the airflow is turned on, then off. The top chamber temperature was -15°C , whilst the lower chamber temperature was -28°C . The pump controlling the crystal flow past the target was turned on at certain times to measure the charging current in order to prevent the tube containing the target from rime closing. At time $t=0$, the trapdoor was opened and the pump was activated at $t=20\text{s}$; the sign of the charging current was positive even though the interactions were occurring below the reversal temperature. The kettle was then switched off and the crystals depleted the cloud and, at $t=90\text{s}$, the sign was negative. At this point, the crystals were evaporating in the unsaturated environment. Vapor was reintroduced at $t=240\text{s}$; shortly afterwards the pump was turned on and the sign was again positive; at this point the liquid water content was estimated to be about

0.5 g m⁻³. The above procedure was repeated with upper and lower chamber temperatures of -23 and -28°C respectively, when the target charged negatively (Figure 39). The small positive peak at the end of the run is due to the very high liquid water content of 3-4 g m⁻³ present in the chamber.

The initial positive charging current was reproducible if the upper chamber temperature was above the reversal temperature; below -18°C the charging was always negative. Negative charging for a warm upper chamber could also be obtained if the liquid water content was below 0.1 g m⁻³. The consequences of these results are discussed later.

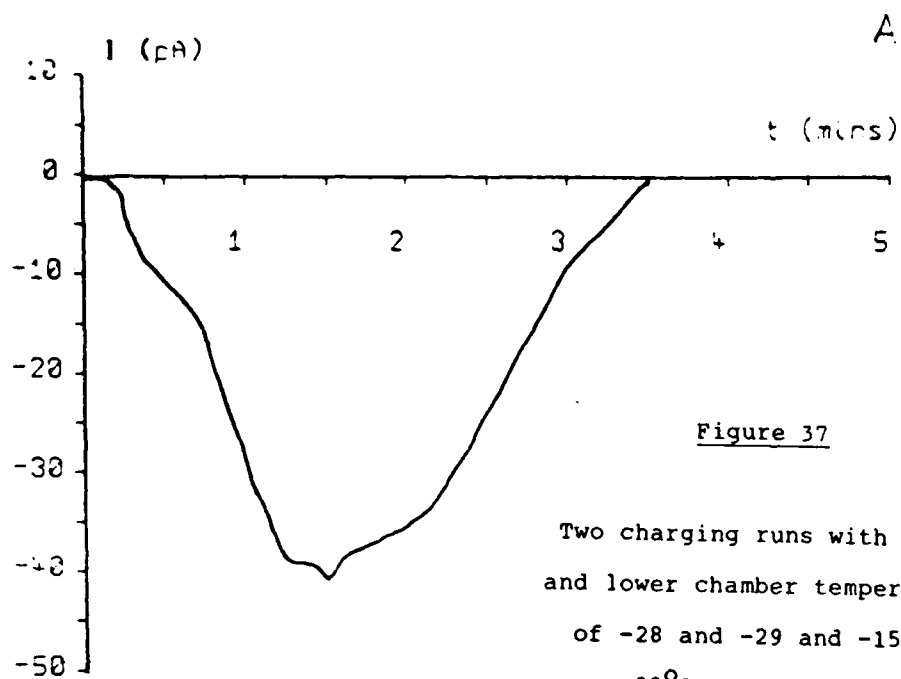


Figure 37

Two charging runs with upper
and lower chamber temperatures
of -28 and -29 and -15 and
-28°C respectively

A : -28/-29°C

B : -15/-28°C

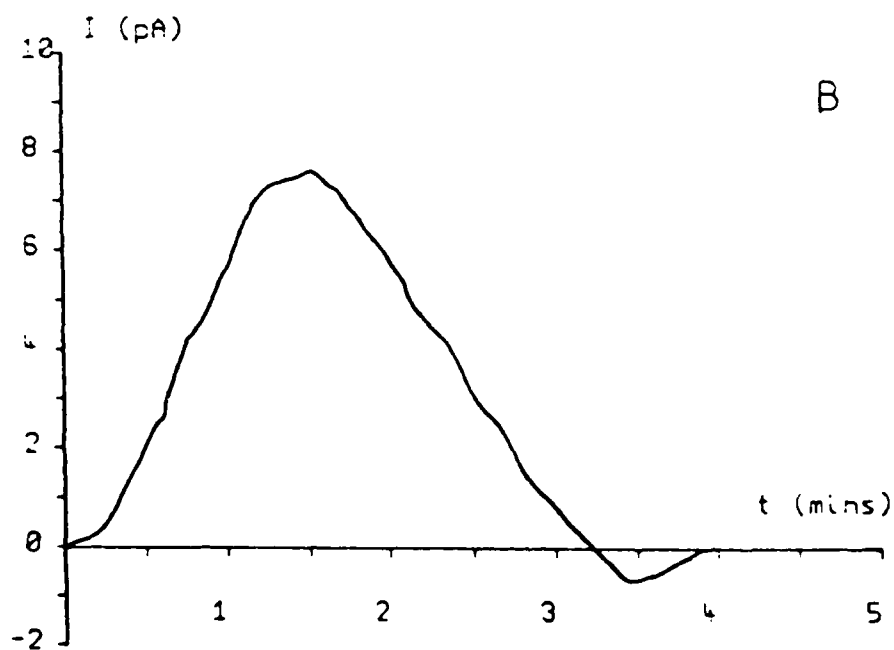


Figure 33

Three charging runs at speeds of 50, 25 and 10 m/s for an ice crystal growth temperature of -15°C

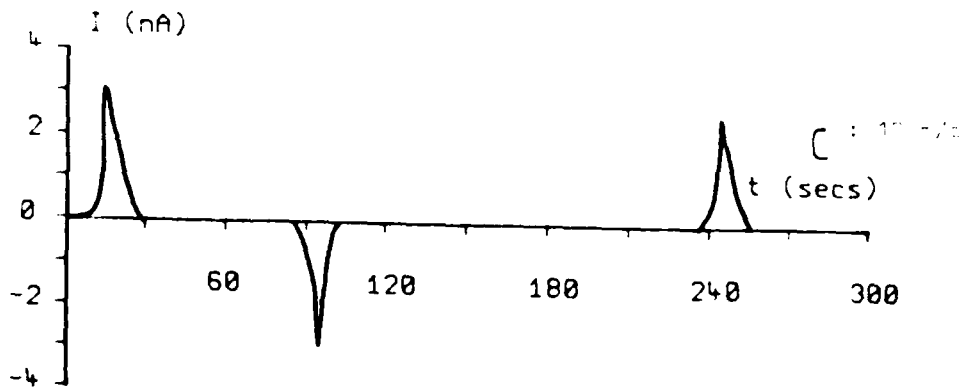
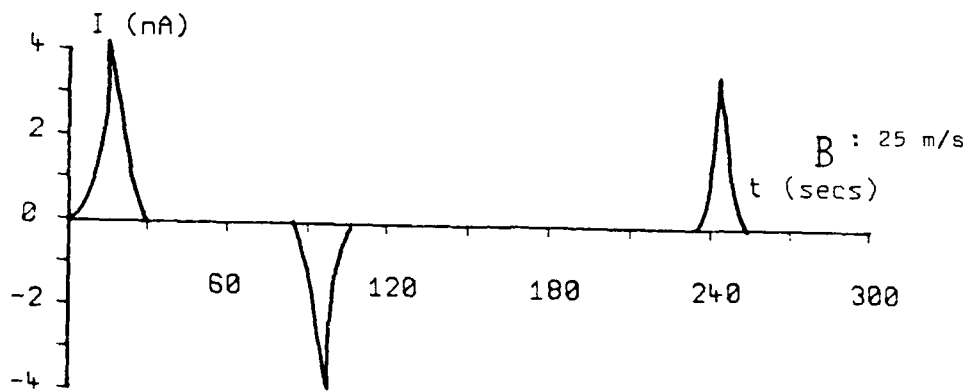
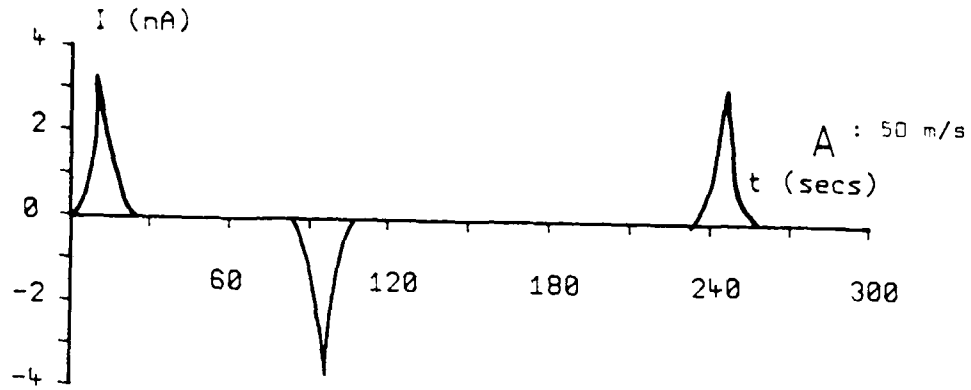
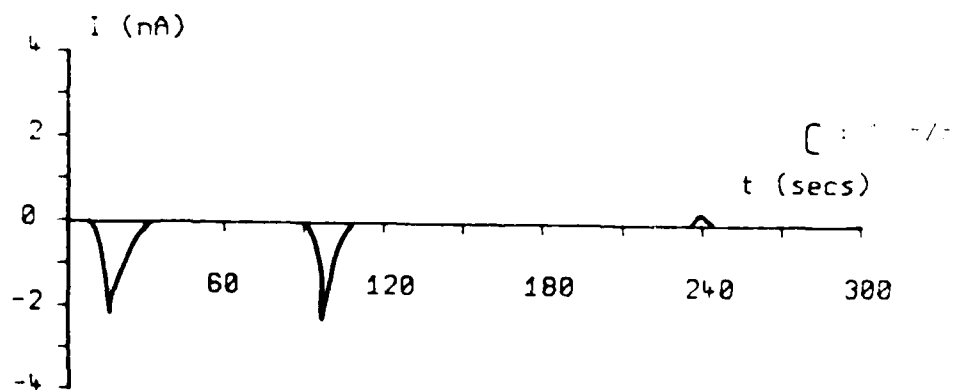
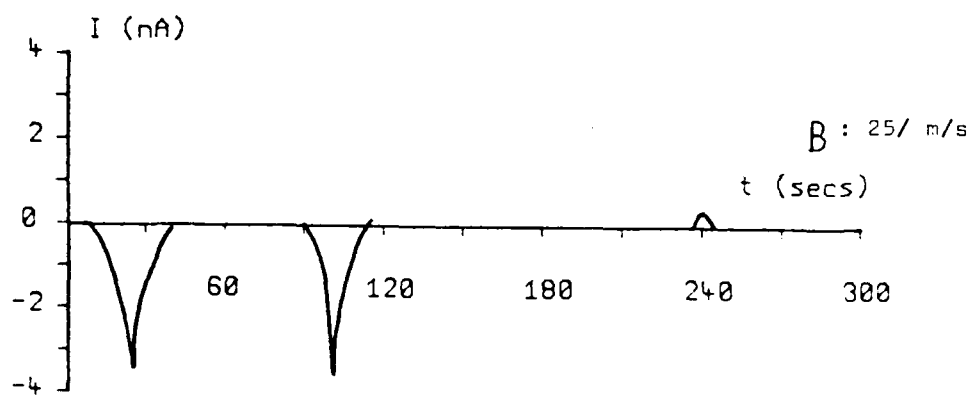
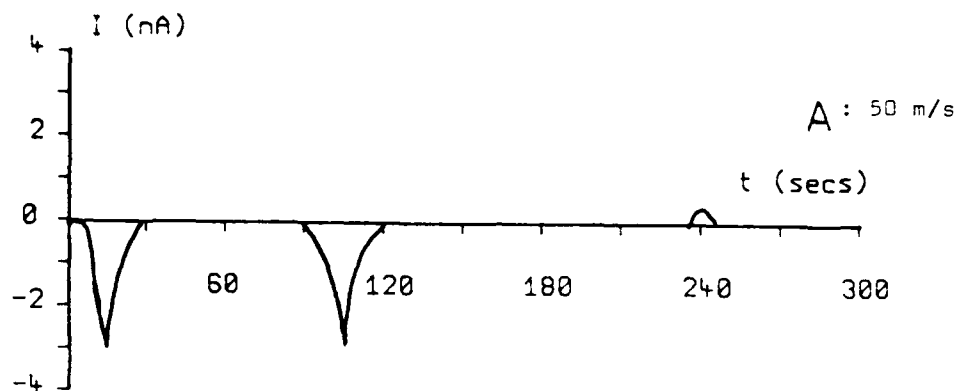


Figure 39

Three charging runs at speeds of 50, 25 and 12 m/s for an ice
crystal growth temperature of -23°C



Charging in the Presence of Ice Crystals Alone

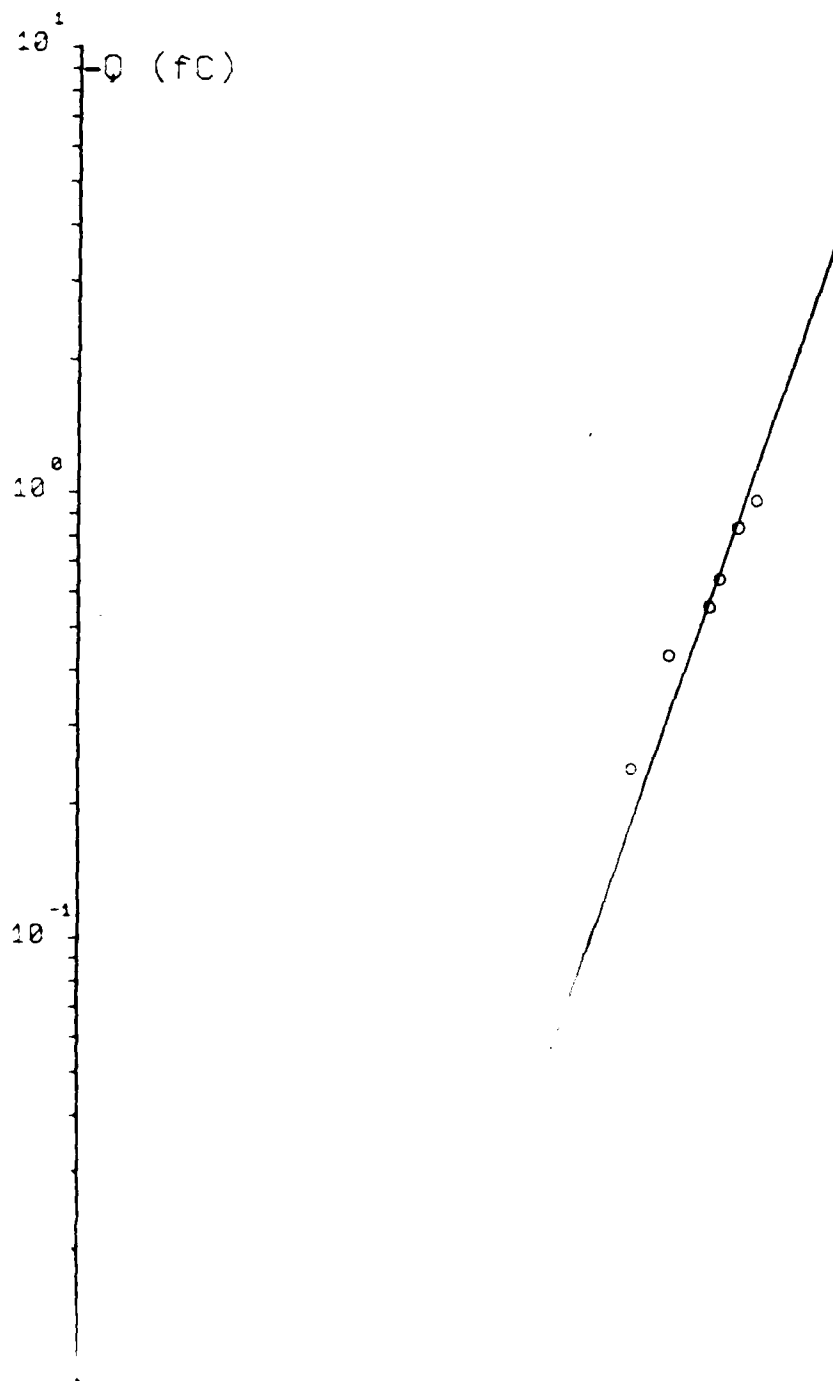
A cloud consisting of ice crystals only was obtained by seeding a supercooled cloud of water droplets, switching off the vapor supply and allowing the crystals to use up all the available water vapor. In this manner, experiments could be performed without any water droplets being present. The apparatus was rotated at 3 m s^{-1} through a cloud of $120 \text{ }\mu\text{m}$ plate crystals; no charging was detected above the noise on the amplifier which was consistent with the results of Jayaratne et al. However, when ice crystals greater than $200 \text{ }\mu\text{m}$ in diameter interacted at a speed of 3 m s^{-1} negative charging was measured. Figure 40 shows the charge per event against crystal diameter. The magnitude of the charge per event ranges from -0.1 fC for a $200 \text{ }\mu\text{m}$ crystal to -1 fC for a $500 \text{ }\mu\text{m}$ crystal. These values are about 1 order of magnitude smaller than the values of negative charging obtained at low liquid water content, and two orders of magnitude lower than the positive charging obtained at -15°C at a liquid water content of 1 g m^{-3} .

Low Velocity Charging

Jayaratne et al. (1983) found that the charge per event increased with impact velocity raised to the power 3.2 for small ice crystals. Similar experiments were performed with $200 \text{ }\mu\text{m}$ ice crystals in a mixed cloud at -12°C and -25°C . The maximum permissible velocity with the rotating apparatus was 6 m s^{-1} . The cloud liquid water content was controlled to give the same rim accretion rates for all the velocities investigated. Figures 41 and 42 show the charge per event at different velocities at the two temperatures. The figures also show the results discussed in the following section at 10 and 25 ms^{-1} .

FIGURE 40

Q vs α at 3 m/s for ice crystals only



AD-A189 490

ICE PARTICLE CHARGE TRANSFER STUDIES(U) UNIVERSITY OF
MANCHESTER INST OF SCIENCE AND TECHNOLOGY (ENGLAND)
DEPT OF PHY SICS C P SAUNDERS 30 SEP 87 EOAD-TR-87-10
AFOSR-85-0282 F/G 20/3

2/2

UNCLASSIFIED

NL

100
100
100
100

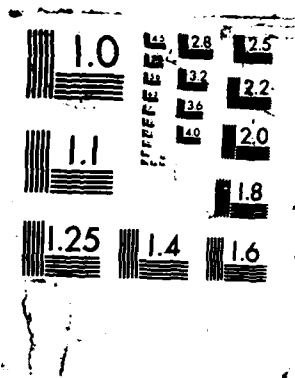


Figure 41

Dependence of the charge per event on the impact velocity at -12°C

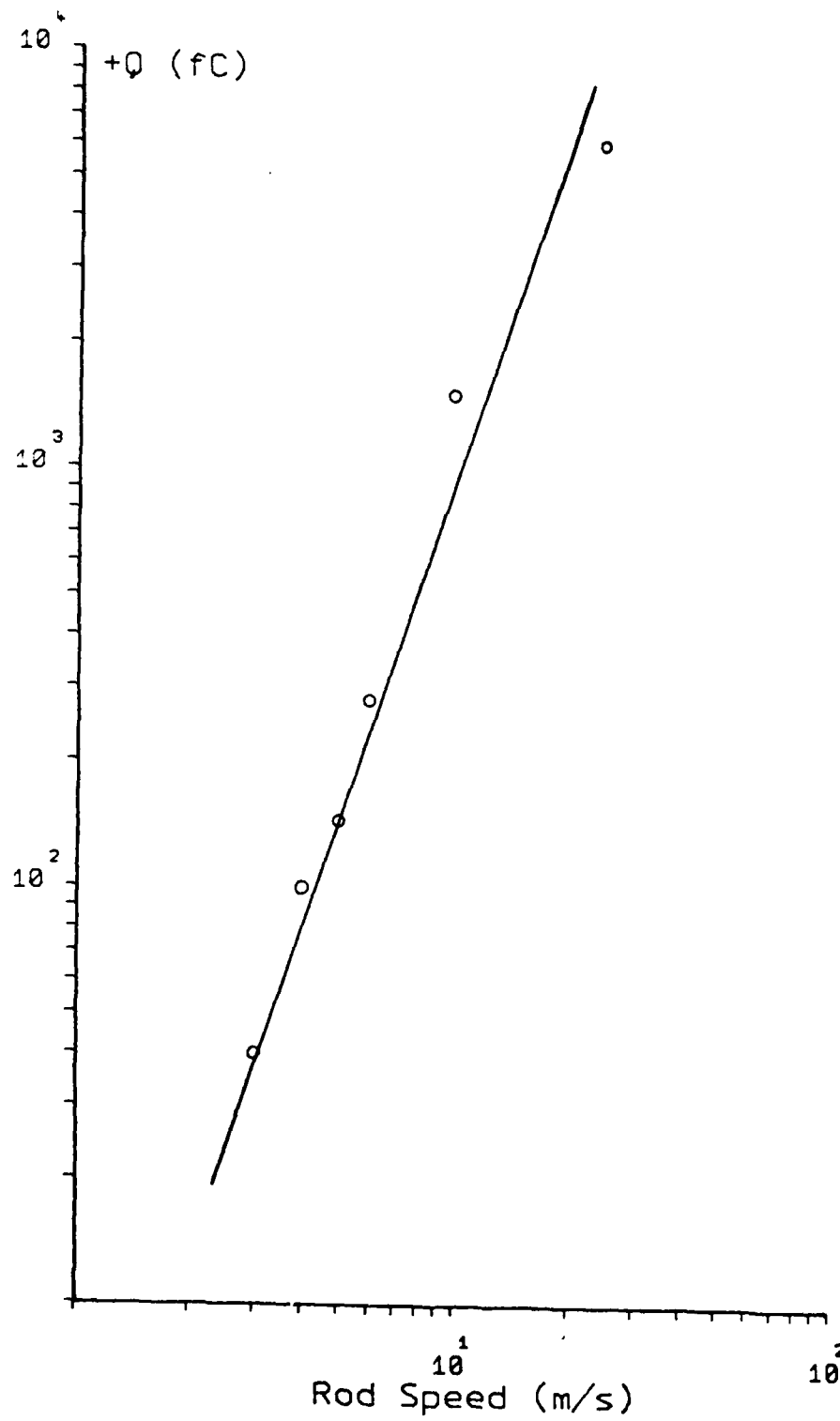
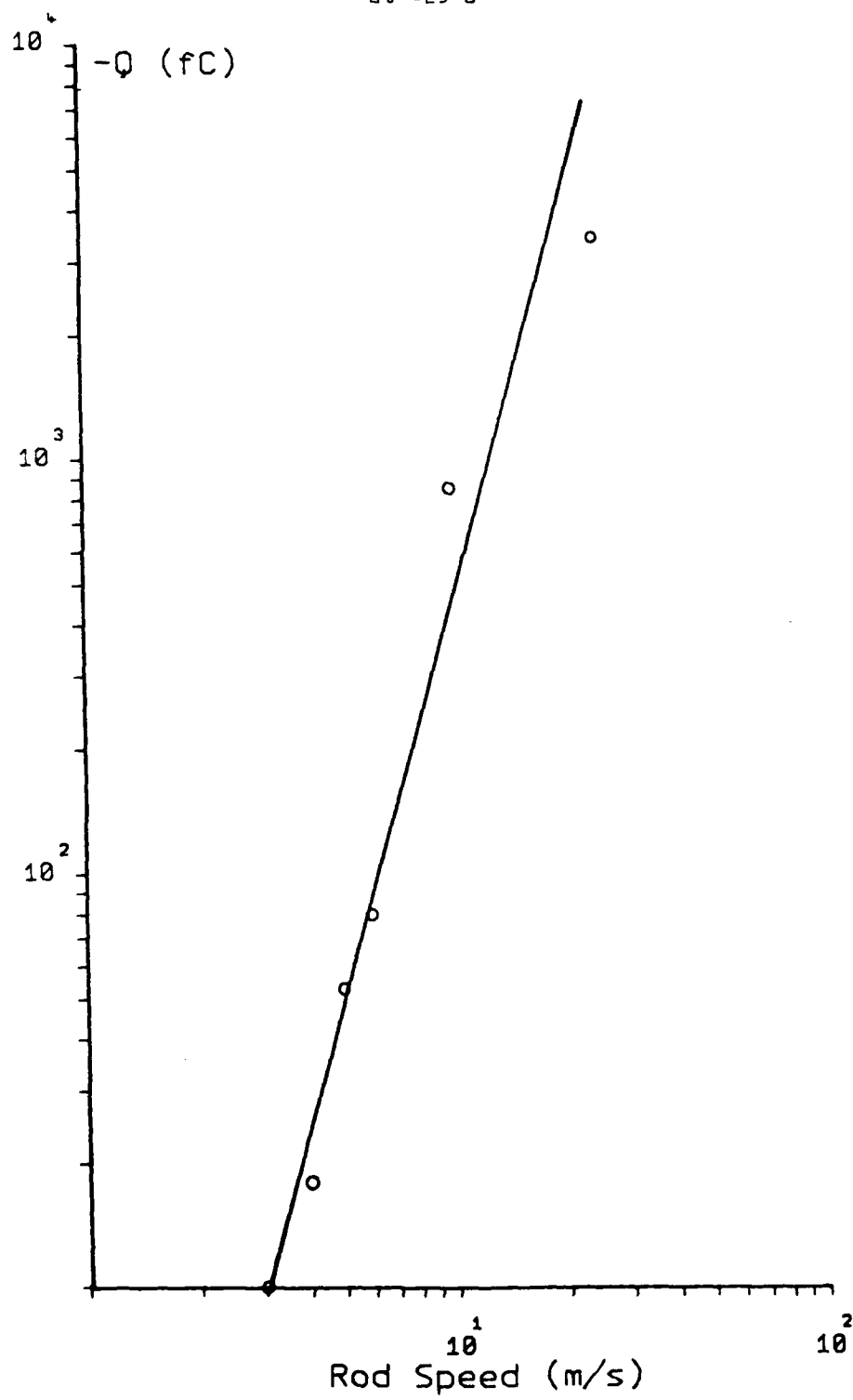


Figure 42

Dependence of the charge per event on the impact velocity
at -25°C



High Velocity Charging

Charging with Ice Crystals Alone

In these experiments, the amplifier ratio was changed so that $1\text{mV} \equiv 10^{12}\text{ A}$. At the greater sensitivity the amplifier was swamped by the large charges being separated. The crystal cloud was produced in the usual way, and the crystals were allowed to fall out until only a small concentration of about 10^4 m^{-3} remained.

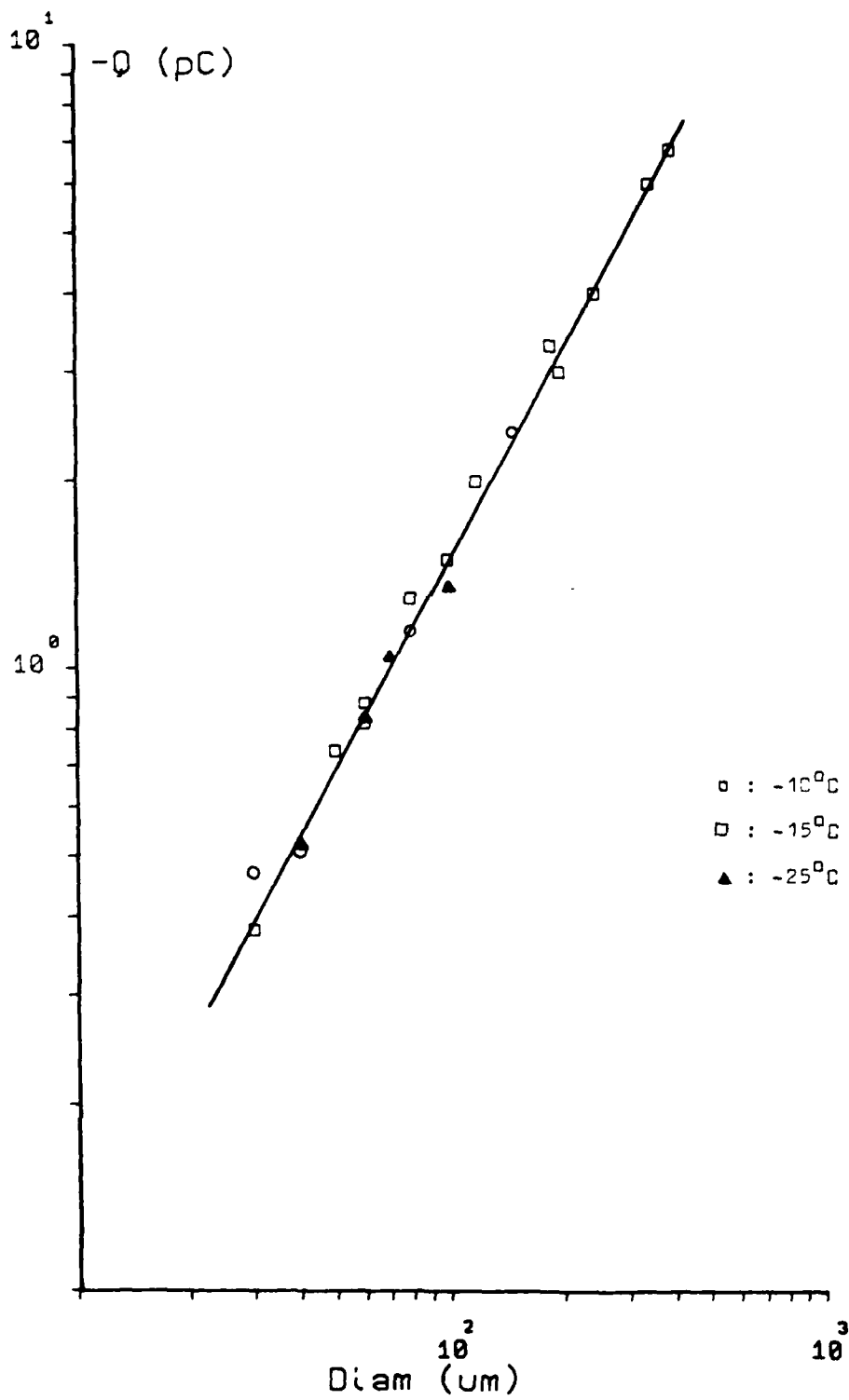
The pure crystal cloud was drawn past a 5mm diameter metal target at a speed of 110 m s^{-1} . The crystal concentration was determined from a microscope slide just before the pump was switched on. It was assumed that the crystal concentration drawn past the target for the first 15 seconds of a run was constant, after which time the crystal concentration was depleted. The charge per event was calculated from the crystal concentration and the initial negative peak. The event probability was found to be unity, as there was no evidence of any crystals on the target at the end of a run. Strong negative charging was measured at all temperatures and all crystal diameters.

Figure 43 shows the charge per event against crystal diameter at a speed of 110 m s^{-1} . In agreement with Jayaratne et al., the sign of the charging current is negative when the target is evaporating. The figure illustrates that large amounts of charge are being separated; for example, a $500\text{ }\mu\text{m}$ crystal separates about -10 pC , which is 3 orders of magnitude greater than the charge measured at 3 m s^{-1} .

These experiments were repeated with a previously rimed target. The target was rimed for a few seconds; the cloud was then seeded and the experiments conducted as before at 110 m s^{-1} . There was no effect due to the presence of the rime, as illus-

Figure 43

Q vs d at 110 m/s for crystals only



trated by Figure 44 which plots points from the two sets of experiments at equal values of crystal sizes. There is a close 1:1 relationship between the charge per event of the rimed target, QR, with that of the unrimed target, Q.

Charging in a Mixed Cloud

The riming experiments were conducted with the stationary target by allowing a few droplets to remain in the ice crystal cloud. The Macklin and Payne equation (Appendix II) shows that at these high velocities, a very low liquid water content of 0.1 g m^{-3} will lead to a temperature rise from which a rime accretion rate of $14 \text{ mg}^{-3} \text{ min}^{-1}$ may be calculated.

The apparatus was modified so that the cloud could simultaneously be drawn past three targets at different speeds, which enabled direct comparison between three speeds under the same cloud conditions to be made. The target diameter was 1.6 mm and the flow speeds used initially were 75, 50 and 25 m s^{-1} . The event probability is unity for all crystal diameters at these velocities. Figure 45 shows currents from the three targets at a temperature of -15°C . The fact that the shape of the curves is the same verifies that the targets are experiencing the same cloud conditions. Figure 46 shows positive charge per event against crystal diameter for these three velocities. It can be seen that the three lines are roughly parallel but that more charge is separated at the lower speed.

The apparatus was also used at a temperature of -25°C . The sign of the charging was negative but the same pattern of velocity dependence was observed. Figure 47 shows the charging current to the targets at this temperature. The shape of the current versus time is the same for all the targets, thus con-

Figure 44

Q vs QR at 110 m/s

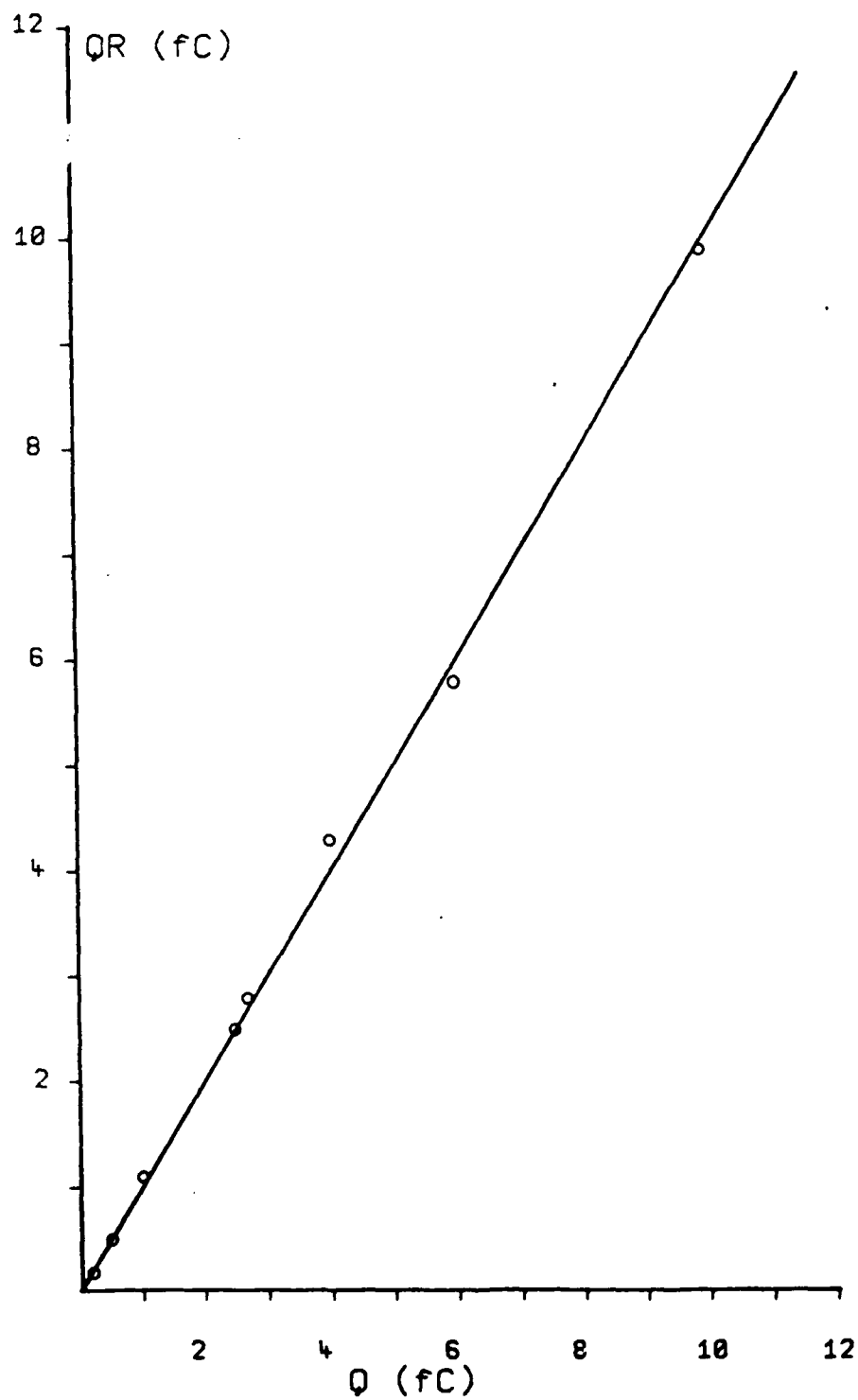


Figure 45

Typical charging run at -15°C for speeds of 75, 50 and 25 m/s

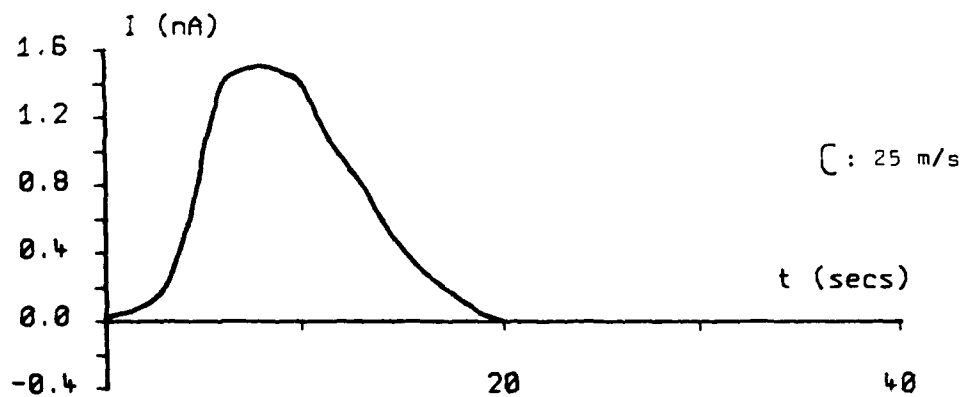
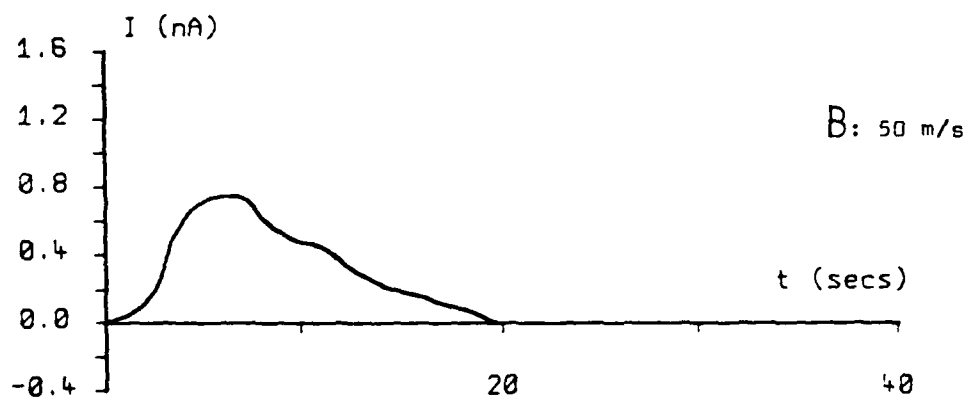
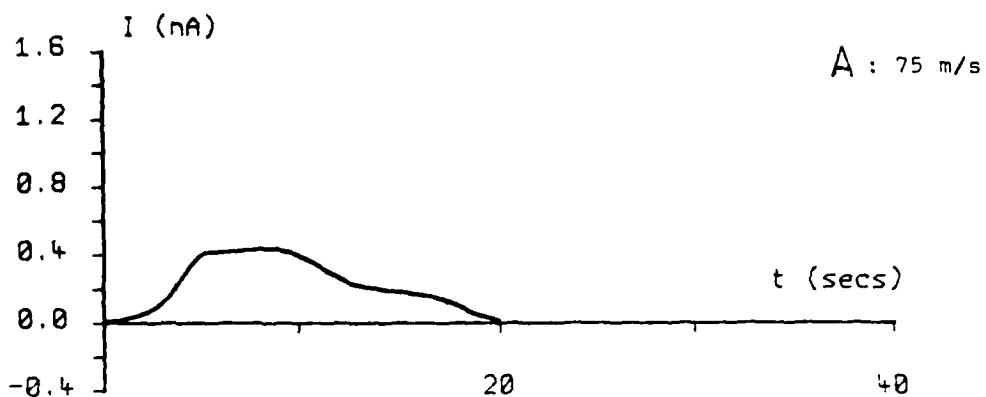


Figure 46

Q vs d for speeds of 75, 50 and 25 m/s at temperature
of -15°C

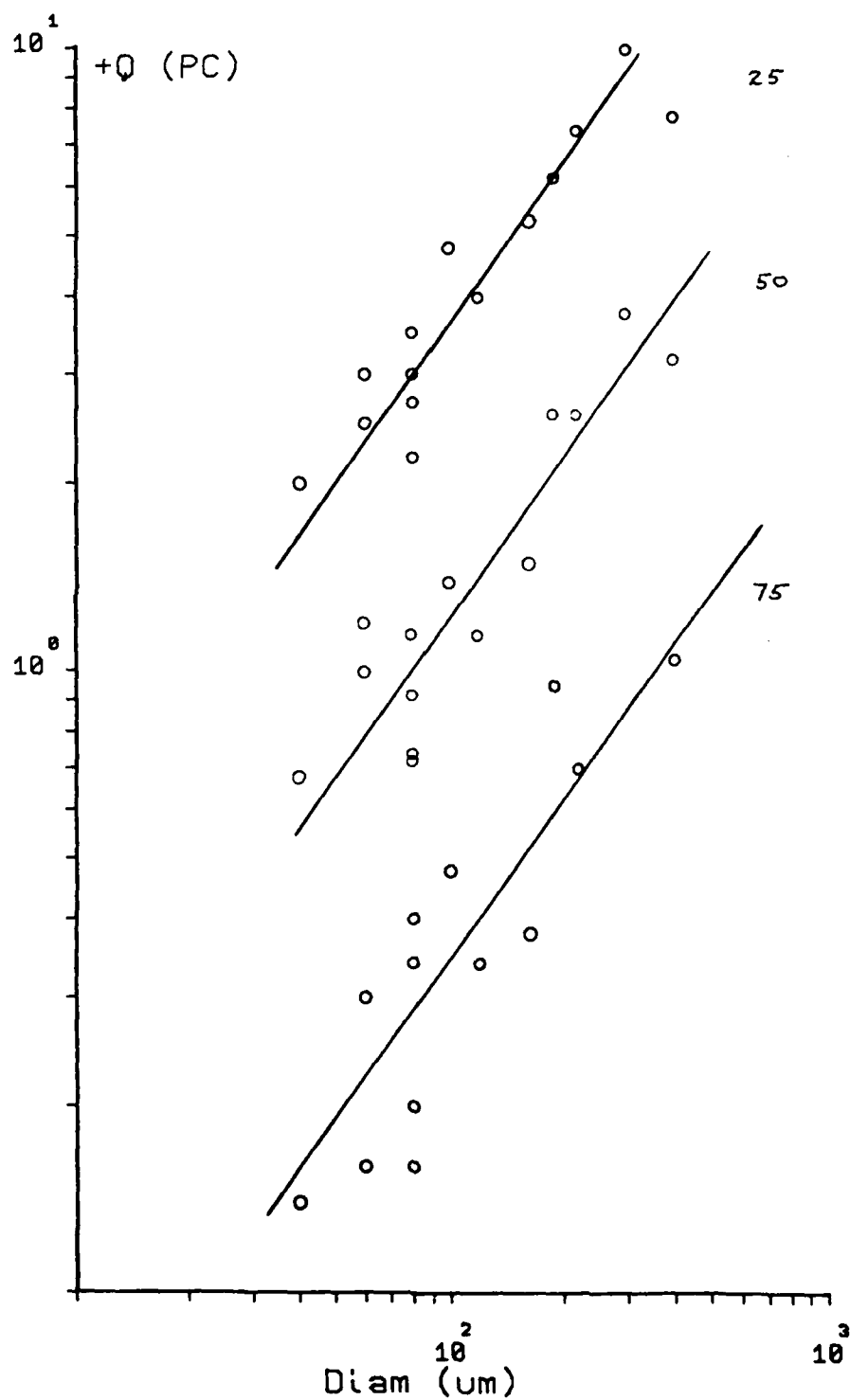
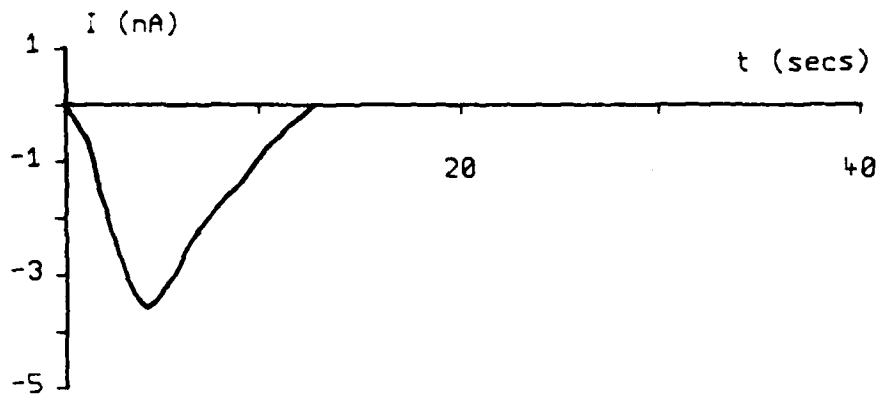


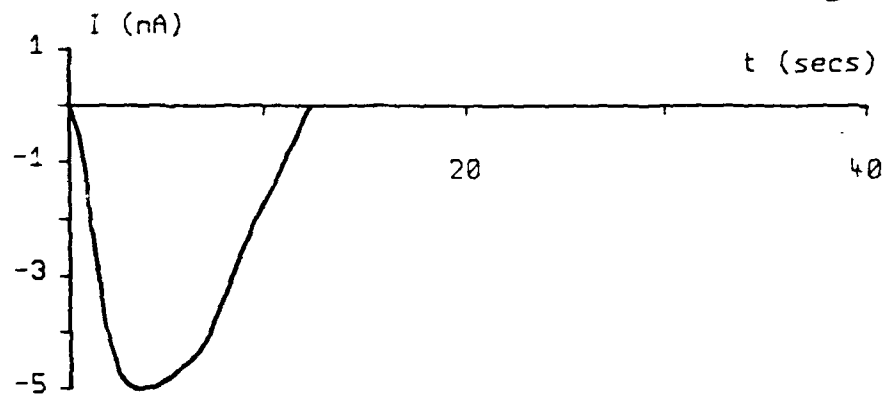
Figure 47

Typical charging run at -25°C for speeds of 50, 25 and
10 m/s

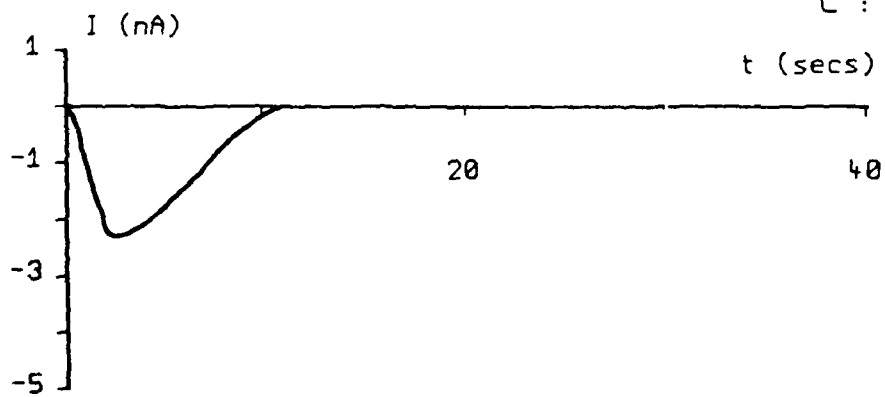
A : 50 m/s



B : 25 m/s



C : 10 m/s



firming that they are experiencing the same cloud conditions. Figure 48 shows the charge per event against crystal diameter, with maximum values at 25 m s^{-1} . The gradients of the graphs for both positive and negative charging is 0.7. A possible explanation for the velocity dependence is discussed in the following section.

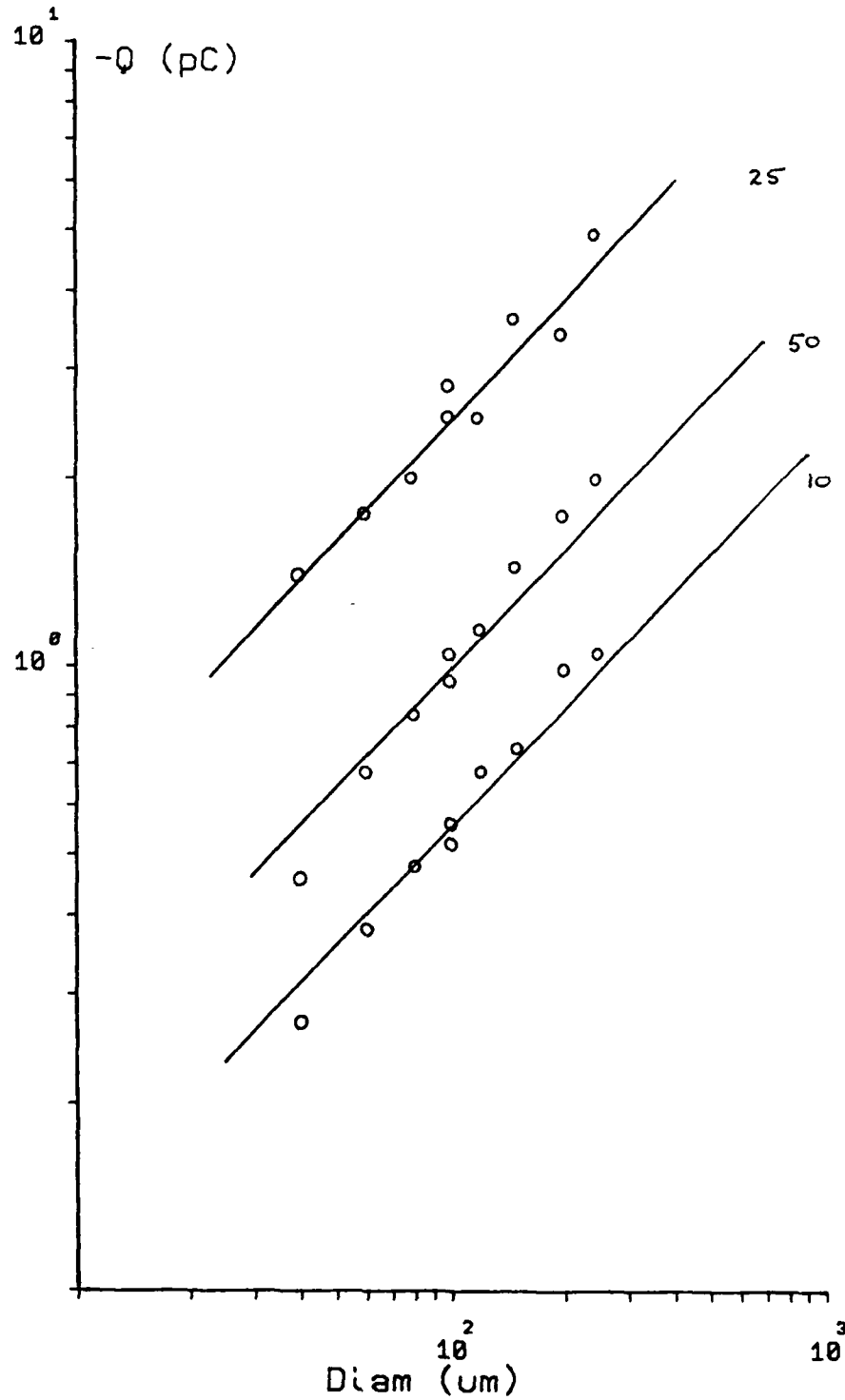
Discussion

Large amounts of charge are generated when an ice crystal hits and rebounds from a riming hailstone. The magnitude and sign of the charge is dependent on the rime accretion rate, the ice crystal diameter, the impact speed and the cloud temperature. Jayaratne et al. (1983) found the dependence of the charge per event with crystal diameter up to $120 \mu\text{m}$. These positive charging results were extended to a diameter of $800 \mu\text{m}$ and both sets of results, which have been corrected with revised values of event probability determined in the present study, are shown in Figure 49. It can be seen that the charge per event changes shape at $150 \mu\text{m}$ and $480 \mu\text{m}$. For example, a $350 \mu\text{m}$ crystal, according to the Jayaratne prediction, would separate $+1.25 \text{ pC}$, whereas these experiments have shown that it only separates $+0.1 \text{ pC}$, roughly one order of magnitude less. This would suggest that there is some mechanism which is limiting the amount of charge being separated. There was no dependence of the charge per event on crystal type.

In the negative charging regime, the deviation from the Jayaratne experimental line occurs at $210 \mu\text{m}$; Figure 50 shows both the new and the Jayaratne data. The deviation from the previous data is greater than for the positive case; for example, a $350 \mu\text{m}$ crystal, from the Jayaratne data, is predicted to sep-

Figure 48

Q vs d for speeds of 50, 25 and 10 m/s at temperature of
-25°C



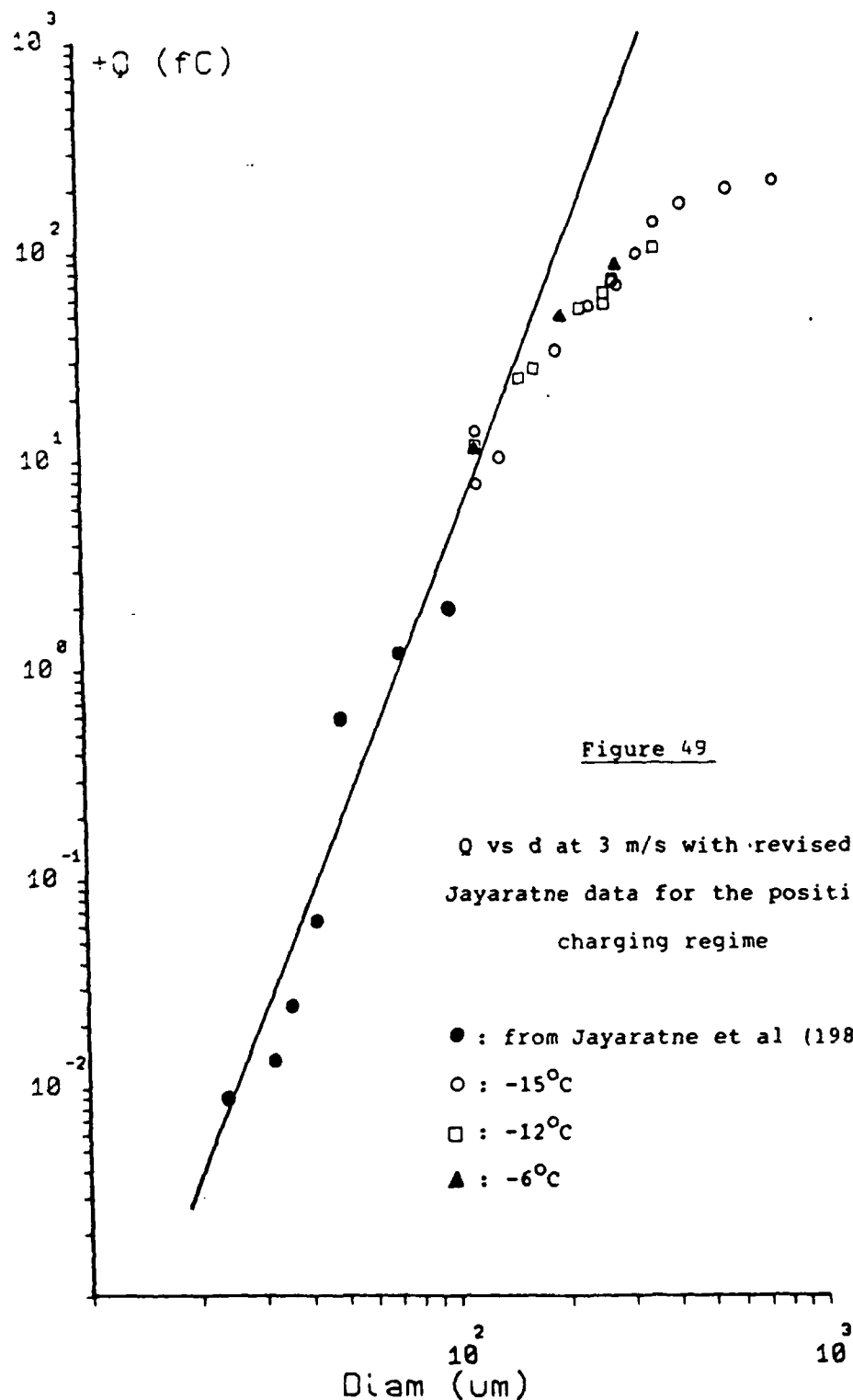
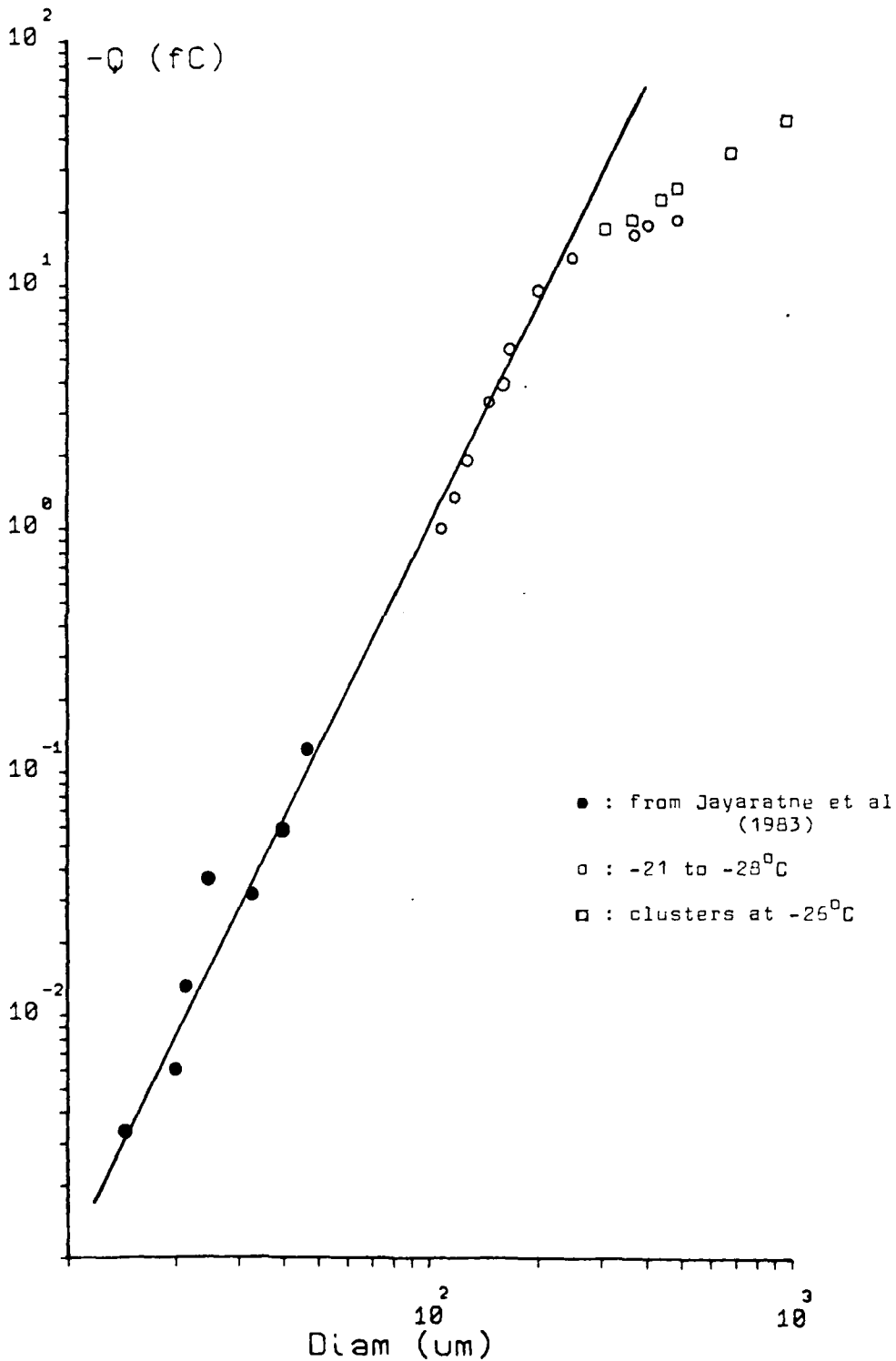


Figure 50

Q vs J at 3 m/s with revised Jayaratne data for the negative charging regime

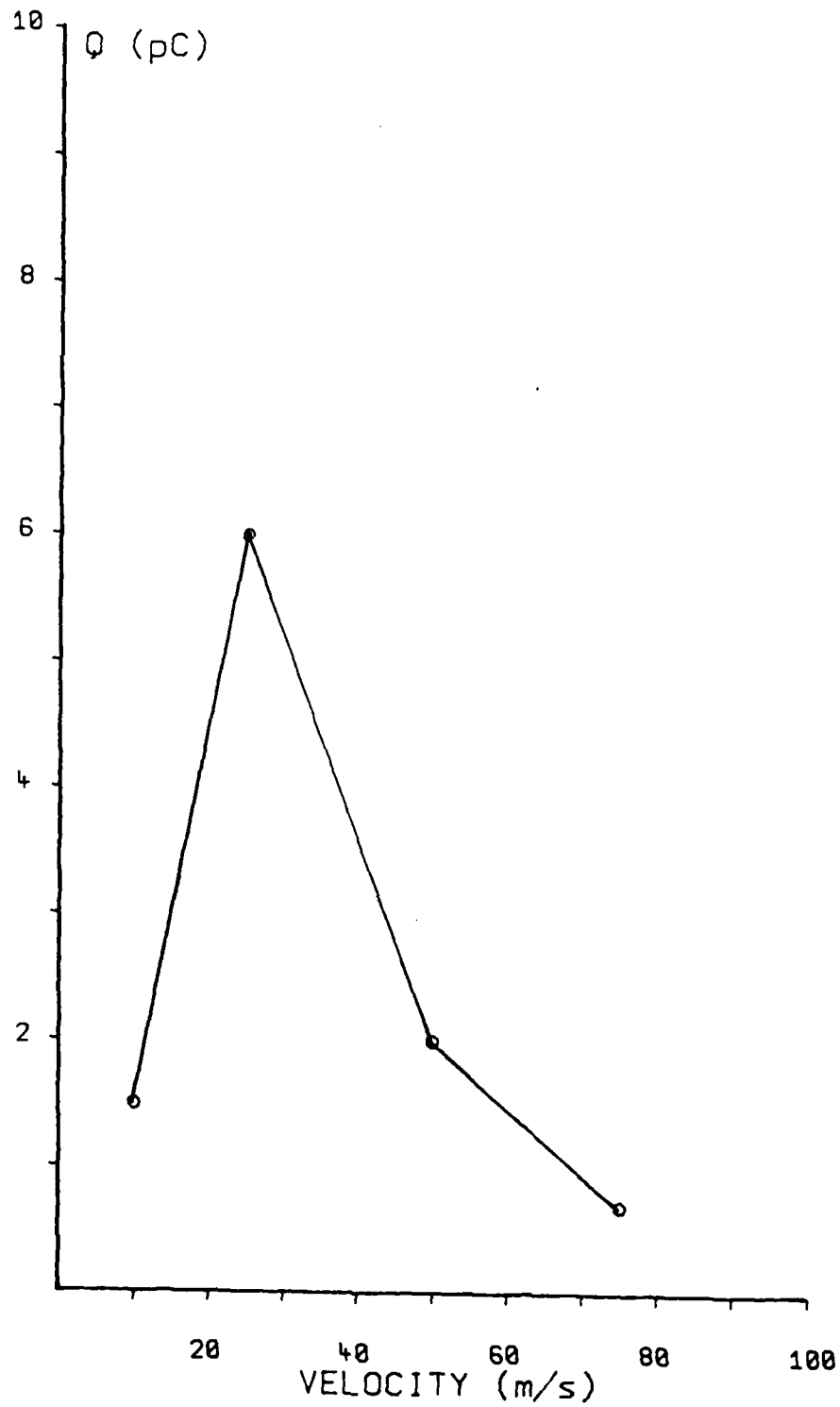


arate 57 fC but, in reality, it only separates 1.8 fC. The largest crystal produced in this regime was 500 μm . The charge per event for the bullet clusters was greater than that for a single crystal of the same size due to the cluster shattering on impact.

The high speed collision experiments were designed to simulate the charging of an aircraft as it flies through a cloud. In regions of zero liquid water content, the target charged negatively at all temperatures. However, the collection efficiency for water droplets at these speeds is such that a very low liquid water can give a high rime accretion rate and consequently lead to positive charging. This was the case with the 1.6mm targets; under cloud conditions which gave negative charging to the 5mm target, the smaller target measured positive charging due to its greater collision efficiency. Thus, it was quite difficult to ensure a zero liquid water content in the crystal only experiments with the 1.6mm targets. The velocity dependence was opposite to that expected, in that the high velocities produced less charge than at lower velocities. Figure 51 illustrates the charge per event for a 200 μm crystal against air speed. It shows that the charge per event is a maximum at about 25 m s^{-1} . This can be explained in terms of the contact time and the sticking efficiency. As the contact time between the hailstone and the ice crystal increases, the charge transfer also increases until some equilibrium between the particles is reached and the charge transfer decreases. Thus, if the contact time for an impact speed of 110 m s^{-1} is less than that at 25 m s^{-1} , then less charge would be separated at the higher speed.

Figure 51

Charge per event for 200 μm crystals at impact speeds
of 75, 50, 25 and 10 m/s



SECTION 7

DISCUSSION, CONCLUSION AND FUTURE WORK

The hot-wire device discussed in Section 3 is useful for measurements of the liquid water content in clouds. The novel approach here is that the wire is heated by a chain of fixed amplitude voltage pulses whose mark-space ratio is varied to control the mean power dissipation in the wire. A wire temperature of 76°C was chosen for maximum sensitivity and to avoid the formation of an insulating layer of liquid over the wire surface at high temperatures. The output is simply calibrated using a cloud of known liquid water content (determined by another longer and more tedious method). The device is accurate to 4% at 1 g m^{-3} .

A cylindrical target has a collection efficiency for water droplets which is dependent on the target diameter, the air temperature and the droplet diameter. Theoretical collision efficiencies have been calculated for smooth targets; however, rough targets present a more difficult problem. The experiments described in Section 4 show that the collision efficiency is increased at temperatures below -10°C and at air speeds below 5 ms^{-1} due to the growth of 'rime feathers' on the target surface. At higher speeds, the growth of the feathers is inhibited. An equivalent collector diameter has been defined as the diameter of a smooth collector whose collection efficiency is the same as that of the rimed collector. At temperatures below -10°C at an air speed of 3 m s^{-1} the equivalent collector diameter of a 5mm rimed target is 3.2mm. At 5 m s^{-1} for the same conditions the diameter is 4.8mm. At the lower speed, the weighted collection efficiency is increased by almost 50% due to the presence of the

rime feathers.

The collision efficiency of a cylindrical target for ice crystals has not been modelled theoretically and has only been studied in a limited way before. The results described in Section 5 show that the collision efficiency is unity for crystals greater than 80 μm at a flow speed of 3 m s^{-1} . A simple relationship between crystal diameter, target diameter and flow speed was found.

The target, moving at 3 m s^{-1} , did not undergo detectable or significant charge transfer in a cloud consisting only of crystals if they were smaller than 120 μm . Above this size, a weak negative charge was measured which was dependent on crystal size. At high speeds strong negative charging of about 1 pC per event was measured at all temperatures. The charge per event was found to be dependent on the impact speed with a maximum value at around 25 m s^{-1} . Impacts on airplanes at high speeds may, therefore, not lead to charge transfer.

The above mentioned work was all preliminary to the achievement of the main objectives of this study. In order to calculate the charge separated by an individual crystal bouncing off an ice target in the laboratory experiments, the concentration of crystals in the cloud is needed, the collection efficiency or, in our case, the event probability is required, and the current to the ice target must be measured to provide a value of the charge per event.

Experiments carried out have followed the lines of previous investigations, with the exception that larger ice crystals than have been available before have been used. Studies of charge transfer for both the positive and negative regimes at temperatures on either side of the reversal temperature, have been made

with ice crystals up to 800 μm in diameter. Previous results with crystals up to 100 μm had shown that the charge/size dependence was to the fourth power. This result has been verified. However, at larger sizes the charge transfer power dependence decreases dramatically, falling to a value of order unity for crystals around 500 μm . This decrease with larger crystal sizes is noted for both positive charging and negative charging, which suggests that the charge transfer mechanism is the same for both signs of charging. With crystals alone in the cloud the charge transfer was weak and this situation is probably not of significance in thunderstorms.

Jayarathne and Saunders (1985) extrapolated their d^4 relationship to larger sizes than those investigated in the laboratory experiments to account for lower positive charge centers (LPCC). They calculated that a 3mm diameter graupel particle falling 1 km through a crystal concentration of 10^4 m^{-3} would acquire a charge of +35 pC if the charge separated in each interaction was 500 fC. They assumed that the size of the crystals was 200-300 μm with an event probability of 0.1. However, the results presented here show that a 300 μm crystal will separate about 80 fC and that a 3mm graupel particle has an event probability of 0.5 at 3 m s^{-1} . Thus the particle will acquire about 29 pC. Surprisingly, therefore, the lower than expected values of charge transfer for larger crystals have not led to a significant fall in the total charge transfer, simply because of the increased values of event probability with the larger crystals.

The charge separated when an ice crystal of diameter d rebounds from a hailstone can be calculated from the following relationship: $Q = Ad^a v^b$ where v is the impact velocity. Jayaratne et al. found that the constants a and b take the values

4 and 3 respectively. The present study has shown that $b=2$ for low velocities and a takes values to between 0.3 and 2. The range of values of a is due to the dependence on crystal size. Calculations are now under way which include these latest results in a thunderstorm model, so that the rate of magnitude of electrification may be compared with the field data.

A new theory of the charge transfer mechanism is being considered. A vast array of experiments have now been performed using a range of experimental conditions and any theory must be consistent with the results. Recently, Baker et al. (1987) suggested that the charge transfer is associated with the relative growth rates of the interacting particles; effectively, the surface which grows from the vapor fastest, charges positively. However, the present results suggest that it is the history of the growth process that is important - for example, crystals grown at -15°C and interacted at -28°C charged the target positively; whereas, at -28°C , negative charging is expected. A possible explanation that is being investigated, is that the freezing time of droplets on the target controls the concentration of dislocations in the ice lattice and, similarly, the ice crystals include more dislocations in their surface when they grow rapidly from the vapor. A difference in dislocation concentrations on the two interacting surfaces leads to charge transfer because the dislocations are charged. Evidence for charged dislocations is available, but more work is needed before this concept can be assumed to be the charge transfer mechanism.

The size dependence results need to be extended to still larger crystal sizes, preferably up to 1-2mm diameter crystals, to discover if the observed dependence continues. Also, interactions between millimetre-sized graupel particles having had

different growth histories may be important. One method of growing graupel in the cloud chamber would be to introduce some form of recirculation into the cold room in order to extend the crystal lifetime and to promote riming of the ice crystals.

The moving target experiments presented here simulate a soft-hail stone moving through a cloud; however, the height of the cold-room would allow ice spheres of different diameters to be dropped through a mixed cloud in a realistic manner. A series of induction rings may be arranged vertically to measure the charge on the riming hailstone as it falls. It can be calculated that the hailstone will be falling at its terminal velocity in the bottom half of the cloud chamber, and given typical crystal concentrations and sizes the charge acquired by the hailstone will be in the region of 1 pC. A further extension of these experiments would be to introduce an electric field into the chamber, thus allowing inductive ice-ice collisions and inductive water-ice collisions to be performed in order to confirm that the conductivity of ice is too low for the ice-ice mechanism to work, and to show that even one in a thousand droplets splashing off a riming target is insufficient to explain thunderstorm electrification.

Hailstones which occur in thunderstorms carry charges up to -100 pC. The simulated hailstones used here and elsewhere have all been conditionally neutral because the charge acquired by the target flows to earth via the amplifier and chart recorder. It would be useful to place a charge on the target of about -100 pC and then rotate the target through a mixed cloud to determine the effect of the hailstone charge on the charging process; it has been suggested that this may limit the charge transferred.

The work involving large ice crystals is continuing at

present with support from a new USAF contract. The objectives are to extend the present work in ways outlined above, and also to investigate the scavenging nature of large ice crystals.

APPENDIX I

THE REPLICATION OF CLOUD PARTICLES

A.1 The Continuous Formvar Replicator

The use of the replicator has been described in detail by Hallett (1976a,b) and Jayaratne (1981). The device is used for making replicas of the cloud particles, be they water droplets or ice crystals. The cloud particles are drawn past a moving film which is coated with formvar solution and they are trapped by the sticky surface. The formvar dries and the particles evaporate leaving a plastic replica.

The replicator consists of a film support arm, take-up reel and the drive motor. The support arm (of length 60 cm) fits into a smooth metal tube of the same length, which then protrudes into the cloud chamber. The transparent 16mm film was transported by two dc motors; one turns the take-up reel, and the other is attached to five of the rollers mounted on top of the replicator. The formvar solution was pumped through a metal tube to the applicator head at the end of the support arm. As the film moves past the applicator it is covered in a fine coat of formvar, the thickness of which could be controlled.

At the side of the outer metal tube, there is a rectangular slot of dimensions 5.5 x 2.0mm. The end of the tube is connected to a suction pump. When the support arm is in the tube the slot is located just after the applicator head. The cloud is drawn past the film and impacts on it. The film must be dry before being taken up by the reel, and so the film is moved through the rollers on top of the replicator. In order to speed up this process, cold dry air is blown across the film. The flow speed was measured with a flowmeter and was normally 4 m s^{-1} . The slot

was heated with a current element to prevent rime building up and obstructing the flow.

Water resistant pens were used to mark the film at certain points. Thus the information on the film could be correlated with the charging current shown on the chart recorders.

Analysis of the Formvar Film

The film was viewed under a microscope with a x400 magnification. The smallest graticule division was $4.6 \mu\text{m}$. The film was analysed at the required time on the film corresponding to the marks on the chart recorder. A time interval of 1 second was analysed with at least 10 measurements being made within that section.

The droplet and ice crystal concentrations per cubic metre could be calculated from the number of particles visible on the film, the film speed and the flow speed through the slot.

The film has a finite collision efficiency for water droplets. The equations of Ranz and Wong (1952) can be applied to the droplets, and it can be calculated that the smallest droplet which can collide with the film at the flow speeds used is $3.5 \mu\text{m}$. Therefore, any droplets smaller than $3.5 \mu\text{m}$ are ignored as it is assumed that they are formed by direct condensation. Ice crystals are of different shapes and densities, and so their collision efficiencies cannot be calculated from these equations. However, the crystal concentration was a maximum when the crystal diameter reached about $20 \mu\text{m}$. Thus it was assumed that the collection efficiency of the film was unity for larger sizes.

APPENDIX II

MEASUREMENTS OF THE SURFACE TEMPERATURE OF A RIMING HAILSTONE

Introduction

A platinum resistance temperature sensor was used to measure the surface temperature of a riming cylindrical target. The sensor is the same diameter as the simulated hailstone (5 mm) and will experience the same effective liquid water content; thus the need to calculate the mean collection efficiency is removed. Obviously, if the sensor is thinner than the target it will collect more of the droplets due to its higher collection efficiency, and so would over-estimate the hailstone surface temperature. One of the first attempts to predict the surface temperature under certain conditions was made by Ludlam (1951), and later extended by Macklin and Payne (1967). In both formulations the surface temperature is determined by a balance between the rate at which heat is released on freezing and the rate at which the heat can be liberated to the environment by forced convection and evaporation.

The Ludlam Equation

Ludlam (1951) formulated an equation to calculate the surface temperature of a riming hailstone as it moves through a supercooled cloud. The equation deals with the rate of heat loss by convection and evaporation and heat transfer to the environment. The rime surface temperature, RT , is given by:

$$RT = A\{KCT + Lkdp\} + B\{CT - L_f\} / (Ak + Bc_w)$$

where $A = (0.24(Re)^{0.6})/d$, $B = Emv/\pi$, c_w = specific heat of ice,

T_c = cloud temperature, d = cylinder diameter, Δp = difference in vapor densities at the cylinder surface and the environment, E = collection efficiency, K = thermal conductivity, k = coefficient of diffusion of water vapor, L = latent heat of evaporation, L_f = latent heat of fusion, m = liquid water content, v = impact velocity.

The Macklin and Payne Equation

Macklin and Payne (1967) also calculated the rime surface temperature using a similar method and included terms to account for the forced convection and evaporation. Their equation takes the form:

$$X_1 = A \{ Pr^{1/3} k T_a - Sc^{1/3} L_v D (p_s - p_e) \}$$

$$X_2 = B \{ L_f + c_w (T_a - T_m) + c_i T_m \}$$

$$X_3 = A Pr^{1/3} k + B c_i$$

$$T_s = (X_1 + X_2) / X_3$$

where $A = (0.24(Re)^{0.6})/d$, $B = EW_v/\pi$, c_i = specific heat of ice, c_w = specific heat of water, d = cylinder diameter, D = coefficient of diffusion of water vapor, E = collection efficiency, k = thermal conductivity of air, L_f = latent heat of fusion of water, L_v = latent heat of vaporisation of ice, Pr = Prandtl number: $Pr = \gamma_a/K_a$, p_e = density of water vapor in environment, p_s = density of water vapor at surface, Sc = Schmidt number: $Sc = \gamma_a/D$, T_a = ambient temperature, T_s = time surface temperature, T_m = melting temperature, v = airspeed, W = liquid water content, γ_a = kinematic viscosity of air.

APPENDIX III

THE GROWTH RATE OF CLOUD HYDROMETEORS

Mason (1971) states that the general equation for the rate of increase in ice crystal mass by vapor diffusion takes the form:

$$\frac{dm}{dt} = 4\pi CD(\rho_w - \rho_i) \quad (A.1)$$

where the constant C depends on the shape of the crystal, D is the diffusion coefficient of water vapor in air and ρ_i and ρ_w are the vapor densities at the crystal surface and the cloud respectively.

For a hexagonal plate, C has the value of $2r/\pi$ if it is considered to be a circular disc. At -10°C , $(\rho_w - \rho_i)$ is 0.21 g m^{-3} and the rate of increase in mass of a $30 \text{ }\mu\text{m}$ diameter plate is approximately 10^{-8} g s^{-1} . The rate of increase of mass per unit area may be calculated from the original area if $dr \ll r$ and is approximately $4 \times 10^{-5} \text{ g cm}^{-1} \text{ s}^{-1}$.

There are two contributions to the growth rate of the hailstone; firstly, the vapor flux to the surface from the deep field vapor supply and, secondly, the vapor flux from a single droplet freezing on the hailstone surface. These two contributions can be calculated from the equations given by Baker et al. (1987).

(i) The deep field vapor flux to the surface is given by:

$$\Psi_1 = fD(\rho_w - \rho_i)/R \text{ g m}^{-2} \text{ s}^{-1}$$

where f is the ventilation coefficient. Thus if $f=15$, $d=2 \times 10^{-5} \text{ m}^2 \text{ s}^{-1}$, $R=2.5 \times 10^{-3} \text{ m}$ and $(\rho_w - \rho_i)=0.2 \text{ g m}^{-3}$ then $\Psi_1 = 2.4 \times 10^{-3} \text{ mg cm}^{-2} \text{ s}^{-1}$.

(ii) The mass growth rate due to the vapor arriving at the surface from a single freezing droplet is given by:

$$\frac{dm}{dt} = 3\pi fDa(\rho_o - \rho_i) \quad g \, s^{-1}$$

The mass to droplet lost as vapor is all assumed to deposit on the hailstone surface and is given by:

$$M = 3\pi fDa(\rho_o - \rho_i)t_f \quad g$$

where t_f is the freezing time.

Typically: $f=15$, $d=2 \times 10^{-5} \, m^2 \, s^{-1}$, $(\rho_o - \rho_i)=4 \, g \, m^{-3}$,
 $a=5 \, \mu m$ $t_f=1 \, ms$ and so $M=5.6 \times 10^{-11} \, g$.

The target used by Jayaratne et al. was rotated at $3 \, m \, s^{-1}$ in a cloud of droplets of diameter $5 \, \mu m$ and concentration $1000 \, cc^{-1}$. From the present work the collection efficiency of the target for this droplet diameter is 0.2% and the number of droplets swept out per unit area per second is $300 \times 1000 \times 0.002 = 600 \, cm^{-2} \, s^{-1}$.

Thus the available mass flux, Ψ_2 , is:

$$= 5.6 \times 10^{-11} \times 6 \times 10^2 = 3.36 \times 10^{-8} \, g \, cm^{-2} \, s^{-1}$$

The total rate of increase of mass per unit area of the hailstone is just the sum of Ψ_1 and Ψ_2 . Thus,

$$\frac{dm}{dt} = 2.43 \times 10^{-6} \, g \, cm^{-2} \, s^{-1}$$

The ratio of the rate of increase of crystal mass to that of the hailstone is:

$$\frac{4 \times 10^{-5}}{2.43 \times 10^{-6}} = 16.44$$

that is, the ice crystals are growing some sixteen times faster than the hailstone in this situation. In any case the collection of droplets in the range $5-8 \, \mu m$ range due to the rime feathers

still does not provide as much vapor as from the droplets in the cloud. Therefore, the conclusion of Jayaratne et al., that the charge transfer in these experiments is controlled by the vapor diffusion to the target surface from droplets in the cloud still stands.

APPENDIX IV

THE EVENT PROBABILITY OF A CYLINDRICAL TARGET

The collection efficiency of a cylindrical target for super-cooled water droplets, can be considered to be the same as the collision efficiency as only a few droplets, 1 in 1000, Aufdermaur and Johnson (1972), will rebound; the rest will freeze on impact. For ice crystals, however, the collection efficiency is not the same as the collision efficiency, as the ice crystals have a finite separation probability which increases with crystal size and impact velocity. The event probability is defined as the probability of a crystal impacting on a target and rebounding. Therefore, the event probability is a product of the collision efficiency and the separation probability. The collision efficiency equations of Ranz and Wong are not applicable to ice crystals due to their different shapes and densities. Jayaratne (1981) states that the event probability of ice crystals is directly proportional to the total charge separated in a given time.

The simulated hailstone targets consist of a rod and wire of diameters R_r (5.0 mm) and D_w (0.5 mm) respectively. It is assumed that the two targets experience the same cloud conditions at all times. The charging currents to the rod and the wire are I_R and I_w respectively. The volume of cloud swept out by either target is directly proportional to the target diameter and the charging current is directly proportional to the event probability. If the event probabilities of the two targets are E_R and E_w respectively, then:

and therefore:

$$E_R D_R / E_w D_w = I_R / I_w$$
$$E_R = D_w E_w I_R / D_R I_w$$

The wire diameter is small compared to the rod diameter, and so it is assumed that it has an event probability of unity, and if the diameters are substituted, then:

$$E_R = 0.5 I_R / 5 I_W$$

This relationship is valid for all crystal sizes and impact velocities (except very low velocities), because E_W is assumed to be unity.

The values of the event probability given by the ratio of the charging currents were confirmed by the experiments described in Section 5.

REFERENCES

- Aufdermaur A N & Johnson D A, 1972
"Charge separation due to riming in an electric field"
Q J Roy Met Soc, 98, 369-382
- Baker B, Baker M B, Jayaratne E R, Latham J & Saunders C P R, 1987
"The influence of diffusional growth rate on the charge transfer accompanying rebounding collisions between ice crystals and hailstones"
Q J Roy Met Soc, 113 (In press)
- Boussinesq J, 1905
J de Mathematics, 1, 285-332
- Bradley S G & King W D, 1980
"Frequency response of CSIRO liquid water probe"
J Appl Met, 18, 361-366
- Brun R J, Lewis W, Perkins P J & Serafin J S, 1955
"Impingement of cloud droplets and procedure for measuring liquid water content and droplet sizes in supercooled clouds by rotating multi-cylinder method"
NACA Tech Notes 1215
- Church C R, 1966
"The electrification of hail"
PhD Thesis, Univ of Durham
- Dong Y Y & Hallett J, 1986
"Structure, fall orientation and secondary ice formation by graupel"
Paper 22.4, Conf on Cloud Physics, Am Met Soc, Snowmass, Colo.
- Freytmuth P, 1977
"Frequency response and electronic testing for constant temperature hot-wire anemometers"
J Phys, E10, 705-710
- Hallett J, 1976a
"Measurement of size, concentration and structure of atmospheric particulates, by the airborne continuous particle replicator"
Air Force Geophys Lab, Rep No AFGL-TR-0149
- Hallgren R E & Hosler C L, 1960
"Ice crystal aggregation"
Geophys Monogr, 5, 251-260
- Harimaya T, 1975
"Riming properties of snow crystals"
J Meteor Soc Japan, 53, 384-392
- Hosler C L & Hallgren R E, 1960
"The aggregation of small ice crystals"
Trans Farad Soc, 30, 200-207
- Jayaratne E R, 1981
"Laboratory studies of thunderstorm electrification"
PhD Thesis, Univ of Manchester

- Jayaratne E R, Saunders C P R & Hallett J, 1983
"Laboratory studies of the charging of soft hail during ice crystal interactions"
Q J Roy Met Soc, 109, 609-630
- Jayaratne E R & Saunders C P R, 1985
Reply to "comments on the 'rain gush', lightning and the lower positive charge centre in thunderstorms"
J Geophys Res, 90, 10755
- Jayaratne E R & Saunders C P R, 1985
"Thunderstorm electrification: the effect of cloud droplets"
J Geophys Res, 90, 13063-13066
- Kennelly A E, Wright C A & Van Bylevelt J S, 1909
"The convection of heat from copper wires"
Trans AIEE, 28 363-393
- King L V, 1914
"On the convection of heat from small cylinders in a stream of fluid"
Phil Trans Roy Soc, London, A214, 373-
- King W D, Parkin D A & Handsworth R J, 1978
"A hot-wire liquid water device having fully calculable response characteristics"
J App Met, 17, 1809-1813
- King W D, Maher C T & Hepburn G A, 1981
"Further performance tests on the CSIRO probe"
J App Met, 20, 195-202
- King W D, Strapp J W, Baumgardner D & Huffman D, 1984
"Icing wind tunnel tests on the CSIRO liquid water probe"
Private communication
- Latham J & Saunders C P R, 1970
"Experimental measurements of the collection efficiencies of ice crystals in an electric field"
Nature, 96, 257-265
- Löffler F & Muhr W, 1972
"Die Abscheidung von Feststoffteilchen unter Tropfen an Kreisylindern infolge von Tragheitskreften"
Chemie Ing-Techn, 44, 510-514
- Lowaski E P, Stallabrass J R & Hearty P F, 1983
"Icing of an unheated, non-rotating cylinder. Part II: icing wind tunnel experiment"
J Cli App Met, 22, 2063-2074
- Ludlam F M, 1951
"The heat economy of a rimed cylinder"
Q J Roy Met Soc, 77, 663-666
- Macklin W C, 1962
"Density and structure of ice formed by accretion"
Q J Roy Met Soc, 87, 30-50

- Macklin W C & Payne G S, 1967
"A theoretical study of the ice accretion process"
Q J Roy Met Soc, 93, 195-213
- Mason B J, 1971
"The Physics of Clouds"
Oxford Univ Press
- Merceret F J and Schricker T L, 1975
"A new hot-wire liquid water meter"
J Appl Met, 14, 319-325
- Morris J T, 1912
"The electrical measurement of wind velocity"
Electrician, 69, 1056-1059
- Mossop S C, 1984
"Production of laboratory clouds"
Q J Roy Met Soc, 110, 275-279
- Ono A, 1969
"The shape and riming properties of ice crystals in natural clouds"
J Atmos Sci, 26, 138-147
- Pitter R L, 1977
"A re-examination of riming on thin ice plates"
J Atmos Sci, 34, 684-685
- Ranz W E & Wong J B, 1952
"Impaction of dust and smoke particles on surface and body collectors"
Indus Eng Chem, 44, 1371-1381
- Reynolds S E, Brook M and Gourley M F, 1957
"Thunderstorm charge separation"
J Met, 14, 426-433
- Rodgers D C, 1974
"Collection efficiency of ice spheres for ice crystals"
Res Report, No AR110, Dept of Atmos Resources, Univ of Wyoming,
Laramie, Wyo.
- Rodgers D C, Baumgardner D & Vali G, 1983
"Determination of supercooled liquid water content by measuring the
riming rate"
J of Cli and App Met, 22, 153-162
- Saunders C P R & Wahab N W A, 1973
"The replication of ice crystals"
J Appl Met, 12 1035-1039
- Saunders C P R, Wheeler M F S, Jallo N and Jayaratne E R, 1984
"Ice crystal interactions with a riming target: charge transfer and
collection efficiencies"
J Geophys Res, 90, 6047-6050
- Saunders C P R and Zhang C C, 1987
"Rime density, radial forces and atmospheric electricity"
Submitted for publication to Atmos Res.

Schaefer V J, 1962

"The vapour method for making replicas of liquid and solid aerosols"
J Appl Met, 1 413-418

Stallabrass J R, 1978

"An appraisal of the single rotating cylinder method of liquid water content measurement"

National Research Council of Canada Report, LTR-LT-92 21pp

Takahasi T, 1978

"Riming electrification as a charge generation mechanism in thunderstorms"

J Atmos Sci, 35, 1536-1548

Van de Hage J, 1969

"A variation of Schaefer's formvar technique for obtaining replicas of small ice crystals"

J Rech Atmos, 3, 49-50

Wilkins R D & Auer A H Jr, 1970

"Riming properties of hexagonal ice crystals"
Conf on Cloud Physics, Ft Collins, Colo. 81-82

Wyngaard J C & Lumley J L, 1967

"A constant temperature hot-wire anemometer"

J Sci Instru, 44, 363

END

DATE
FILMED

3 88